In-Process Cooling of Friction Stir Extruded Joints for Increased Weld Performance via Compressed Air, Water, Granulated Dry Ice and Liquid Nitrogen

By

Benjamin Anton Snyder

Thesis

Submitted to the Faculty of the

Graduate School of Vanderbilt University

in partial fulfillment of the requirements

for the degree of

Master of Science

in

Mechanical Engineering

May 14th, 2021

Nashville, Tennessee

Approved:

Alvin M. Strauss., Ph.D.

Kenneth R. Pence, Ph.D.

Acknowledgements

I would like to thank my incredible wife Alex for loving me endlessly, believing in me, and being by my side every step of the way. As well as my parents, Jack, Kristi, and Ron, and my brother, Eli, for their love and continued support in all that I do.

I would also like to thank all of those who helped in the many aspects involved in completing this degree. Dr. Alvin Strauss for introducing me to friction stir welding, his guidance in school, research, as well as all things planes and nuclear. Dr. Ken Pence for also guiding me through school and agreeing to be a reader for my thesis. Adam Jarrell, Kelsay Neely, Connor Strawn, Lucas Wilkins, Brayden Terry, and Henry Gunner for being such wonderful mentors, lab mates, and lifelong friends from whom I gained invaluable knowledge and shared endless laughs through memes and pranks. Phil Davis for all the life advice, machining assistance, and unveiling my passion for running. Tom Kourlis and Frank Buncom for being such amazing friends and providing feedback for this thesis. All my professors and additional mentors throughout my graduate career: Dr. Tom Withrow, Dr. Jason Mitchell, Dr. Ken Frampton, Dr. Haoxiang Luo, Dr. Greg Walker, Dr. Eric Barth, Dr. Nilanjan Sarkar, and Dave Berezov. As well as those who helped with resources and testing procedures for my research: Anuj Rastogi for help with liquid nitrogen procurement, Rossane Delap for allowing me to borrow a liquid nitrogen dewar, and Mark Thelen for helping with hardness and shear testing.

Thank you to Vanderbilt University and the NASA Tennessee Space Grant Consortium as this project would not have been possible with their financial support.

Table of Contents

List of Tables

List of Figures

Figure Page

Nomenclature

AC	Air Cooled
AS	Advancing Side
BM	Base Material
CAD	Computer-Aided Design
DI	Dry Ice
FSE	Friction Stir Extrusion
FSF	Friction Stir Forming
FSW	Friction Stir Welding
HAZ	Heat Affected Zone
IMC	Intermetallic Compounds
IPC	In-Process Cooling
IPM	Inches Per Minute
LN	Liquid Nitrogen
MIG	Metal Inert Gas
NC	Non-Cooled
RPI	Revolutions Per Inch
RPM	Revolutions Per Minute
RS	Retreating Side
STC	Specific Thermal Contribution
TMAZ	Thermo-Mechanically Affected Zone
USTS	Ultimate Shear Tensile Strength
UTS	Ultimate Tensile Strength
VUWAL	Vanderbilt University Welding Automation Laboratory
WC	Water Cooled
WNZ	Weld Nugget Zone
WP	Weld Pitch
YS	Yield Strength

Chapter I

Introduction

Friction Stir Welding

Friction stir welding (FSW) is a solid state-joining process developed by The Welding Institute (TWI) of the U.K. in 1991[1-17]. While the development of this joining process was for aluminum, its use has expanded to various other materials such as copper, magnesium, brass, titanium, steel, and plastics [3]. This form of joining has found applications in the aerospace, automotive, railway, and naval industries due to its relatively low operating temperatures, ability to join difficult or previously unweldable materials, reduction in joint residual stress, and lack of resolidification effects which results in cracking, second phase formation, porosity, and embrittlement [4]. In a study comparing butt joints of aluminum alloys AA7050 and AA2024 joined by FSW and by metal inert gas (MIG), a form of conventional welding, Kulekci et al. found that the tensile strength of the FSW joints was 3% lower than the base material (BM) whereas the strength of the MIG joints were 51.3% lower than the BM [3]. Comparing these two tests revealed that the FSW joints had an 88% tensile strength improvement over MIG welding which can be explained by the advantages of FSW listed previously. Like fusion welding, FSW can weld workpieces in several joint configurations, the most common of these being the lap joint, butt joint, and T-joint.

The FSW process starts by plunging a rotating non-consumable tool into the weld material until the shoulder of the tool is in contact with the workpiece. The rotating tool then begins to traverse along a seam line or desired weld path causing additional heat generation into the work material due to friction and plastic deformation from the tool. This generated heat allows the work material to reach a temperature in which the metal plasticizes and can flow or "stir" without reaching the material's melting temperature. Welding parameters that directly affect the heat generation and weld quality during FSW include tool rotation speed, welding

speed, plunge depth, tilt angle, tool shoulder geometry, and tool probe geometry [18]. To better describe the regions of the FSW process, different areas of the tool material interface have been given specific names, all of which can be seen in Figure 2 below. The advancing side (AS) of the weld is the edge of the weld line in which the rotational vector of the tool travels the same direction as the linear vector of the traversing workpiece. The retreating side (RS) is the opposite edge of the weld line where the direction of the rotational vector of the tool opposes the direction of the linear vector of the traversing workpiece. The localized tool speed is lower on the RS than the AS. While the tool is moving through the workpiece, the leading edge is the front side of the tool moving through unwelded material while the trailing edge is the back side of the tool leaving behind an "onion ring" structure [5].

There are a variety of tool geometries used during the FSW process which include shoulder features such as scrolled, convex, and concave surfaces. They can also feature a probe that has variable cross-sectional shapes such as a circle, triangle, or square and may include threads, flutes, or flats. In addition to heating the workpiece, the tool prevents flash by containing plasticized material, breaks up workpiece oxide layers, provides sufficient forging pressure, and wipes material from the leading side to the retreating side in order to properly fill the weld path and create the "onion ring" surface structure, which is a desirable weld characteristic that illustrates a high-quality friction stir weld [11–13].

When analyzing the cross-section of FSW, there are four classifications to describe the various microstructure zones known as the base material (BM), heat affected zone (HAZ), thermo-mechanically affected zone (TMAZ), and weld nugget zone (WNZ). The BM is unaffected by heat and deformation during the welds. The HAZ is only affected by heat while the TMAZ is affected by both heat and deformation which causes dynamic recrystallization also known as grain refinement [19]. Depending on the parent materials used in FSW, the whole TMAZ may not experience dynamic recrystallization which then results in an embedded WNZ [18]. All these microstructure zones are present in most materials and all welding configurations used in FSW. Figure 1 below shows the various microstructural zones in the cross-section of a friction stir weld.

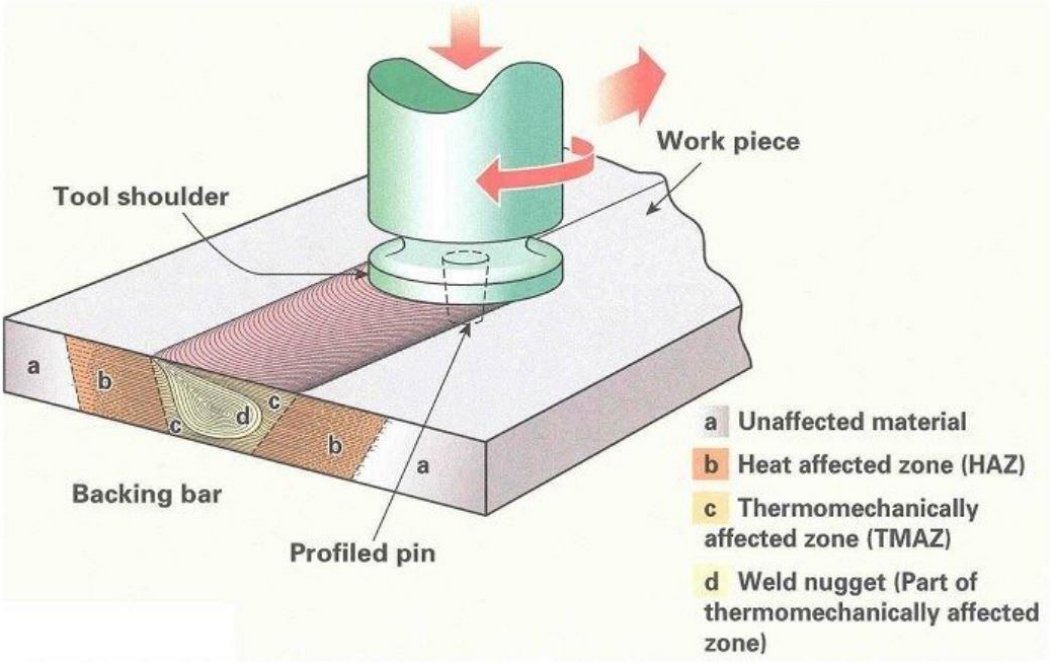

Figure 1 – Microstructural zones formed during the FSW process [1]

Friction Stir Extrusion

This thesis focuses on the use of a welding process known as friction stir extrusion (FSE). FSE is a derivative process of FSW that extrudes parent material into a grooved material with a precut groove or cavity. This process creates an interlocking mechanical joint that joins the parent and base materials. Due to the formation of intermetallic compounds (IMCs) and severe tool wear from vast differences in material properties, FSW has many challenges in joining dissimilar materials such as steel and aluminum [20]. FSE eliminates these challenges because only the parent material is being altered, which also tends to be the softer material, therefore minimizing any surface penetration of the harder material, IMC formation, and tool wear. One of the first known instances of FSE was the development of friction stir forging (FSF) by Nishihara where various aluminum alloys were joined to carbon steel plates by welding across horizontally drilled holes [7]. The dovetail extrusion used in this paper and developed by Evans et al. differs from FSF in that the welding line is along the groove instead of traversing over multiple grooves. Through experimentation in the Vanderbilt University Welding Automation Lab (VUWAL), past lab mates have determined that an O-ring dovetail groove shape results in solid joint strength and is easily manufacturable. This dovetail groove has been used in various orientations and weld

types such as lap welds, T-Joint welds, and thin sheet welds [20-22]. The FSE process and materials used in this research can be seen below in Figure 2.

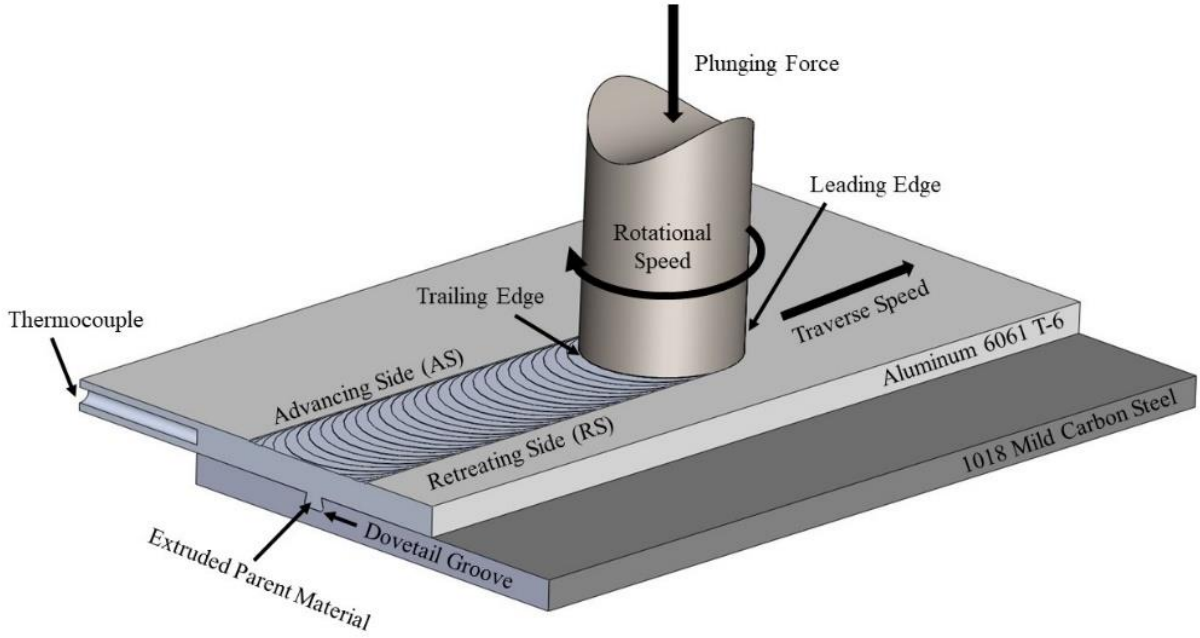

Figure 2 – FSE diagram highlighting important FSW parameters and terminology as well as indicating the material used in this research, location of the thermocouple for weld temperature measurements, and dovetail extrusion.

Chapter II

Literature Review

This thesis focuses on the combined effects of in-process cooling (IPC) and variable weld pitch (WP) on the improvement of FSE joints. Therefore, this section offers an in-depth definition and literature review of these processes and parameters.

Variable Welding Parameters

Weld pitch (WP) is a welding parameter that compares the rotational velocity of the tool and translational velocity of the weld to provide quick insight into the quality and specific heat input of the weld [8]. More specifically, WP signifies the number of revolutions per length that the tool advances and directly correlates with heat flux in the weld. A smaller WP means that there are fewer revolutions per unit length forward and less heat input whereas a higher WP means that there are more revolutions per length forward and greater heat input into the welded material. The equation for this parameter can be seen below in equation 1 where ω is the rotational speed of the tool in revolutions per minute (RPM) and υ is the translational speed of the weld in inches per minute (IPM) [8]:

$$WP = \frac{\omega}{v} \tag{1}$$

There have been a handful of publications that study the effects of varying WP during the FSW process. Park et al. studied the effect of shoulder diameter and WP on the lap weld of aluminum alloys AA6111 and AA5023. They found that increases in the WP caused a reduction in the weld nugget zone (WNZ) while decreases in the WP improved the hardness values of the thermo-mechanically affected zone (TMAZ), heat affected zone (HAZ), and WNZ [8]. Both conclusions stem from the WP being positively correlated with heat input and peak weld

temperature. The larger heat input and weld temperatures result in increased grain growth in the aluminum microstructure which increases the size of the weld nugget and reduces the hardness of the metal as the lattice grows.

Abbasi et al. studied the influence of WP on the mechanical properties of magnesium alloy AZ31 friction stir welds. This publication unveiled similar discoveries to Park et al. and cited that the weld nugget growth was due to the increased frictional and plastic-work heat produced as WP increases [23]. Chowdhury et al. studied the effects of pin tool thread and weld pitch in the FSW of a magnesium alloy. Unlike Park et al. and Abbasi et al., Chowdhury et al. defined WP in their paper as translational velocity over the tool rotational velocity or rather the inverse of the WP defined above. This publication similarly concluded that the grain growth is proportional to the WP defined in the equation above. Additionally, they found that increasing WP, causes a linear decrease in both yield strength (YS) and ultimate tensile strength (UTS) of the lap weld [9]. The relationship between WP and the YS and UTS can be seen in equations 2 and 3 below where α_1, β_1, α_2, and β_2 are material dependent parameters [9] :

$$YS = \alpha_1 + \beta_1 \frac{v}{\omega} = \alpha_1 + \frac{\beta_1}{WP} \quad (2)$$

$$UTS = \alpha_2 + \beta_2 \frac{v}{\omega} = \alpha_2 + \frac{\beta_2}{WP} \quad (3)$$

In summary, WP is the ratio of rotational to translational velocity in a weld and provides rapid insight to better understand the heat input and peak temperature of the system. As WP increases, the weld nugget grows while hardness values, YS, and UTS decrease.

In-Process Cooling

A common method of improving the performance of FSW is the introduction of in-process cooling (IPC). IPC uses varying combinations of passive and active cooling during the welding process in the form of moving or stationary fluids. The success behind this additional process in FSW comes from the removal of heat when the weld is surrounded by a fluid cooler than the FSW temperature. The inspiration for this research came from the publications of Fratini et al. and Sharma et al. which will be discussed at length below.

Active In-Process Cooling

Fratini et al. published multiple articles where they used aluminum alloys AA2024-T4 and AA7075-T6 to make various dissimilar and homogenous friction stir welds in multiple weld configurations such as butt, lap, and T-joints [10–12]. For these welds, the group had a set of welds joined under normal conditions and another set that used a FSW tool trailing water flux with a flow rate of 0.5 $\frac{L}{min}$. In addition to introducing IPC into their welds, they also used three different weld pitches (84.9 revolutions per inch (RPI), 173.0 RPI, and 362.9 RPI) which they labeled as specific thermal contributions (STC) levels of low, medium, and high respectively [10]. Within their publications, Fratini et al. found that IPC varied in its efficacy depending on the STC level through hardness testing, tensile testing, and grain size analysis. When conducting tensile tests, the group found that fracture on non-cooled welds occurred between the HAZ and TMAZ on the advancing side (AS) of the joint whereas the IPC welds shifted their fracture location. More specifically, the low STC weld fractured in the nugget at the center of the weld line in the WNZ while the medium and high STC fracture locations were somewhere between the non-cooled and low STC fracture zones. For hardness testing, all of the water cooled samples produced higher micro-hardness values than normal joints with the medium and high STC differences being minor and the low STC difference being significant [12]. The reason for this superior performance in relation to the non-cooled welds is due to the limitation of the weld temperature caused by reduction in weld heat flux from variable WP and IPC. With the reduction of the weld temperature, welds do not reach solubilization temperatures where precipitates are primarily formed. Thus, the limitation of heat flux into the welds improves performance due to the reduction in grain growth and precipitation solubilization during the welding process [10]. In summary, Fratini et al. found that the introduction of a water flux during the welding process improved the performance of the welds in tensile, micro-hardness, and precipitate forming as well as the reduction of residual stresses (by up to 20% for butt joints) [11]. The group concluded that this method of IPC was most effective for their low STC sample and thus future work should be done with other cooling sources to increase the weld performance at higher STCs or WP.

While Fratini et al. focused on the use of water cooling in their IPC research, Sharma et al. expanded the cooling media used in their IPC research [24]. Within their research, Sharma et al. used compressed air, liquid nitrogen, and water to investigate the effects of IPC on butt welds of aluminum alloy AA7039. They analyzed these welds through grain size analysis as well as

tensile and microhardness testing. All coolants within this research were dispensed 30 mm behind the FSW tool and along the weld center line with flow rates of 60 $\frac{L}{min}$ for air, 1.5 $\frac{L}{min}$ for water, and .25 $\frac{L}{min}$ for liquid nitrogen. Sharma et al. found that IPC decreased the size of the TMAZ and HAZ and decreased the grain size inside of the WNZ. Additionally, the group found that IPC hardness values were highest in the HAZ rather than the WNZ and TMAZ which is the opposite of the trend found in non-cooled welds. Comparing the different cooling types, Sharma et al. found that water performed the best in increasing the strength and material properties of the weld while air cooled joints performed the worst. The water cooled welds had an ultimate tensile strength of 73.5% and a percent elongation of 86.8% to that of the base metal. Additionally, the water cooled joints caused the fracture location to migrate from the boundary of the HAZ and TMAZ to approximately the weld center line with a fracture line that was "curved and perpendicular to (the) applied load" [24] compared to the normal joint that fractures in a straight line inclined at 45º to the loading direction.

In addition to the work done by Fratini et al. and Sharma et al., there have been numerous other groups that researched the effects of IPC, some of which are summarized below.

Kumar et al. discussed the effects of active cooling during the FSW process on residual stress in weldments [5]. They found that the introduction of a cooling media adjusted the thermal field during the welding process which greatly reduced residual stress in the welded structure caused by the fixturing of the raw material. In addition to reducing the residual stress, active cooling also changed the residual stress of the weld from being tensile to compressive [5].

Mehta et al. conducted non-cooled and water cooled FSW of aluminum alloy AA6061 and magnesium alloy AZ31B in a butt weld configuration [25]. They found that water cooling during the FSW process at a flow rate of 100 $\frac{mL}{min}$ resulted in a reduction of intermetallic compounds (IMCs), an increase in tensile strength and micro hardness, as well as a higher joint efficiency of ~73% in comparison to non-cooled welds that had a joint efficiency of ~53% [25]. The group concluded that with the reduction in IMCs, cooling assisted friction stir welds are characterized by lower average hardness values.

Peng et al. incorporated forced air cooling in their process of butt friction stir welding of aluminum alloys AA5A06-H112 and AA6061-T651 to analyze the effects of forced convective cooling in comparison to non-cooled welds [13]. The introduction of forced air accelerated the

cooling process during the welding which reduced the peak temperatures and high temperature dwell times. As a result, the air cooled welds demonstrated superior mechanical properties to the non-cooled welds with a 10% increase in UTS and an increase in hardness values in the HAZ due to the suppression of coarsening grains and reduction of precipitate dissolution [13].

Passive In-Process Cooling

In addition to research conducted to analyze the weld improvements of active IPC, there have also been many publications researching the similar effects of passive IPC such as welding underwater to yield stronger and more mechanically sound welds.

Fathi et al. researched the effects of underwater friction stir butt welding of aluminum alloy AA6061-T6 [26]. This group also introduced variable WP to simultaneously investigate the optimal FSW parameters. Like others, this research concluded that the strengthening of the HAZ was the main component that enhanced the joint strength which resulted in an increase of tensile strength by 16% and hardness by 12.5% in comparison to a non-cooled weld. As for the optimal WP, Fathi et al. claimed that their 20 mm diameter FSW tool at a rotational speed of 600 RPM and a travel speed of 80 $\frac{mm}{min}$ produces maximum hardness values [26].

Similarly, Liu et al. also researched underwater friction stir butt welding but instead used aluminum alloy AA2219 [14]. To investigate the effects of WP in the underwater FSW process, Liu et al. maintained a constant tool rotational speed of 800 RPM but selected various translational welding speeds in the range of 50 $\frac{mm}{min}$ to 200 $\frac{mm}{min}$. This research revealed that groove defects appear when the translational speed approaches 200 $\frac{mm}{min}$. Additionally, the grain size is lowest at 50 $\frac{mm}{min}$ and 200 $\frac{mm}{min}$ but peaks as the welding speed approaches 150 $\frac{mm}{min}$. The maximum tensile strength measured across all WP was 80% of the BM at 347 MPa. With the variable WP, the fracture location during tensile testing for 50 $\frac{mm}{min}$ occurred in the HAZ on the retreating side (RS) where an increase in welding speed to 150 $\frac{mm}{min}$ shifted the fracture location to the TMAZ on the AS [14].

Benavides et al. constructed a clay containment system with a steel backing plate to prevent leaking of stationary liquid nitrogen that engulfed aluminum alloy AA2024 plates during friction stir butt welding [27]. The group inserted a thermocouple 1 cm from the tool path and

measured a peak temperature of 140 ºC which is approximately half of the peak temperature measured for the non-cooled welds. The introduction of the liquid nitrogen bath resulted in increased hardness in the HAZ and a considerable reduction in grain size, specifically an average of 8 µm at the top of the non-cooled weld and 2 µm at the bottom of the non-cooled weld compared to 2 µm at the top of the liquid nitrogen weld and 0.5 µm at the bottom of the liquid nitrogen weld [27].

Mofid et al. friction stir butt welded plates of magnesium alloy AZ31 and aluminum alloy AA5083 H34 while submerged in both water and liquid nitrogen to compare the effects of the two cooling mediums to uncooled welds [28]. As expected, Mofid et al. found that the grain size in the centerline of the TMAZ reduced from 20 µm for the uncooled weld down to 6.3 µm for the underwater weld and 2.5 µm for the liquid nitrogen submerged weld [28]. As for hardness, the group did not notice much of a change between the three weld types except for high hardness values in the TMAZ of the uncooled weld which is attributed to the formation of IMCs.

Post-Process Cooling

While IPC and submerged FSW seem to be the more popular topics of research in the improvement of FSW joints, additional research in post-process cooling via water and cryogenic fluids has been conducted by Bansal et al. They investigated the effects of subjecting completed Al-Zn-Cu alloy AL7050-T7451 friction stir butt welds to deep cryogenic treatment, specifically the soaking of joints in a liquid nitrogen cryogenic container at a temperature of 88 K for 8 hours [15]. To avoid the introduction of drastic residual stresses, the cryogenic chamber was reduced from room temperature to its minimum temperature over a period of 2 hours and returned to room temperature at the same rate after the cryogenic treatment. These experiments were compared to untreated welds and thus concluded that cryogenically treated welds resulted in a reduction in grain size and an increase in the hardness, impact toughness, YS, and percent elongation values [15].

The research presented in this thesis differs from that presented in this literature review as it provides a study of the effectiveness of IPC at varying WP by using four different cooling media on friction stir extrusion (FSE) weld joints.

Chapter III

Methods and Materials

The naming conventions, weld parameters, and cooling source details for the twenty welds analyzed in this research can be found below in Table 1. This table additionally shows the plunge depth, the tilt angle, and the lateral location of the friction stir welding (FSW) tool based on the global welder position. In FSW, the plunge depth refers to penetration depth of the FSW tool into the work material and the tilt angle is the angle of the FSW tool away from being orthogonal to the workpiece. As for cooling, the table shows amount dispensed, flow rate, and temperature of the in-process cooling (IPC) fluids.

Table 1 - The weld and cooling parameters used for each of the IPC welds

Matrix Number	Rotational Speed (RPM)	Traverse Speed (IPM)	Plunge Depth	Tilt Angle	Lateral Location of Plunge	Length of Weld	Amount of Cooling Fluid	Flow Rate of Cooling Fluid	Temperature of Fluid
(1,1)	1500	3	.22"	1.5°	~2.42"	6.5"	N/A	N/A	N/A
(2,1)	1500	2	.22"	1.5°	~2.42"	6.5"	N/A	N/A	N/A
(3,1)	1000	3	.22"	1.5°	~2.42"	6.5"	N/A	N/A	N/A
(4,1)	1000	2	.22"	1.5°	~2.42"	6.75"	N/A	N/A	N/A
(1,2)	1500	3	.22"	1.5°	~2.42"	6.375"	N/A	12.0 m/s	8.9 ºC (Parallel)/ 11.58 ºC (Perpendicular)
(2,2)	1500	2	.22"	1.5°	~2.42"	6.5"	N/A	12.0 m/s	8.9 ºC (Parallel)/ 11.58 ºC (Perpendicular)
(3,2)	1000	3	.22"	1.5°	~2.42"	6.5"	N/A	12.0 m/s	8.9 ºC (Parallel)/ 11.58 ºC (Perpendicular)
(4,2)	1000	2	.22"	1.5°	~2.42"	6.375"	N/A	12.0 m/s	8.9 ºC (Parallel)/ 11.58 ºC (Perpendicular)
(1,3)	1500	3	.22"	1.5°	~2.42"	6.375"	2254.2 mL	17.68 mL/s	24.55 ºC
(2,3)	1500	2	.22"	1.5°	~2.42"	6.5"	3447.6 mL	17.68 mL/s	24.55 ºC
(3,3)	1000	3	.22"	1.5°	~2.42"	6.25"	2210 mL	17.68 mL/s	24.55 ºC
(4,3)	1000	2	.22"	1.5°	~2.42"	6.5"	3447.6 mL	17.68 mL/s	24.55 ºC
(1,4)	1500	3	.22"	1.5°	~2.42"	6.25"	20 TBSP	3.785 g/s	-80.57 ºC
(2,4)	1500	2	.22"	1.5°	~2.42"	6.5"	30 TBSP	3.639 g/s	-80.57 ºC
(3,4)	1000	3	.22"	1.5°	~2.42"	6.5"	20 TBSP	3.639 g/s	-80.57 ºC
(4,4)	1000	2	.22"	1.5°	~2.42"	6.375"	30 TBSP	3.711 g/s	-80.57 ºC
(1,5)	1500	3	.22"	1.5°	~2.42"	6.5"	1.875 L	14.42 mL/s	-194.6 ºC
(2,5)	1500	2	.22"	1.5°	~2.42"	6.5"	3 L	15.38 mL/s	-194.6 ºC
(3,5)	1000	3	.22"	1.5°	~2.42"	6.5"	1.875 L	14.42 mL/s	-194.6 ºC
(4,5)	1000	2	.22"	1.5°	~2.42"	6.5"	3.1 L	15.89 mL/s	-194.6 ºC

Welder and Data Collection Systems

The friction stir welder used in this research is a 1944 Milwaukee Model K manual mill that has been modified with additional motors to allow for automated control of x, y, z motion with in-house computer programs. Images of the modified welder are found throughout the rest of this section specifically in Figures 3-8. The weld programs use C# and MATLAB code as well as Simulink structures developed by current and previous graduate researchers in the Vanderbilt University Welding Automation Lab (VUWAL) to complete various weld types. Auxiliary instrumentation allows for the collection of cartesian position, cartesian forces, and torque about the FSW tool. The instrumentation used for position monitoring includes string potentiometers, optical encoders, and linear encoders. A Kistler 9123C piezoelectric dynamometer mounted above the spindle records forces and torque during welds. To ensure that the dynamometer does not exceed manufacturer specified temperature limits, air from a vortex tube is directed at heat fins attached to the dynamometer. The process measurements and forces output from the mentioned instrumentation and dynamometer not only serves to provide data for research but also ensures that these outputs do not exceed manufacturer-defined safety limits to prevent damage to the tool, dynamometer, welder, or its users.

Raw Material

This research used 0.25” thick plates of aluminum alloy AA6061-T6 and mild carbon steel that were cut to 3” in width and 8” in length. In preparation for welding, the aluminum plate was scrubbed with steel wool followed by isopropyl alcohol to clear the oil and oxide layers. The steel plates had dovetail grooves milled lengthwise 1” from the edge of the plate. Each of the dovetail grooves was milled using a CNC machine with a 0.172 diameter 2 flute dovetail cutter with a taper angle of 48^{o} and a corner radius of 0.031”.

Experimental Setup

The experimental layout used in this research can be seen in Figure 3 below. All the clamps and work pieces were attached to the containment table, labeled below as the “IPC enclosure.” The table was aligned with the front of the mill anvil and then mounted using four step clamps with the purpose of containing any fluids such as water or liquid nitrogen during in-

process cooling (IPC). Bloodworth built and designed this table to investigate the effects on metallurgic and mechanical effects of underwater friction stir welding (FSW) of AA6061-T6 [16]. The steel and aluminum used during the IPC FSW process were offset by an inch to allow adequate work holding for tensile testing. To ensure that the steel plates maintained a relatively constant position in relation to the tool and to ensure that the weld line was parallel to the precut dovetail groove, two alignment posts were attached to the containment table and used to line up the steel plate before clamping the work pieces with four step clamps.

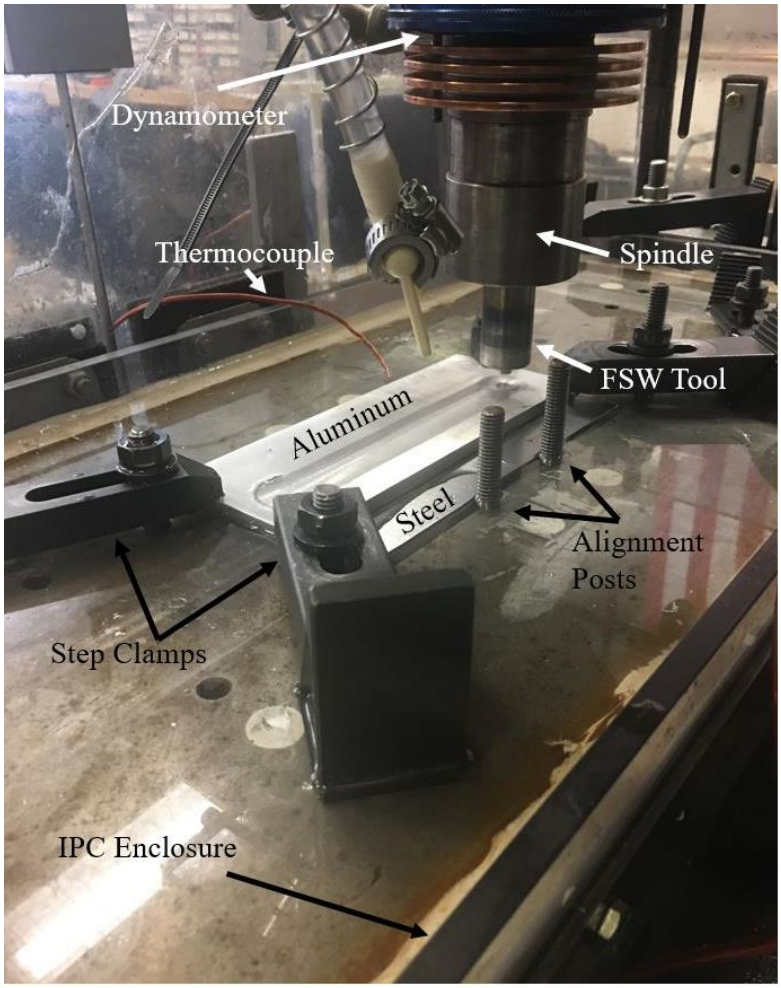

Figure 3 – Water cooled weld that shows the experimental set up for the IPC welds

As previously mentioned, there are several variants and combinations of tools used in FSW, but the tool design used in this research can be seen below in Figure 4. This tool is made of H13 tool steel and features a convex scrolled shoulder with a diameter of 1” and a shoulder

angle of 6.71º as well as a threaded pin with a 0.25” diameter. The scrolled features on the shoulder play an integral role in sweeping material from the outer edge of the shoulder back in towards the pin [17]. This legacy design for VUWAL has been selected for research due to its ease of manufacturing and its ability to create high quality friction stir welds under various welding parameters and materials.

Figure 4 –FSW tool design used for this research featuring a convex scrolled shoulder and threaded pin

Variable Welding Parameters

The most used weld parameters in VUWAL for friction stir extrusion (FSE) are a rotational speed of 1500RPM and a translational velocity of 3IPM (1500RPM-3IPM) with a tilt angle of 1.5º. These parameters were selected through quality analysis of friction stir welds over several parameter studies. To fully investigate the effects of IPC, this research varies the weld pitch (WP) between welds to determine if varying heat input and dwell time on the welds impact

the efficacy of IPC. The WP, rotational speed, and translational speed of sample groups used in this research can be seen below in Table 2.

Table 2 - The weld pitch of the four different weld groups used in the IPC research

Samples Matrix Number	Rotational Speed (RPM)	Translational Speed (IPM)	Weld Pitch (RPI)
(1,:)	1500	3	500
(2,:)	1500	2	750
(3,:)	1000	3	333.33
(4,:)	1000	2	500

Cooling Methods

To test the effectiveness of in-process cooling (IPC) on the improvement of strength and quality of friction stir extrusion (FSE) welds, four methods of cooling were compared to the uncooled weld. These methods of cooling include compressed air (AC), water (WC), granulated dry ice (DI), and liquid nitrogen (LN). Cooling media was deposited on the trailing edge of the tool path.

Air Cooling

Air cooling (AC) of the extrusion weld was achieved using a Model 3825 EXAIR Adjustable Spot Cooler. As mentioned above, this vortex tube has been fit to the welding machine to maintain the dynamometer at an appropriate operating temperature. The compressed air that powers the vortex tube comes from the ~80 PSI facility air supply. The air temperature and velocity are directly proportional and can be adjusted based on the penetration of the vortex tube nose cone. Therefore, the fastest flow setting on the vortex tube outputs the warmest air while the slowest flow setting outputs the coldest air. To have a moderately fast flow rate with a cooler temperature, the vortex tube was set at the middle of its flow setting. This setting resulted in an air temperature of 8.9 ºC when the thermocouple was parallel to the flow and 11.58 ºC when the thermocouple was perpendicular to the flow measured with an Omega type K thermocouple. Additionally, this flow had a velocity of 12 $\frac{m}{s}$ as measured by an anemometer.

The air outlet was oriented ~1.625” behind the FSW tool and ~1.25” above the surface of the aluminum, directed at the weld. The application of the compressed air was terminated two minutes after the end of the weld.

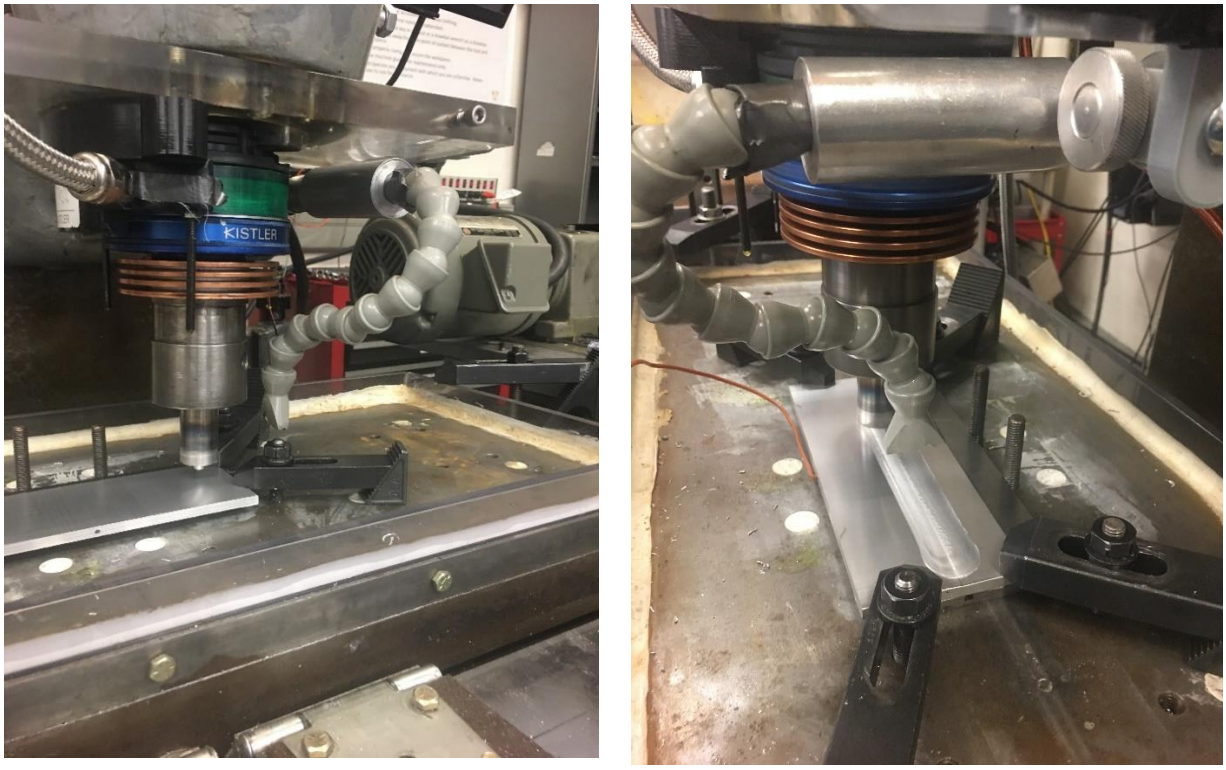

Figure 5 – (Left) The vortex tube orientation before the start of the weld. (Right) The AC process with the vortex tube in action along the weld line.

Water Cooling

In-process water cooling (WC) was achieved by hanging a 5-gallon Stansport Jumbo Camp Shower Bag to the fume hood above the machine. The bag came with a rotary lever valve which made the flow rate easy to adjust but difficult to create a reproducible flow rate across multiple welds. To standardize the flow rate, a lever stopper was 3D printed to limit the lever’s movement at the desired flow rate. This stopper is a small PLA cylinder that has a height reduction for a quarter of its circumference to allow for limited movement of the lever. Once the user found a desirable flow rate from the bag, they rotate the stopper to limit the travel of the lever to that flow rate. To make sure that the stopper would not move after being set, a slit was cut into the stopper to attach a modified hose clamp that would lock-in the stopper which then allowed for a

reproducible flow rate. To allow the water to dispense closer to the weld, a modified vortex tube holder was made which secured the dispensing tube with a Velcro strap. Additionally, a custom spring made from soldering wire was wrapped around the tube which was then inserted into the holder for rigidity. This setup can be seen below in Figure 6 and a close up of the valve stopped can be seen in Figure 7. For the welds, the shower bag was filled up with approximately 2.5 gallons of tap water and ice to reduce the water temperature. The measured temperature during the welds was 24.55 ºC. Both measurements were made using the same thermocouple previously mentioned. The flow rate for these welds was determined manually by measuring the volume dispensed into a graduated cylinder over 10 seconds. This process was repeated five times to yield an average flow rate of 17.68 $\frac{mL}{s}$. The measured data recorded to yield this flow rate can be seen below in Table 3. The orientation of the water nozzle was pointed at the weld and aligned ~2.25" behind the FSW tool along the weld direction. The application of the water was terminated once the FSW tool pulled out of the aluminum.

Table 3 - The volume measurements used to determine the average flow rate of the Stansport shower bag

Water Cooling Flow Rate Measurements		
Measurement Interval (s)	**Measured Volume (mL)**	**Flow Rate (mL/s)**
10	180	18.00
10	192	19.20
10	170	17.00
10	172	17.20
10	170	17.00
	Averaged Flow Rate	17.68

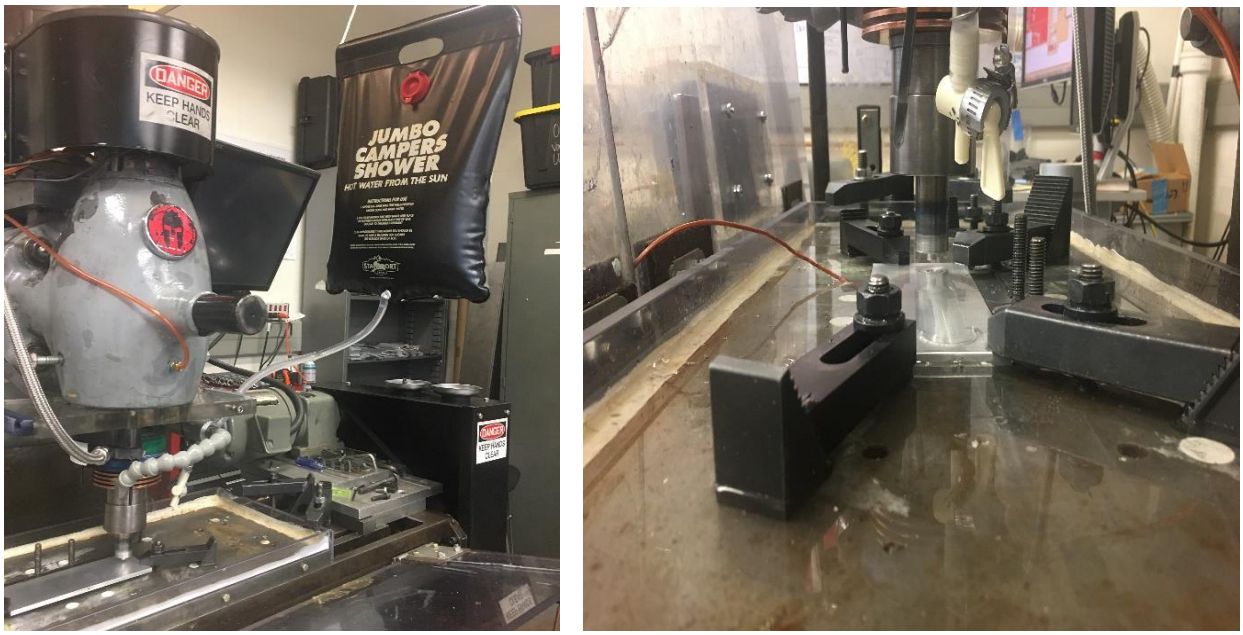

Figure 6 – (Left) The Jumbo Campers Shower Bag for WC welding mounted to the exhaust hood. (Right) Post WC weld which shows standing water around the weld, the valve, and the 3D printed valve stopper.

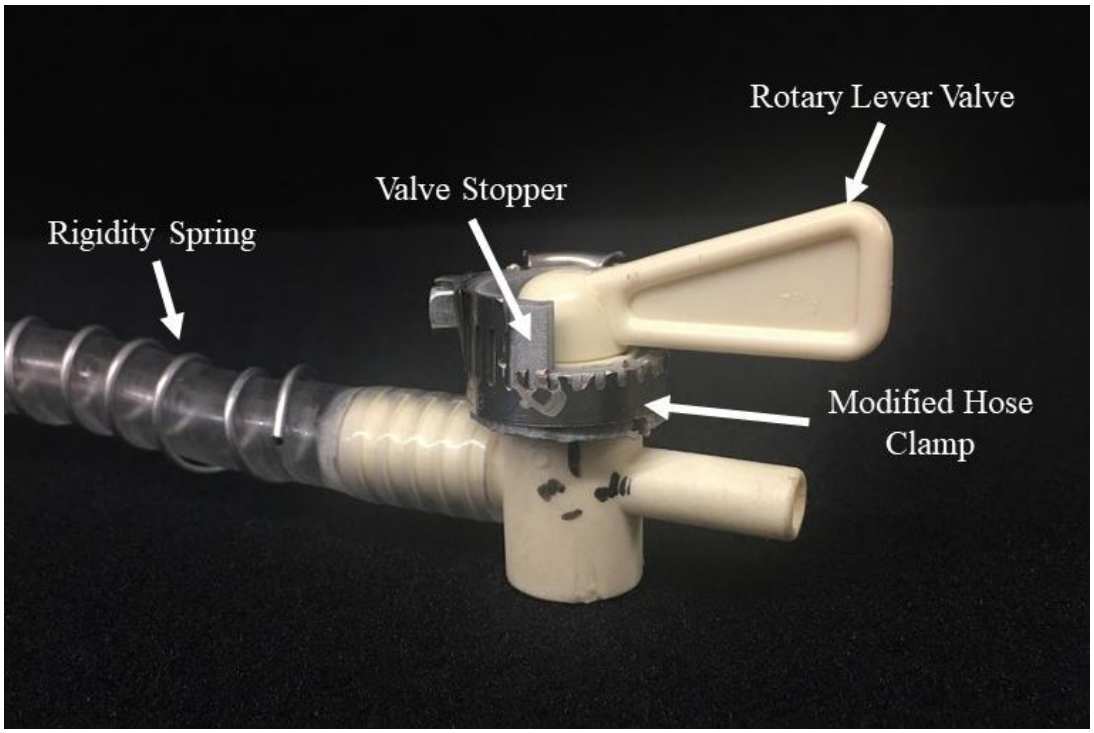

Figure 7 – Close up of the Shower Bag valve, custom fit with a modified hose clamp, valve stopper, and rigidity spring

Dry Ice Cooling

The dry ice (DI) was manually applied using a plastic tablespoon. The DI used in this process was purchased in five-pound slabs and was then granulated by pounding the slab with a sledgehammer. Granulation increases the cooling capacity of the DI by minimizing the heat transfer resistance due to the Leiden frost effect. This effect appears when a liquid or mass comes into contact with a surface that has a temperature that is significantly hotter than the boiling or sublimation temperature of that medium. As a result of vaporizing or sublimating upon contact, gas suspends the droplet or granule and thus minimizes the surface contact and in turn greatly slows down the heat transfer between the liquid or solid and the surface [29]. Although the granulated DI should combat this effect, the cooling source still piled up on the weld (see Figure 8) indicating that the Leiden frost effect was not eliminated. The measured temperature of the granulated DI using the thermocouple was -80.57 ºC. The application of the DI began once the FSW tool began to traverse in the aluminum. Each scoop of DI was applied immediately behind the traversing FSW tool thus allowing the cooling source to build up on the surface of the aluminum. Since the welds were run at two different traverse rates, there were two different volumes of DI applied to the welds. For the 3IPM welds, ~474 g of DI was applied. Alternatively, the 2IPM welds used ~711 g during the welding process. When considering the weld length and amount of applied DI, the approximate application rate of the DI on the welds was 3.7 $\frac{g}{s}$. The manual application of the DI terminated when the FSW tool pulled out of the aluminum.

Figure 8 – (Left) The DI weld with the FSW tool traversing towards the camera. (Right) The trailing end of the DI weld which shows DI piled onto the weld using a tablespoon measurer.

Liquid Nitrogen Cooling

The application of liquid nitrogen (LN) for IPC was also performed manually. This process included pouring LN from the storage dewar into a two-liter polypropylene beaker housed in a Styrofoam container for safety precautions. The LN was then poured into a funnel mounted to the welder. The mounting of the funnel was achieved using a laser cut medium density fiberboard (MDF) box mounted to an acrylic plate on the head of the welder. The funnel was chosen to concentrate the pouring of the LN on the weld line. While this method was not perfectly precise in applying the LN behind the traversing FSW tool, it was more effective than direct pouring because it provided a consistent disposal location on the weld line. The funnel, containment box, and application of LN can be seen below in Figure 9. The flow rate of LN was determined by measuring the consumed LN and then dividing the volume by the duration of the weld. When dispensing the LN during the welds, the funnel was oriented along the weld so that the LN would dispense ~2” behind the FSW tool. Unlike the other forms of cooling, the manual

dispensing of this cooling source did not begin until the nozzle of the funnel was above the aluminum and concluded when the FSW tool pulled out of the aluminum.

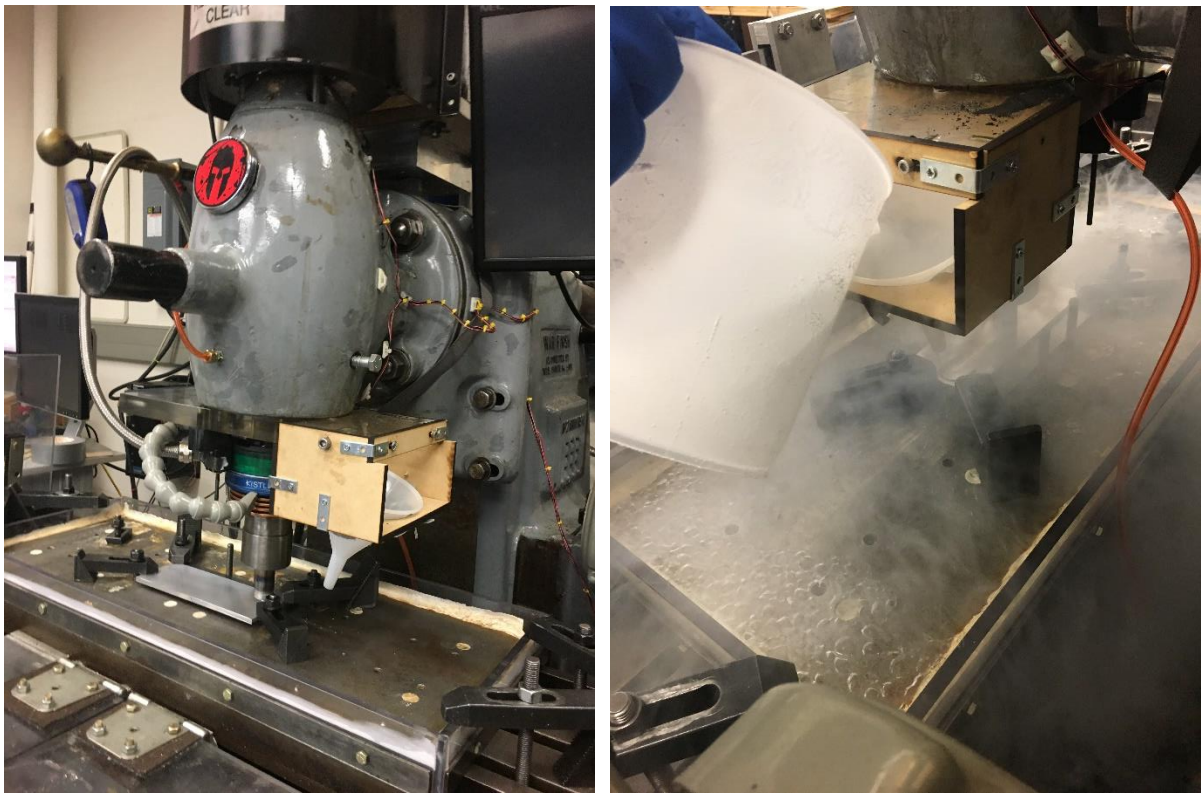

Figure 9 – (Left) The setup for the LN welds which shows the MDF holder and funnel mounted to an acrylic plate above the spindle. (Right) LN in-process cooling, dispensed using a plastic beaker.

Chapter IV

Testing Methodology

Sample Preparation

Upon completion of all the in-process cooling (IPC) welds, the next step in conducting this research was to cut up the welds into samples for testing. To obtain more accurate testing results, five samples were taken from each weld, resulting in 100 samples for testing. These samples were cut using a horizontal band saw. Due to the lack of precision of a bandsaw, the thickness of these samples varied up to ~0.05” from the intended thickness of 0.3”. The first sample from each weld was cut ~2.375” from the edge of the initial plunge to avoid any initial weld behavior and to allow ample time for the IPC to impact the weld. Additionally, sample locations were carefully chosen so that the thermocouple hole would not interfere with sample hardness testing. A model showing the approximate location and size of the five samples cut from each weld can be seen below in Figure 10.

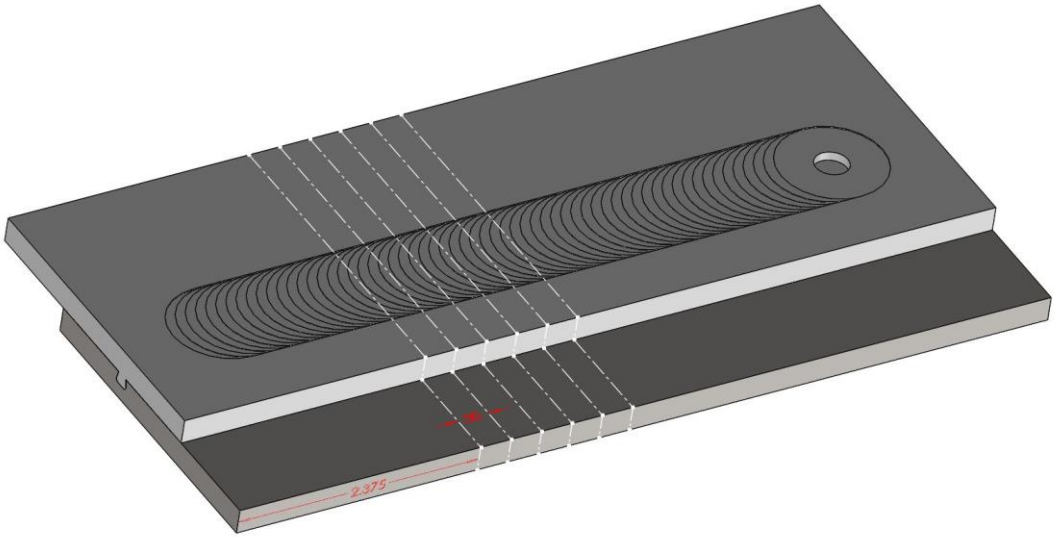

Figure 10 – Model of an extrusion weld that demonstrates the location of the five samples taken for the IPC testing.

The variable thickness across the samples did not matter for the hardness testing since the hardness testing results are consistent above a minimum thickness. For this portion of testing, all the samples were used. To prepare the samples for hardness testing, each sample was sanded to a uniform finish with 600 grit sandpaper to ensure that the testing surface was flat for increased testing accuracy. Some of the samples needed to be sanded on both sides due to uneven cutting finishes from the horizontal bandsaw. After completion of the hardness testing, the first four samples from each weld were taken for tensile shear testing.

Force and Temperature Data

All temperature data for the cooling sources and IPC weld temperature profiles was recorded using an Omega type K thermocouple. Before use, the thermocouple was calibrated by checking the temperature of boiling water. This thermocouple was attached to a TC-08 PicoLog data acquisition (DAQ) board which fed into a computer program to output temperature data into an excel file. For the temperature measurement of the cooling sources, the thermocouple was submerged in the fluid until the temperature reading reached steady state. To obtain the temperature profiles of the IPC welds, a hole was drilled into the side of the aluminum plate facing outwards from the welder. The DAQ board was then mounted to the protective acrylic shield of the machine in an acrylic box and the thermocouple was inserted into the hole until it was ~0.25” outside of the weld path. Since the thermocouple was not directly under the friction stir welding (FSW) tool, the temperature measured will be lower than the true weld temperature but allows for comparison between the different IPC welds.

Hardness Testing

After cutting and sanding the welds, hardness testing was conducted using a Rockwell hardness tester. The Rockwell harness testing method produces dimensionless reference values which can be used to determine physical characteristics of metals such as tensile strength, wear resistance, and ductility. Upon putting the sample onto the platform of the machine, a total test force (which is measured in kgf) is selected depending on the type of indenter as well as the material being tested. The combination of indenter type and total test force produces different dimensionless hardness values which are denoted by scale symbols such as HRF (Rockwell F-

Scale Hardness) or HRB (Rockwell B-Scale Hardness). Upon selecting the appropriate hardness scale, the sample is then raised to the stationary indenter. After initial contact with the indenter, the sample is then slowly risen by the user allowing the indenter to deform the material until it reaches a preliminary test force load. Once this test force load is met, the machine dwells while measuring a baseline depth of indentation. Then the force of the indenter increases at a steady rate until the user-specified total test force is achieved where it will then dwell for a specified amount of time. The indenter will then revert to its preliminary test force load to measure the new depth of indentation after the application of the total test force. This difference in heights between the baseline depth and the final depth of indentation is then used to calculate a hardness value in the specified scale symbol. The equation used to calculate the resultant hardness value from the indentation when using a ball indenter can be seen below in equation 4 where *h* is the difference of the baseline and final indentation depths measured in mm [29]:

$$Rockwell\ Hardness = 130 - \frac{h}{0.002} \tag{4}$$

The HRF scale was used which requires a $\frac{1}{16}$" ball indenter and a total test force (major load) of 60 kgf with a preliminary test load (minor load) of 10 kgf. Previous VUWAL work has shown this scale to be the most insightful for friction stir extrusion (FSE) samples. To test the effectiveness of the various cooling methods, a matrix was originally designed to test hardness values across the sample's horizontal and vertical cross-section. The various horizontal hardness values provide insight into the impact of the cooling on the modified granular structures within varying zones and the vertical hardness values provide insight into the penetrative effects of the IPC. To ensure accurate hardness values, the ASTM E-18 standard for Rockwell hardness testing was followed. This standard indicates that the indent must be $2.5*d_{indenter}$ away from the edge of the material and the indents must have a spacing of $3*d_{indenter}$ [30]. Since the aluminum used in the weld only had a thickness of 0.25" and the indenter had a diameter of $\frac{1}{16}$", only one row of hardness values could be obtained from the center of the aluminum cross-section. Adhering to the spacing requirements, this row contained 15 hardness values per sample. Additionally, the hardness value of each extrusion was tested, but the validity of this number is questionable since there was not enough material to maintain the spacing standard. Ideally, this research would have

had access to a Vicker's hardness tester which has the capability of testing a matrix of points along a cross-section given a specified distance between the points. This capability would have allowed for more precise measurements across all the samples. Since this research only had access to the Rockwell hardness tester where indentation of each location is done manually, a testing jig was created to increase the precision of the hardness measurements throughout the samples. This jig was a laser cut MDF circle with protruding fins. The jig contained a slot large enough for the extrusion cross-section and had lines spaced out by $\frac{3}{16}$" except for the first line from the center which has a spacing of $\frac{5}{32}$". The circle in the jig had the same diameter as the hardness tester platform to allow for positional accuracy. While the placement of the jig was not perfect every time, it was far more reliable than visual alignment. The process of testing with this jig was as follows: insert the extrusion cross-section in the slot, slide the edge of the sample to the first line past the center, ensure the circle and platform were aligned, then obtain a hardness value for that location. For the following hardness values the sample was moved to the next line to ensure that there would be ample distance between the indentations. A sample mounted on the Rockwell hardness tester in the testing jig can be seen below in Figure 11.

Figure 11 – A sample on the Rockwell hardness tester with MDF testing jig

Tensile Shear Testing

The tensile shear peak stress values of the samples were obtained by using a Instru-Met Instron tensile tester. To ensure that the samples fit into the jaws of the tensile tester, all of the samples were milled down to ~0.25" since the samples originally ranged in thickness from the rough sample cutting of the horizontal band saw. After preparation of the samples, they were loaded into the jaws of the tensile tester with the welded aluminum oriented outwards so that the jaws would be pulling along a singular axis. The other orientation of testing the samples, which would have the cross-section facing the user, would result in multi-axial pulling and induce an unnecessary moment on the sample due to the jaw offset from the sample height. The aluminum plate and steel plate were loaded into the top and bottom jaws, respectively which can be seen below in Figure 12. The test run on the samples was a prebuilt tensile test that extended 2 $\frac{mm}{min}$. All of the data from these tests was collected using TestWorks where the output peak load was then converted to a peak shear stress per sample by dividing the load by the area of the dovetail

(width of the dovetail channel, 0.125”, multiplied by the measured thickness of the material). While stress measurement is labeled as a “peak shear” measurement, the failure in the tensile tester is not purely due to shear stress as the edge of the dovetail acts as a stress concentrator that can cause crack formation and propagation. This conversion can be seen in equation 5 below where τ is the shear stress, F is the Instron output load, w is the dovetail groove width, and t is the measured thickness of the sample.

$$\tau_{Peak} = \frac{F_{Peak}}{A} = \frac{F_{Peak}}{w * t_{sample}} = \frac{F_{Peak}}{.125" * t_{sample}} \quad (5)$$

Figure 12 – A sample on the Instron tensile tester

Chapter V

Results and Analysis

Force Data

Figures 13 and 14 below show the plunging force data of all the welds in this research. Figure 13 groups this data between cooling sources while Figure 14 groups this data via welding pitches. The ungrouped force plots can all be seen in greater detail in Figures A6-A14 in the appendix.

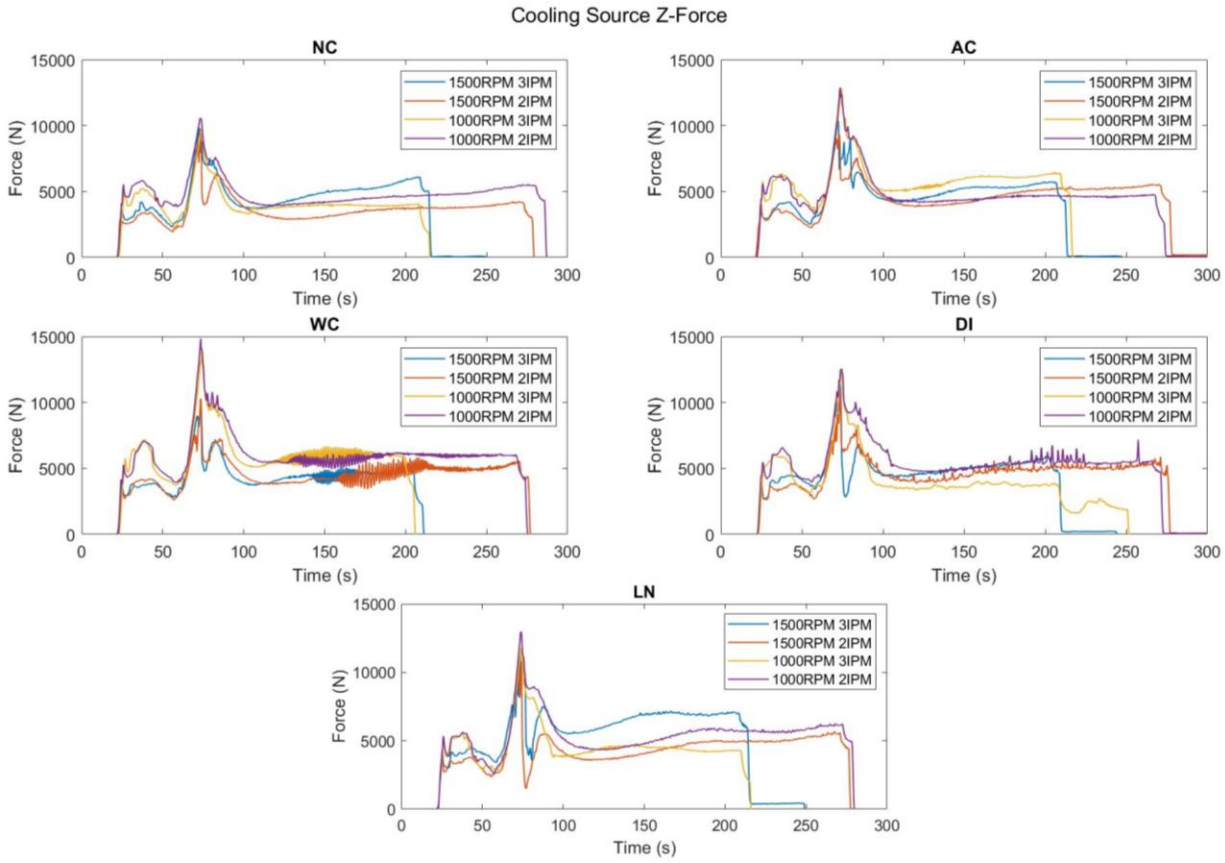

Figure 13 – Cooling source z-force plots of IPC friction stir welds. Each cooling source plot shows the forces for the four weld parameters.

The trends seen in the plunge force plots are governed by the tool geometry. Force data does not appear on the plot for ~25 seconds due to a lag between starting data collection and when the friction stir welding (FSW) tool begins to plunge into the material. The weld program then prompts the welder anvil to raise to the FSW tool. The first spike in these plots is from the pin of the tool plunging into the aluminum which is then followed by the maximum force spike which comes from the shoulder of the tool making contact with the aluminum. When approaching steady state at ~5000 N, there is a slight level off at ~5 seconds after the maximum spike. This behavior is a result of the tool beginning to traverse in the material and having to push through material that bulged from the plunge. The most apparent trend in welding forces is the shorter timespan for the 3IPM welds versus the 2IPM welds. This difference is a result of the workpiece being the same length for every weld but having a different traverse rate which causes the weld to end sooner for the 3IPM welds. Dissecting these plots, the non-cooled (NC) welds generally experience the smallest peak force and tend to have the smallest variability across welding pitches, while the water cooled (WC) welds have the highest peak force during both 1000RPM welds and have the largest variability of forces between different welding pitches. The biggest discrepancy seen in these plots is in the liquid nitrogen (LN) plot between the 1500RPM-3IPM weld and the 1000RPM-3IPM weld. The latter has a steady state plunge force at ~4600 N while the former has a steady state plunge force at ~6000 N. Table 4, below, provides more insight into the average steady state processing forces of each weld measured in N and shows that the WC welds tend to require higher processing forces across most parameters while the NC welds have lower processing forces across all parameters.

Table 4 – Averaged steady state processing forces with the varying cooling sources and weld parameters

	Averaged Steady State Processing Forces (N)			
Cooling Sources	**1500RPM 3IPM**	**1500RPM 2IPM**	**1000RPM 3IPM**	**1000RPM 2IPM**
NC	4714	3686	4181	4909
AC	4940	4715	5940	5062
WC	4444	4646	6100	6244
DI	4952	4810	3910	5780
LN	6041	4438	4681	5527

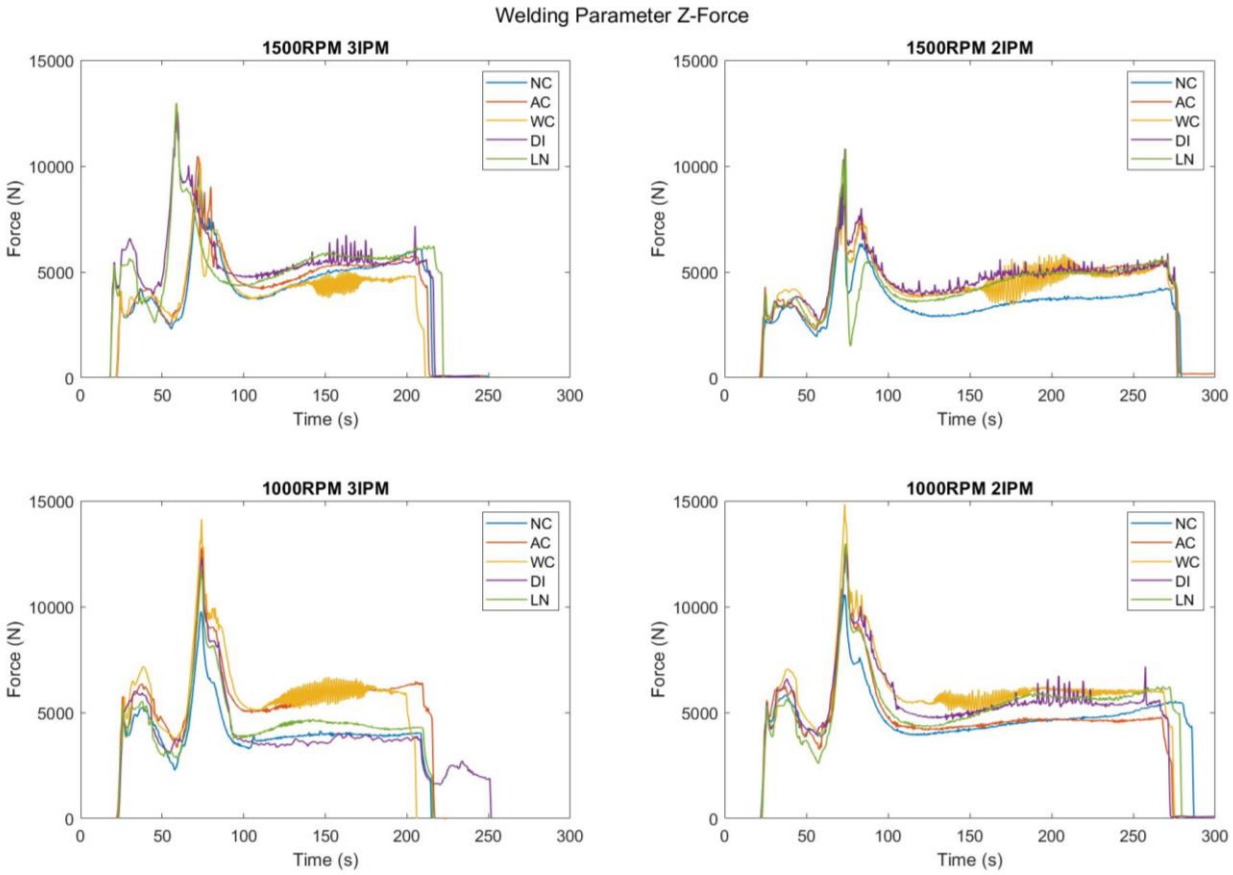

Figure 14 – Welding parameter z-force plots of IPC friction stir welds. Each welding parameter plot shows the forces for the cooling source variations.

The largest force spikes are seen in the WC-1000RPM welds. A general trend among the welding parameter plunge force plots, except for the 1500RPM-3IPM, is that the WC welds tend to produce the highest plunge force while the NC welds tend to produce the lowest plunge force. The reason for these trends is likely because the NC welds allow for more heat propagation throughout the workpiece during the welding process which then reduces the material resistance and thus the plunge force required to weld. On the other hand, the WC welds are effectively extracting heat from the weld, resulting in greater material resistance from a reduced welding temperature. This difference is most apparent in the 1500RPM-2IPM welds where all the IPC welds are at a steady state of ~5000 N while the NC weld is at ~4000 N. These welds are the only set that have a definitive plunge force difference between cooled and non-cooled welds. These plots reveal that as the weld pitch (WP) increases so does the steady state plunge force across all cooling media. Additionally, these plots provide insight into the effectiveness of IPC as

the higher steady state weld forces are likely due to effective heat removal from the weld process in comparison to the NC welds.

Temperature Data

Like the collection of plunge force data, the temperature data collection also began when the user clicked “Start weld.” Figures 15 and 16 below show the temperature data of all the welds in this research. Figure 15 groups this data between cooling sources while Figure 15 groups this data via welding pitches. The ungrouped force plots can all be seen in greater detail in Figures A15-A23 in the appendix.

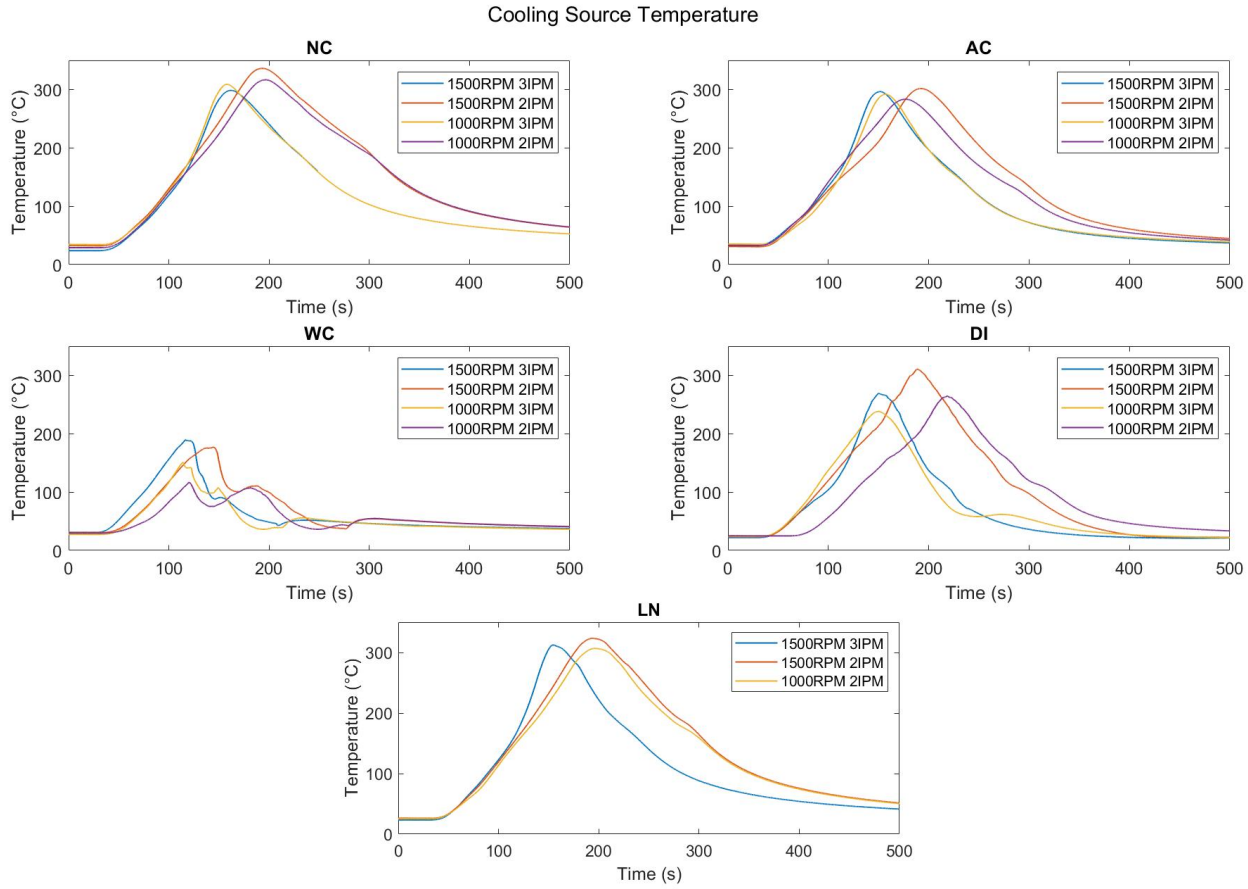

Figure 15 – Cooling source temperature plots of IPC friction stir welds. Each plot shows the temperature profiles for the four weld parameters.

The temperature plots shown in Figure 15 show the general trend of a decreasing peak measured temperature of the weld with the introduction of IPC. While it appears that the WC welds experience the lowest welding temperature, this data is not accurate due to the collection of water in the containment table. As the WC welds ran, water filled up the containment table and eventually filled up the thermocouple hole at ~100 seconds. As a result, the temperature readings immediately began to drop as they were recording water temperature readings instead of the aluminum temperature. In addition to the issues with the data collection with the WC welds, the temperature recording for the NC-1500RPM-3IPM weld was cut short by ~300 seconds and the temperature recording for the LN-1000RPM-3IPM weld is nonexistent due to user error. The plots seen in Figure 15 show that as the weld pitch increases so does the maximum temperature of the weld as expected because there is an increase in heat generation as the weld pitch (WP) increases. The NC-1500RPM-3IPM line is also an outlier because the temperature line goes against the correlation of WP and maximum temperature observed in other plots because it is below the 1000RPM-3IPM temperature line. The reason for this discrepancy is likely due to an error with the thermocouple or the PicoLog DAQ board.

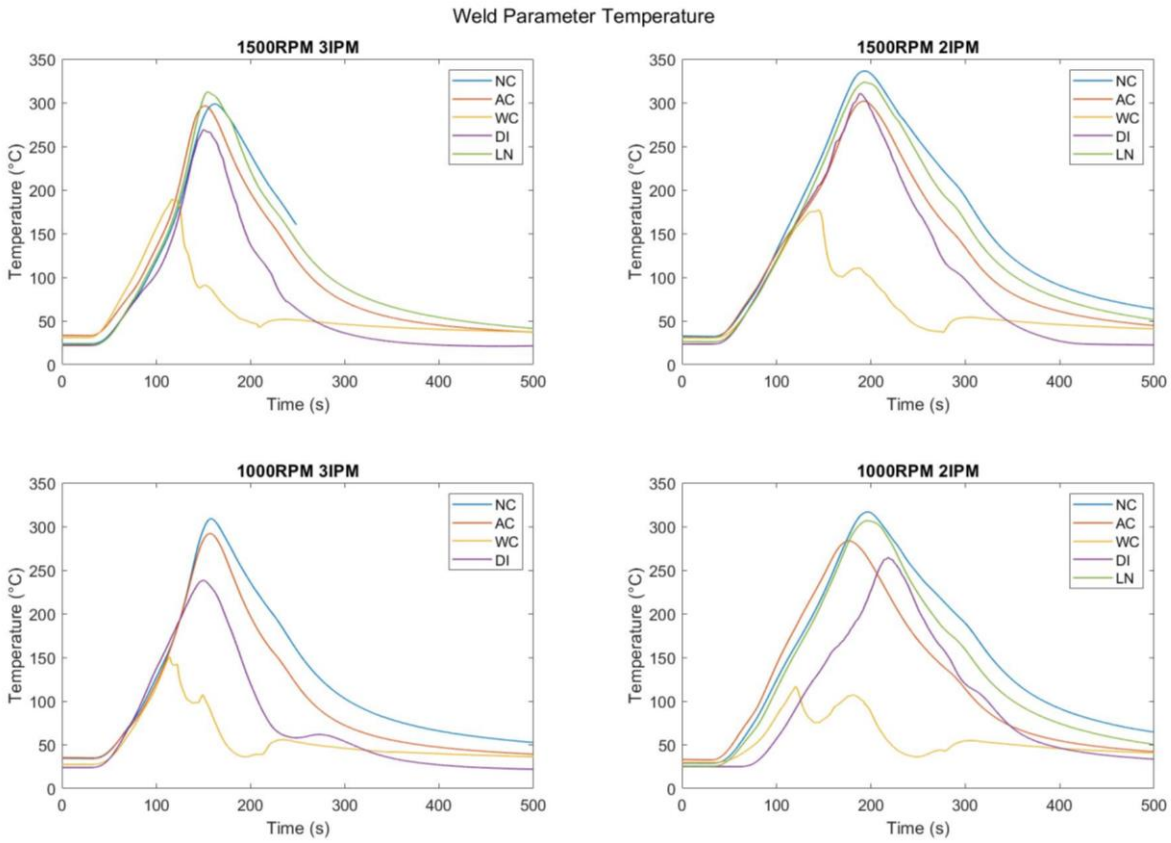

Figure 16 – Welding parameter temperature plots of IPC friction stir welds. Each plot shows the temperature profiles for the five IPC welds.

The WP temperature plots seen above illustrate the differences in cooling source peak temperature across variable WP. The common trend seen among these plots is that temperatures peak in the NC welds and are at their lowest values during the WC welds. As mentioned above, the WC data is likely invalidated due to its submersion in the water after ~100s. The maximum measured weld temperature from hottest to coldest among the cooling sources is NC, LN, AC, DI, and WC. Like the observations in Figure 15, the 1500RPM-3IPM plot also does not follow the observed trend as the NC weld records a peak temperature lower than the LN weld.

Hardness Data

Figures 17 and 18 below show the cross-sectional hardness data of all the welds included in this research. All the points shown in these plots are averages among five samples for each cooling source and weld pitch (WP). Figure 17 groups this data by cooling sources while Figure

18 groups this data via WP. The ungrouped cross-section plots can all be seen in greater detail in Figures A24-A32 in the appendix. The measured hardness value of an unwelded aluminum alloy AA6061 cross-section was ~86.5 HRF which can be seen in Table A6. Additionally, all the raw data obtained from the Rockwell hardness tester and the hardness value of the extrusions can be seen in Tables A1-A5.

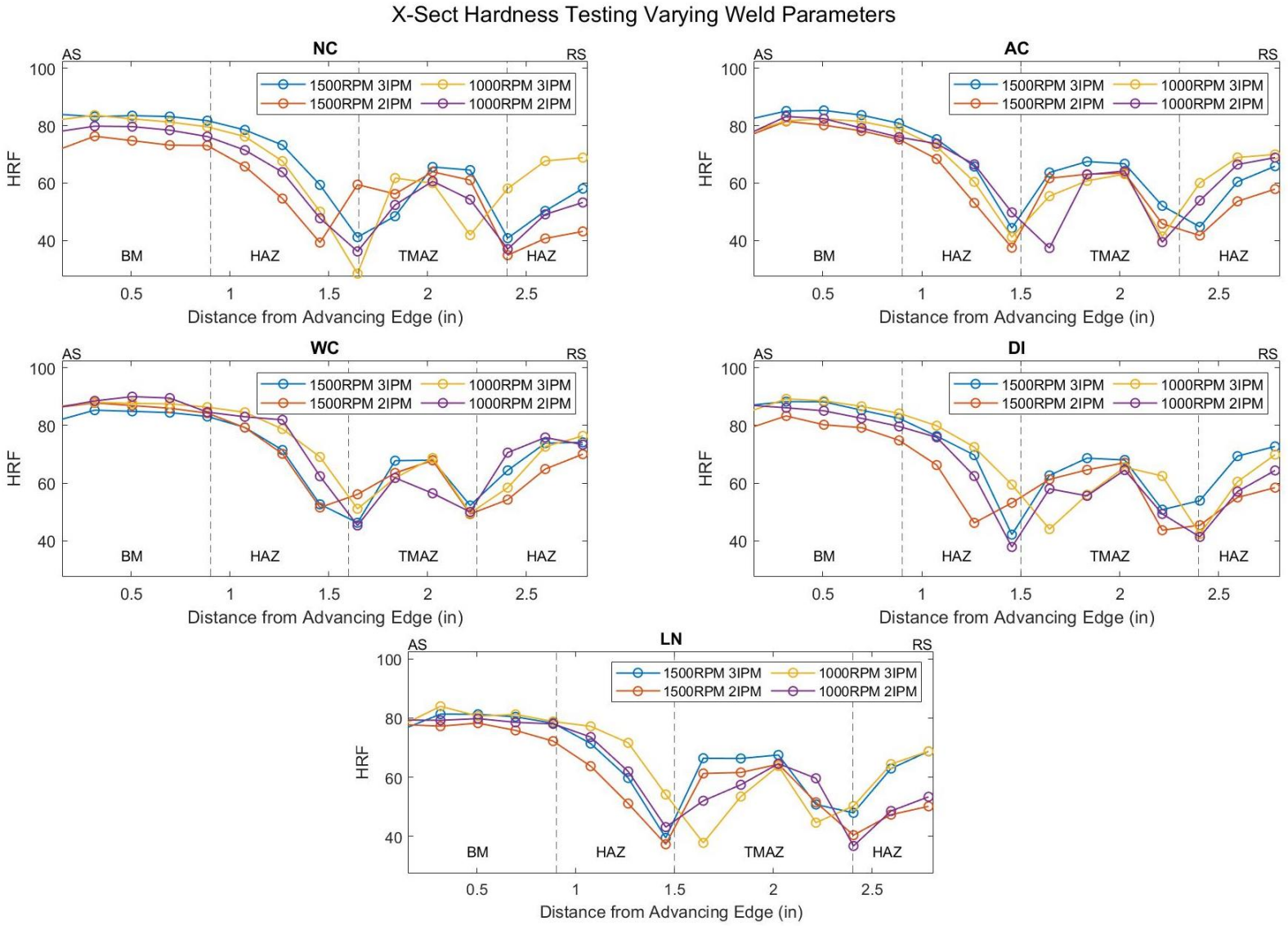

Figure 17 – Cooling source cross-sectional hardness plots of IPC friction stir welds. Each plot shows the hardness profiles measured in HRF for the four weld parameters.

The different microstructural zones become apparent when looking at the cross-section hardness plots. Going from left to right on the plot, the hardness values begin in the base material (BM) where they maintain relatively steady values. Moving to the right, the hardness values begin to dip upon entering the heat affected zone (HAZ) until a local minimum hardness value at the ninth indentation, ~1.5" from the advancing side. At this point, the hardness increases through the thermo-mechanically affected zone (TMAZ) and then decreases to another local minimum when crossing back into the HAZ. There is then a slight hardness increase from this local minimum to the retreating edge of the weld. This distinction of the TMAZ can also be observed optically when looking at the hardness samples as there is a trapezoidal region that starts at the edges of the weld line and encompasses the center of the weld line and the extrusion. This region is observable due to a lighter gray color compared to the surrounding HAZ and BM. The lighter color is a result of the grain refinement and layering from the friction stir welding (FSW) tool in the TMAZ which became visible after polishing the samples. In addition to cleaning the surface finish and preparing for testing, the process of polishing also makes inclusions and other second-phase particles visible in the aluminum which may also play a role in this macroscale observation [31]. The plots in Figure 16 reveal that increasing heat generation due to the increase in WP decreases the performance of the weld cross-sections during hardness testing. This trend can be observed in the NC, AC, DI, and LN plots where 1500RPM-3IPM and 1000RPM-3IPM welds consistently outperform the 1500RPM-2IPM. The reasoning for this observable trend is that as more heat is generated in the welds, the microstructural grains of the aluminum grow which then causes the hardness to decrease as the lattice becomes less compact and less resistant to deformation. The effects of the cooling can be seen in tightening of the variability between the WP for the IPC welds in comparison to the NC weld. The best example of the effects of IPC can be seen in the WC plot. The trend discussed above is no longer visible as the best and worst performing WP for hardness testing change throughout the cross-section. The blurring is due to the WC effectively dissipating generated heat from the variable weld pitches, thus resulting in similar hardness profiles as the aluminum microstructure experiences similar grain growth during the welding process.

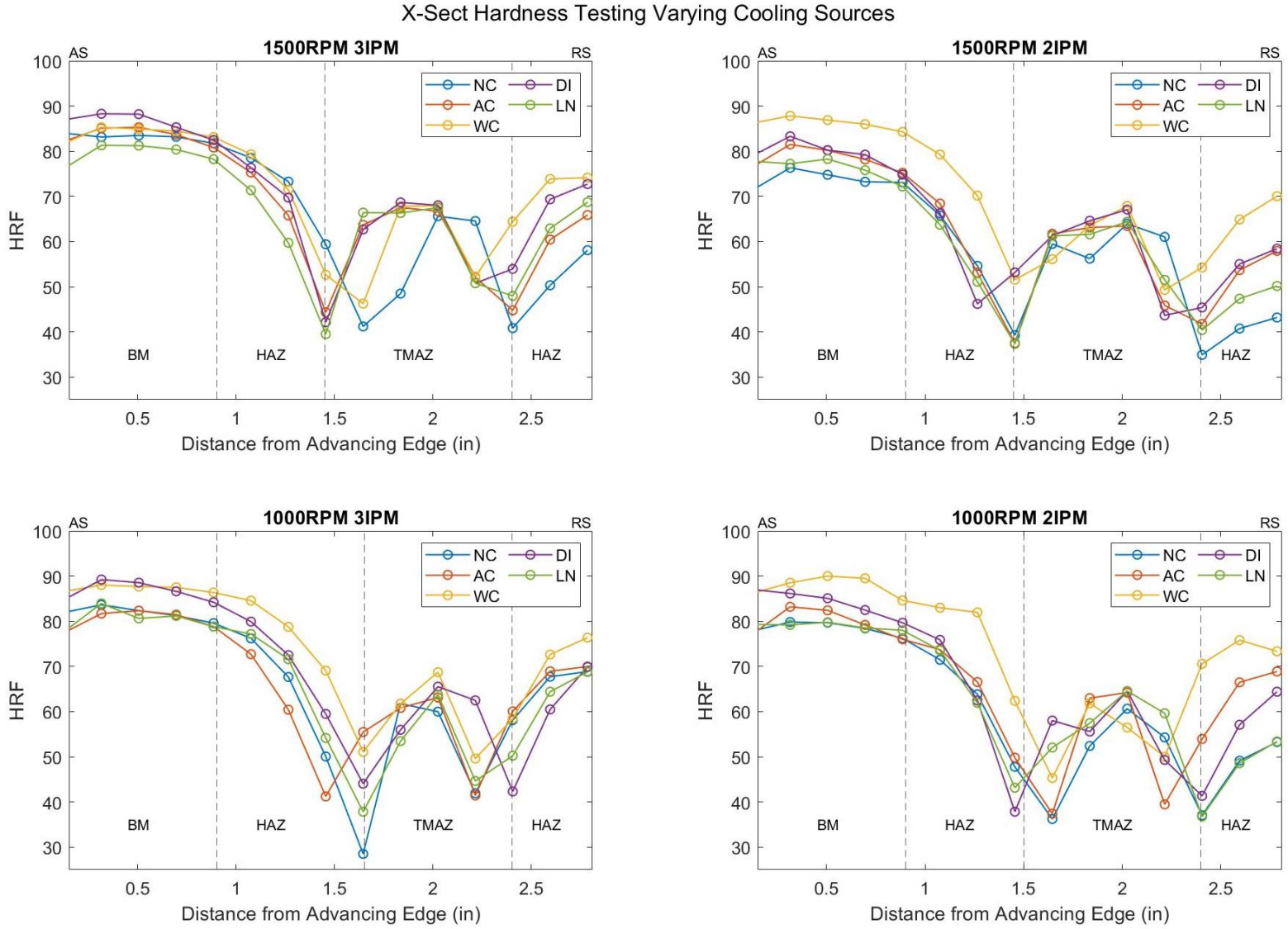

Figure 18 – Welding parameter cross-sectional hardness plots of IPC friction stir welds. Each plot shows the hardness profiles measured in HRF for the five cooling sources.

The hardness profiles seen in Figure 18 provide insight into the performance of the various cooling sources and the NC welds. After analyzing these plots, a few trends become apparent. The first of which being that the WC welds are among the top performing welds in the 1500RPM-3IPM hardness testing and are the best performing among the remaining WP. Additionally, the NC and LN welds tend to be among the worst performing across all the weld pitches. The most interesting trend observed among these plots is the changing variability between WP, specifically looking at the largest WP plot of 1500RPM-2IPM in comparison to the other weld pitches. For this plot, the WC samples perform much better than NC and other IPC samples in the BM and HAZ. This observation is again due to the robustness of IPC from WC amongst varying weld pitches. While the other cooling sources become less effective with an increasing WP, the WC maintains steady performance across the three weld pitches used in the hardness testing for this research. When comparing these IPC hardness values to the unwelded aluminum alloy AA6061 hardness values, the BM hardness measurements of the WC and DI welds showed an improvement in hardness values. Only the values in the BM can be compared to the unwelded sample since the unwelded sample does not have a HAZ or TMAZ. Comparing these values, the WC welds performed better than the unwelded sample in the 1500RPM-2IPM, 1000RPM-3IPM, and 1000RPM-2IPM welds with a maximum hardness (90 HRF) increase of ~4.05% in comparison to the unwelded material. While the DI welds performed better than the unwelded sample in the 1500RPM-3IPM, 1000RPM-3IPM, and 1000RPM-2IPM welds with a maximum hardness (89.2 HRF) increase of ~3.12% in comparison to the unwelded material.

As mentioned above, this improvement in performance in the WC samples is primarily seen in the BM and HAZ zones while the TMAZ shows more uniform performance between the IPC sources which still outperform the NC samples. There are some outliers in these trends mostly in the TMAZ which is due to the presence of a small void in the center of some samples because of the tool being aligned slightly too far away from the groove during the welding process. These points affected by the void can be seen in the hardness data in the appendix and are highlighted red because they are negative or extremely small values. The explanation for the output of these negative values is that there is not sufficient testing area for consistent hardness readings due to the presence of the void [32]. In addition to appearing in the TMAZ, these negative values also appear in most of the extrusion hardness values because of not having enough hardness testing area.

Another source of error for this testing comes from the hardness testing location. While the testing jig used during the hardness testing helped to ensure that the indent locations would be more accurate across all the tested samples, there was still variability about the indent locations. This variability can be seen below in Figure 19 which shows the intended location of the indent versus the average indent location for each cooling group. The indent location of each sample within the cooling groups can be seen in Figures A33-A37 in the appendix. To visualize the shift in hardness testing locations due to the manual operation of the Rockwell hardness tester, Figure 20 shows the NC-1500RPM-3IPM sample overlaid with a CAD model indentation layer.

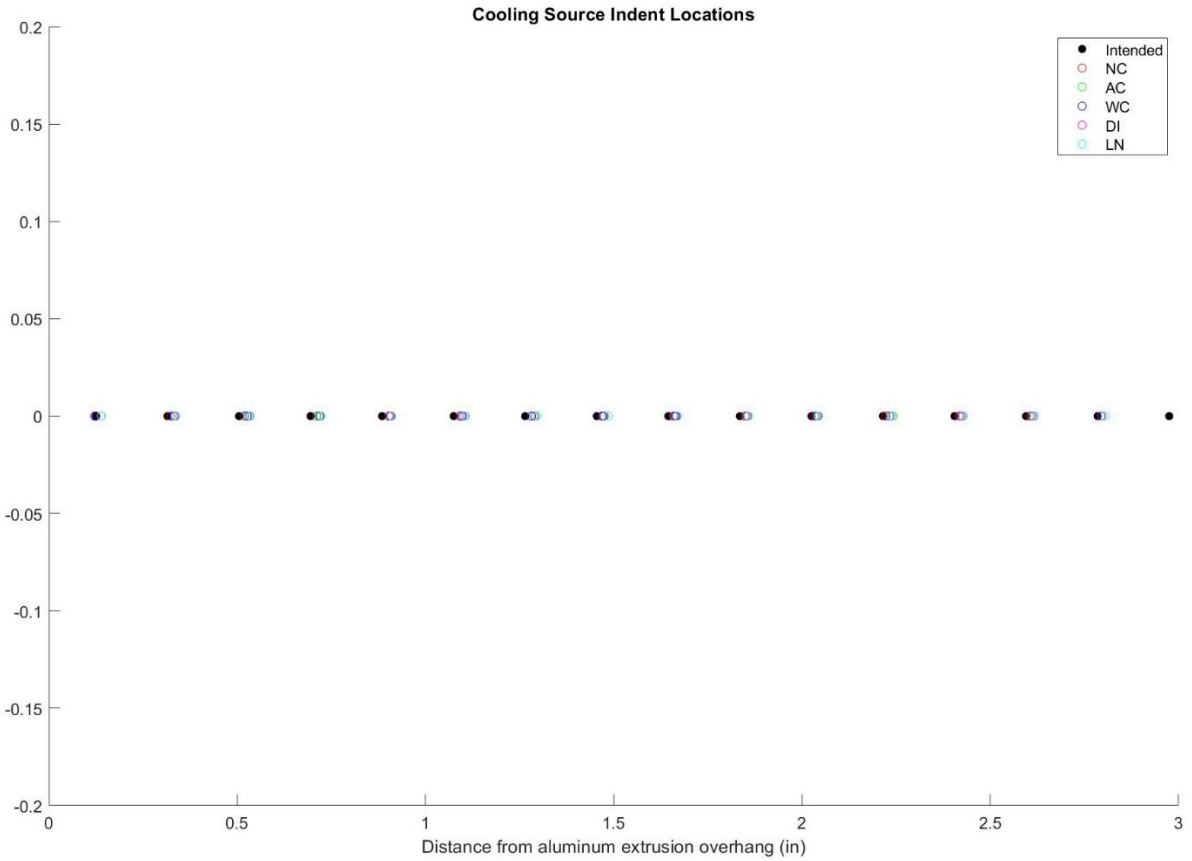

Figure 19 – The average indentation of each sample during hardness testing plotted against the intended indent location.

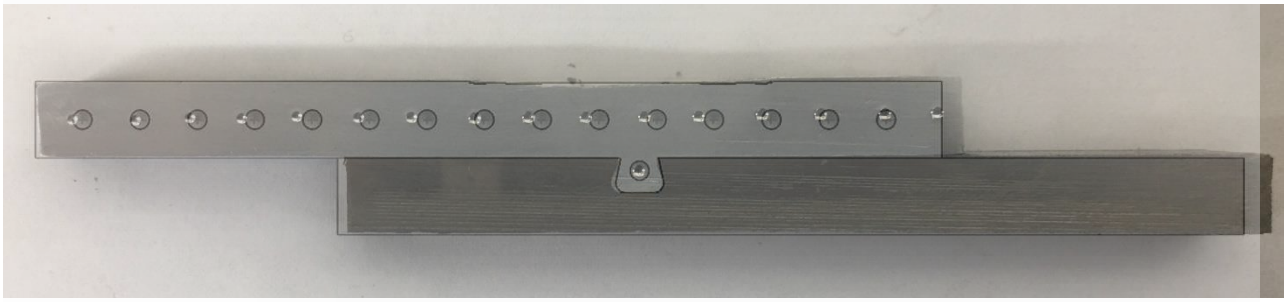

Figure 20 – CAD image of intended indentations during hardness testing on IPC sample overlaid on sample 4 from the NC-1500RPM-3IPM weld which shows the sample's actual indentation marks.

The circles in Figure 19 show the average location of each of the indent locations for all weld samples within an IPC group. This plot shows that there was variability between the hardness testing locations across the samples but the measurements furthest off from the intended location were ~0.048" to the left of the intended location. While this variability is not ideal, it is acceptable as each indentation had sufficient aluminum to provide consistent hardness value readings except for those affected by the voids in the TMAZ. The largest drawback of this variability is that the hardness boundary between the TMAZ and HAZ is not as clear with some of the hardness readings.

Shear Testing Data

The results from the tensile shear testing are shown below in Table 5. Each data point consists of averaged data points across four samples for each cooling source and weld pitch (WP). The "Averaged Welding Parameters" column of this table shows the averaged shear stress performance of all welding parameters within the specified cooling source while the "Averaged Cooling Sources" row shows the averaged shear stress performance among all cooling sources in a specified set of welding parameters. This was done to increase the data sample size to make the comparison between cooling sources statistically significant for visual representation in the box and whisker plot seen in Figure 21. The individual data for each sample can be seen below in Tables A7-A11 in the appendix.

Table 5 – Average shear stress of weld samples across varying welding parameters and cooling sources.

	Averaged Shear Stress of Weld Samples (MPa)				
Cooling Source	**1500RPM 3IPM**	**1500RPM 2IPM**	**1000RPM 3IPM**	**1000RPM 2IPM**	**Averaged Welding Parameters**
NC	126.9	122.1	114.7	115.1	119.7
AC	128.0	127.4	127.0	114.2	124.1
WC	129.5	131.6	123.8	115.4	125.1
DI	131.9	123.7	115.4	124.6	123.9
LN	130.1	121.2	114.6	121.4	121.8
Averaged Cooling Sources	129.3	125.2	119.1	118.1	

The averaged shear stress data in Table 5 shows that except for LN-1000RPM-3IPM samples, the in-process cooling (IPC) samples outperformed the NC samples during tensile shear testing. The best performing cooling source varies by WP. For a welding pitch of 333.3 RPI (1000RPM-3IPM), AC experienced the largest peak shear stress trailed by WC, DI, and LN in that respective order. For a WP of 500 RPI (1500RPM-3IPM and 1000RPM-2IPM), DI experienced the largest peak shear stress trailed by LN, WC, and AC in that respective order. For a WP of 750 RPI (1500RPM-2IPM), WC experienced the largest peak shear stress trailed by AC, DI, and LN in that respective order. Grouping all the cooling source shear stress results which is shown in the "Averaged Cooling Sources" line, the 1500RPM-3IPM welds have the strongest tensile shear strength performance followed by 1500RPM-2IPM, 1000RPM-3IPM, and 1000RPM-2IPM, respectively. The 1500RPM-3IPM welding parameters having the best performance is consistent with previous lab results and is the reason for this set of parameters being the legacy parameters used for friction stir extrusion (FSE) in VUWAL. Alternatively, grouping all the welding parameters to compare the overall performance of the cooling sources reveals that on average the WC process produces the strongest tensile shear welds across variable welding parameters which is then followed by AC, DI, LN, and NC. The use of IPC for welding produced a ~4.49% ultimate shear tensile strength (USTS) increase for WC welds, a ~3.71% USTS increase for AC welds, a ~3.53% USTS increase for DI welds, and a ~1.79% USTS increase for LN welds in comparison to NC welds. These results are visible in Figure 21 below which shows that the WC welds have the highest average shear tensile stress as well as the lowest deviation among the other cooling

sources. Additionally, Figure 22 shows the average peak shear stress of each parameter within each cooling source. This plot shows that the 1500RPM-3IPM parameter yields stronger shear stress FSW joints while the 1000RPM-3IPM and 1000RPM-2IPM parameters yield weaker shear stress FSW joints.

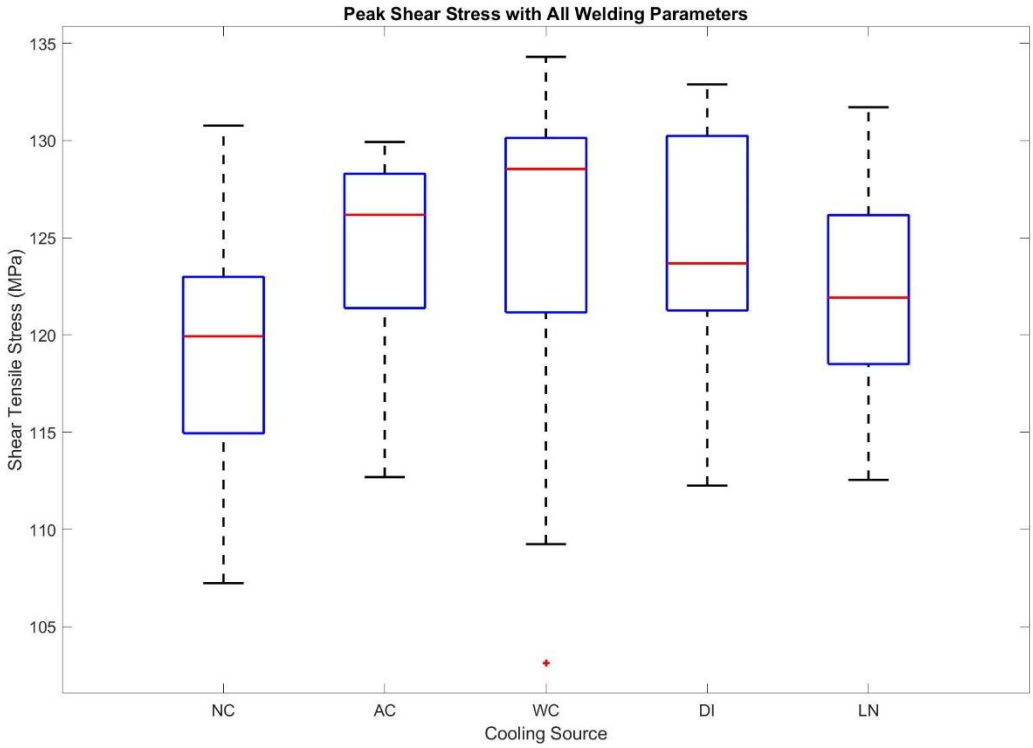

Figure 21 – Comparison of peak shear stress considering all welding parameters across the five cooling sources. Each cooling source has sixteen data points.

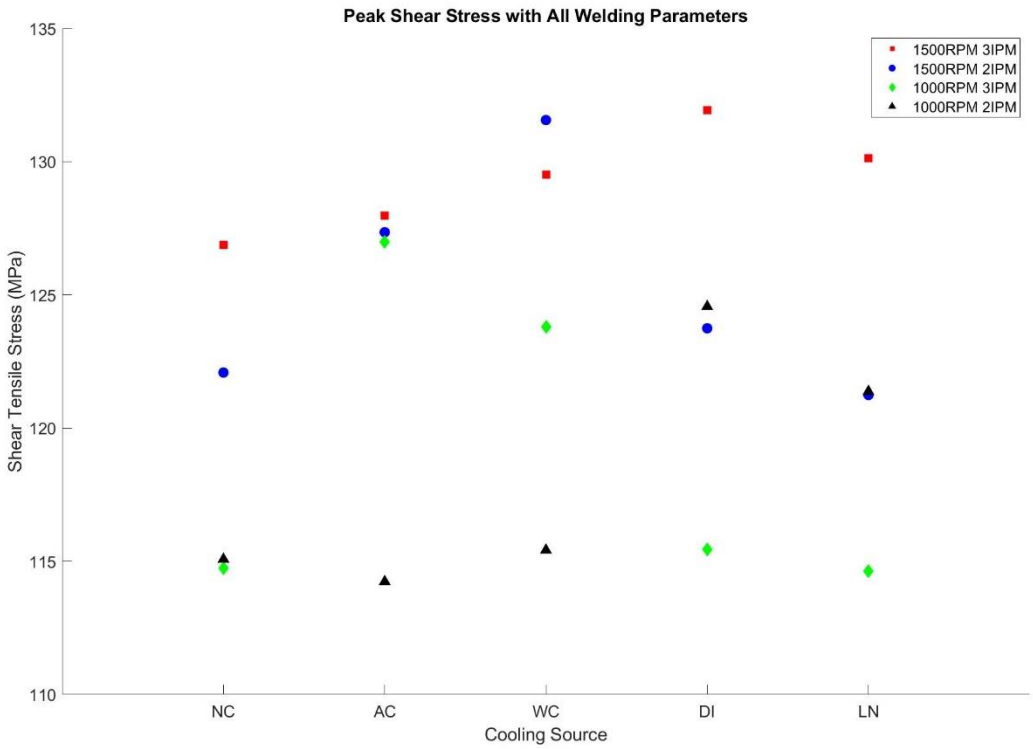

Figure 22 – Comparison of peak shear stress across welding varying welding parameters within each cooling source.

During the shear testing of the samples, there were different types and different locations of failure which was a result of a void in the cross-section of the extruded aluminum. As mentioned in the testing methodology section, the process of testing these extrusion samples produces a moment since the aluminum and steel are offset due to their stacked nature. Therefore, all samples experienced some degree of rotation which can be seen by looking at the extruded dovetail rotation. In addition to this rotation, some of the samples contained a void in the aluminum cross-section which prevented shear testing of the extruded dovetail. All samples affected by this mode of failure have a purple marking in their data cell in the appendix. Some of these void samples completed their tensile shear test upon pulling the extrusion completely out of the steel while others fractured at the void line. The four different sample failures can be seen below in Figure 23 where the top two samples show the two types of void failure while the bottom two show the varying degrees of dovetail aluminum extrusion rotation during tensile shear testing.

Figure 23 – Tensile shear testing samples. The samples included in this image illustrate the variability of failure during shear testing. From top to bottom the samples pictured are sample 4 from NC-1000RPM-3IPM, sample 2 from NC-1000RPM-3IPM, sample 4 from WC-1500RPM-2IPM, and sample 1 from AC-1000RPM-3IPM.

Chapter VI

Conclusions

This research introduced in-process cooling (IPC) to the friction stir extrusion (FSE) joining process to evaluate the effectiveness of joint performance via varying cooling sources including compressed air (AC), water (WC), granulated dry ice (DI), and liquid nitrogen (LN). There were also four pairs of weld parameters which yielded three different weld pitches (WP) to better understand the capabilities of the cooling sources with different heat generation in the welded material. Using hardness testing via a Rockwell hardness tester and tensile shear testing via an Instron tensile tester, the following conclusions about the use of IPC in the FSE process can be drawn:

- IPC produced stronger FSE joints than non-cooled FSE joints regardless of the cooling media implemented.
- For hardness testing, the WC welds and DI welds were the top performing as they increased the observed cross-sectional hardness of the aluminum at maximum values of 90 HRF and 89.2 HRF which is a 4.1% and 3.1% hardness performance increase compared to the uncooled welds, respectively.
- For tensile shear testing, the introduction of IPC increased the observed average joint strength of the FSE joints by 4.5% for WC welds, 3.7% for AC welds, 3.5% for DI welds, and 1.8% for LN welds. When considering the various WP used in this research, the strongest joints for the 750 RPI, 500 RPI, and 333.33 RPI were the WC weld, DI weld, and AC weld, respectively.

While the use of all the various cooling media improved the performance of FSE welds in hardness and tensile shear testing, the effectiveness of the AC, DI, and LN welds dwindled with the increase of the heat generation in the weld due to the increasing WP. The WC welds were the most capable of dissipating the additional heat input to limit the microstructural grain growth.

After considering the performance amongst the various cooling sources and WP in tensile shear strength, hardness testing, and WP heat mitigation, the use of WC in the FSE process is the most consistent in joint strength and hardness improvement. Additionally, the implementation of WC has a much lower barrier to entry than LN and DI cooling since it does not require extreme cooling for storage, the use of cryogenic personal protective equipment (PPE), and is much more cost efficient.

Chapter VII

Future Work

Immediate next steps for the analysis of IPC performance in FSE joints would be to analyze the microstructure of the extrusion cross-section to compare the cooling source average grain size in the various weld zones. These findings would allow for further conclusion on the effectiveness of IPC in the reduction of grain growth during the FSE process. Analysis of the grain structure was attempted for this research using electrolytic polishing in combination with Barker's reagent but was unsuccessful as the revealed grain structure area was not sufficient for grain size analysis. It was apparent from the preformed tests that cooling methods that utilized a working fluid tended to be more efficient even at higher coolant temperatures. This trend suggested a way of enhancing the IPC from dry ice. Super cooling a working fluid such as ethylene glycol or isopropyl alcohol with dry ice could be used to improve the IPC contribution from dry ice. Additional next steps for this research would be the implementation of an aqueous solution for IPC, a direct comparison of active water cooled (WC) IPC to passive WC IPC with underwater FSW as well as the development of a commercialized IPC system that could be used in the naval, aerospace, railway, and automotive sectors.

References

[1] "Friction Stir Welding - TWI." https://www.twi-global.com/technical-knowledge/job-knowledge/friction-stir-welding-147 (accessed Jan. 26, 2021).

[2] W. M. Thomas and E. D. et al Nicholas, "Friction Welding," 5,460,317, 1995.

[3] M. K. Kulekci, U. Esme, and B. Buldum, "Critical analysis of friction stir-based manufacturing processes," *International Journal of Advanced Manufacturing Technology*, vol. 85, no. 5–8, pp. 1687–1712, 2016, doi: 10.1007/s00170-015-8071-5.

[4] B. T. Gibson *et al.*, "Friction stir welding: Process, automation, and control," *Journal of Manufacturing Processes*, vol. 16, no. 1, pp. 56–73, 2014, doi: 10.1016/j.jmapro.2013.04.002.

[5] P. S. D. N. Kumar and R. S. Mishra, *Friction Stir Welding and Processing*. Springer, 2014.

[6] A. C. (NASA M. P. L. Nunes Jr., "A Brief Introduction to the Theory of Friction Stir Welding," 2008.

[7] T. Nishihara, "Development of friction stir forming," *Materials Science Forum*, vol. 426–432, no. 4. pp. 2971–2978, 2003, doi: 10.4028/www.scientific.net/msf.426-432.2971.

[8] S. W. Park, T. J. Yoon, and C. Y. Kang, "Effects of the shoulder diameter and weld pitch on the tensile shear load in friction-stir welding of AA6111/AA5023 aluminum alloys," *Journal of Materials Processing Technology*, vol. 241, pp. 112–119, 2017, doi: 10.1016/j.jmatprotec.2016.11.007.

[9] S. M. Chowdhury, D. L. Chen, S. D. Bhole, and X. Cao, "Tensile properties of a friction stir welded magnesium alloy: Effect of pin tool thread orientation and weld pitch," *Materials Science and Engineering A*, vol. 527, no. 21–22, pp. 6064–6075, 2010, doi: 10.1016/j.msea.2010.06.012.

[10] L. Fratini, G. Buffa, and R. Shivpuri, "Mechanical and metallurgical effects of in process cooling during friction stir welding of AA7075-T6 butt joints," *Acta Materialia*, vol. 58, no. 6, pp. 2056–2067, 2010, doi: 10.1016/j.actamat.2009.11.048.

[11] L. Fratini and S. Pasta, "Residual stresses in friction stir welded parts of complex geometry," *International Journal of Advanced Manufacturing Technology*, vol. 59, no. 5–8, pp. 547–557, 2012, doi: 10.1007/s00170-011-3510-4.

[12] L. Fratini, G. Buffa, and R. Shivpuri, "In-process heat treatments to improve FS-welded butt joints," *International Journal of Advanced Manufacturing Technology*, vol. 43, no. 7–8, pp. 664–670, 2009, doi: 10.1007/s00170-008-1750-8.

[13] G. Peng, Q. Yan, J. Hu, P. Chen, Z. Chen, and T. Zhang, “Effect of forced air cooling on the microstructures, Tensile strength, and Hardness distribution of dissimilar friction stir welded AA5A06-AA6061 Joints,” *Metals*, vol. 9, no. 3, 2019, doi: 10.3390/met9030304.

[14] H. J. Liu, H. J. Zhang, and L. Yu, “Effect of welding speed on microstructures and mechanical properties of underwater friction stir welded 2219 aluminum alloy,” *Materials and Design*, vol. 32, no. 3, pp. 1548–1553, 2011, doi: 10.1016/j.matdes.2010.09.032.

[15] A. Bansal *et al.*, “Influence of cryogenic treatment on mechanical performance of friction stir Al-Zn-Cu alloy weldments,” *Journal of Manufacturing Processes*, vol. 56, no. April, pp. 43–53, 2020, doi: 10.1016/j.jmapro.2020.04.067.

[16] T. Bloodworth, “On the Immersed Friction Stir Welding of AA6061-T6: A Metallurgic And Mechanical Comparison to Friction Stir Welding,” Vanderbilt University, 2009.

[17] D. Sweitzer, “ANALYSIS OF FRICTION STIR WELDING BEHAVIOR OF ALUMINUM CERIUM ALLOY AND VIABILITY FOR INDUSTRIAL APPLICATION,” Vanderbilt University, 2019.

[18] P. L. Threadgill, “Terminology in friction stir welding,” *Science and Technology of Welding and Joining*, vol. 12, no. 4, pp. 357–360, 2007, doi: 10.1179/174329307X197629.

[19] J. Q. Su, T. W. Nelson, R. Mishra, and M. Mahoney, “Microstructural investigation of friction stir welded 7050-T651 aluminium,” *Acta Materialia*, vol. 51, no. 3, pp. 713–729, 2003, doi: 10.1016/S1359-6454(02)00449-4.

[20] W. T. Evans, B. T. Gibson, J. T. Reynolds, A. M. Strauss, and G. E. Cook, “Friction Stir Extrusion: A new process for joining dissimilar materials,” *Manufacturing Letters*, vol. 5, pp. 25–28, 2015, doi: 10.1016/j.mfglet.2015.07.001.

[21] A. W. Jarrell, A. M. Strauss, and G. E. Cook, “Dissimilar Metal T-Joint of Aluminum and Steel Formed by Friction Stir Extrusion,” *Minerals, Metals and Materials Series*, no. 9783319523828, pp. 91–96, 2017, doi: 10.1007/978-3-319-52383-5_10.

[22] A. W. Jarrell, J. Cui, A. M. Strauss, and G. E. Cook, “Friction stir extrusion of thin sheet stock,” *Manufacturing Letters*, vol. 24, pp. 38–42, 2020, doi: 10.1016/j.mfglet.2020.03.008.

[23] M. Abbasi Gharacheh, A. H. Kokabi, G. H. Daneshi, B. Shalchi, and R. Sarrafi, “The influence of the ratio of ‘rotational speed/traverse speed’ (ω/v) on mechanical properties of AZ31 friction stir welds,” *International Journal of Machine Tools and Manufacture*, vol. 46, no. 15, pp. 1983–1987, 2006, doi: 10.1016/j.ijmachtools.2006.01.007.

[24] C. Sharma, D. K. Dwivedi, and P. Kumar, “Influence of in-process cooling on tensile behaviour of friction stir welded joints of AA7039,” *Materials Science and Engineering A*, vol. 556, pp. 479–487, 2012, doi: 10.1016/j.msea.2012.07.016.

[25] K. P. Mehta, P. Carlone, A. Astarita, F. Scherillo, F. Rubino, and P. Vora, “Conventional and cooling assisted friction stir welding of AA6061 and AZ31B alloys,” *Materials Science and Engineering A*, vol. 759, no. May, pp. 252–261, 2019, doi: 10.1016/j.msea.2019.04.120.

[26] J. Fathi, P. Ebrahimzadeh, R. Farasati, and R. Teimouri, “Friction stir welding of aluminum 6061-T6 in presence of watercooling: Analyzing mechanical properties and residual stress distribution,” *International Journal of Lightweight Materials and Manufacture*, vol. 2, no. 2, pp. 107–115, 2019, doi: 10.1016/j.ijlmm.2019.04.007.

[27] S. Benavides, Y. Li, L. E. Murr, D. Brown, and J. C. McClure, “Low-temperature friction-stir welding of 2024 aluminum,” *Scripta Materialia*, vol. 41, no. 8, pp. 809–815, 1999, doi: 10.1016/S1359-6462(99)00226-2.

[28] M. A. Mofid, A. Abdollah-Zadeh, F. M. Ghaini, and C. H. Gür, “Submerged friction-stir welding (SFSW) underwater and under liquid nitrogen: An improved method to join Al alloys to Mg alloys,” *Metallurgical and Materials Transactions A: Physical Metallurgy and Materials Science*, vol. 43, no. 13, pp. 5106–5114, 2012, doi: 10.1007/s11661-012-1314-2.

[29] “Leidenfrost effect | Engineers Edge | www.engineersedge.com.” https://www.engineersedge.com/physics/leidenfrost_effect_13089.htm (accessed Jan. 27, 2021).

[30] “ASTM E18: Standard Test Methods for Rockwell Hardness of Metallic Materials,” *ASTM International*, pp. 1–38, 2014, doi: 10.1520/E0018-14.2.

[31] M. R. Louthan, “Optical Metallography,” in *ASM Handbook, Volume 10: Materials Characterization*, vol. 10, ASM International, 1986, pp. 299–308.

[32] H. Kuhn and D. Medlin, “ASM Handbook: Mechanical Testing and Evaluation,” vol. 8, ASM International, 2000, p. 998.

Appendix

Matrices of Welds

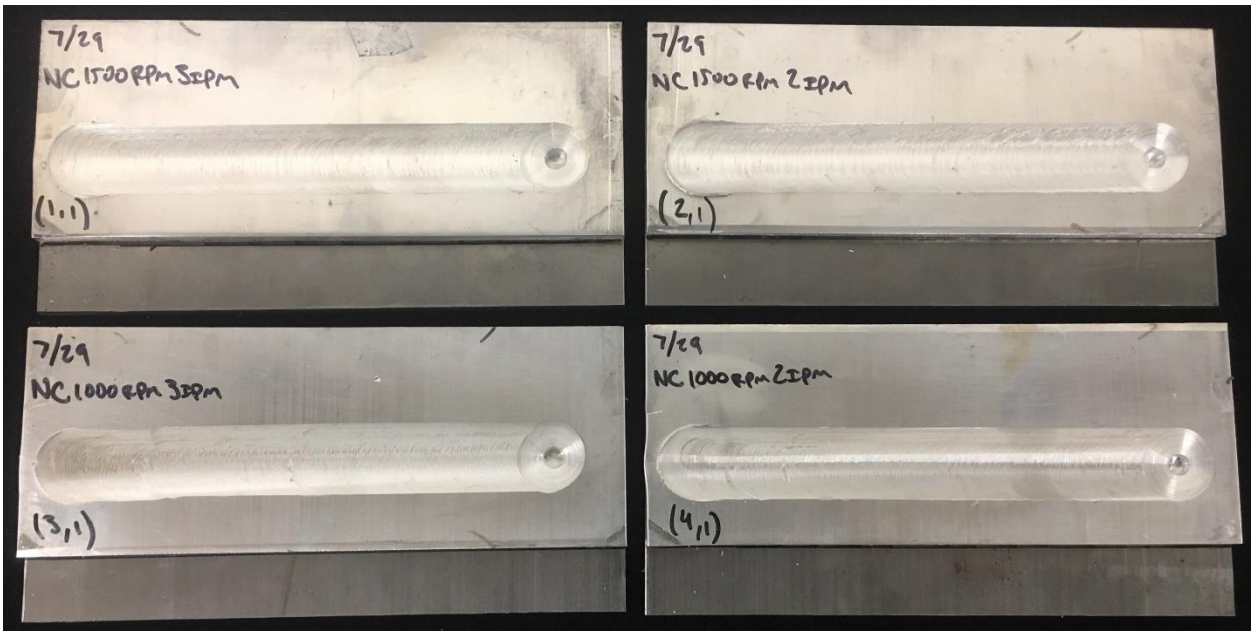

Figure A1 – NC welds with variable WP

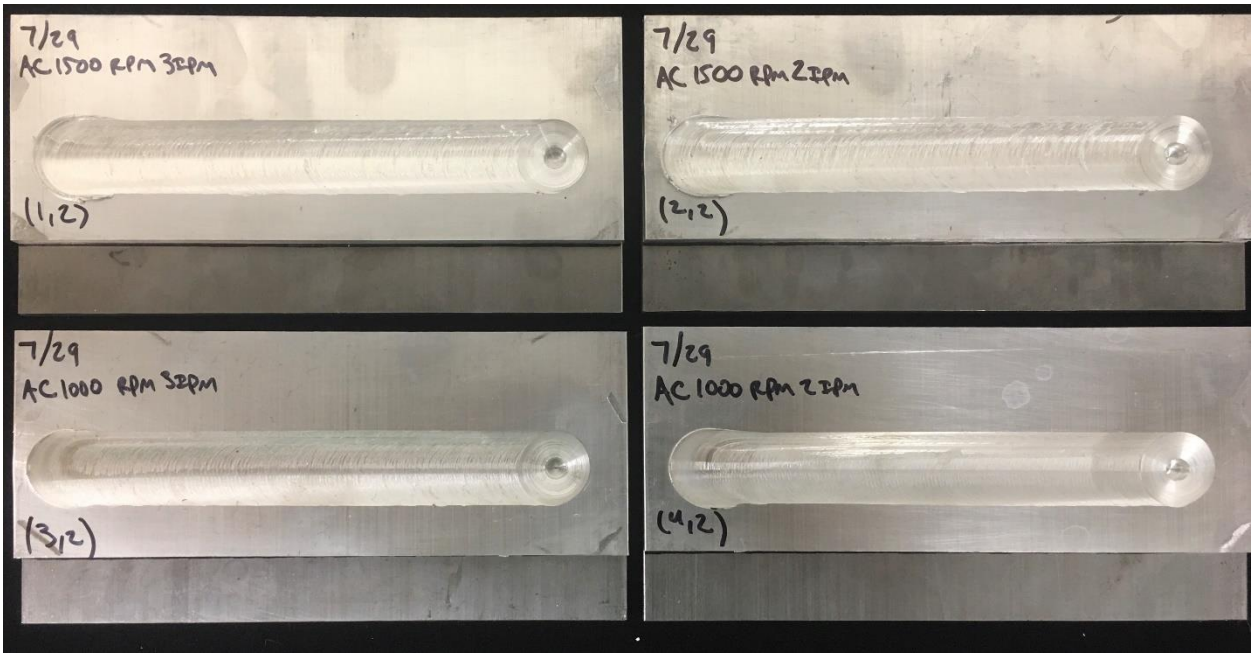

Figure A2 – AC welds with variable WP

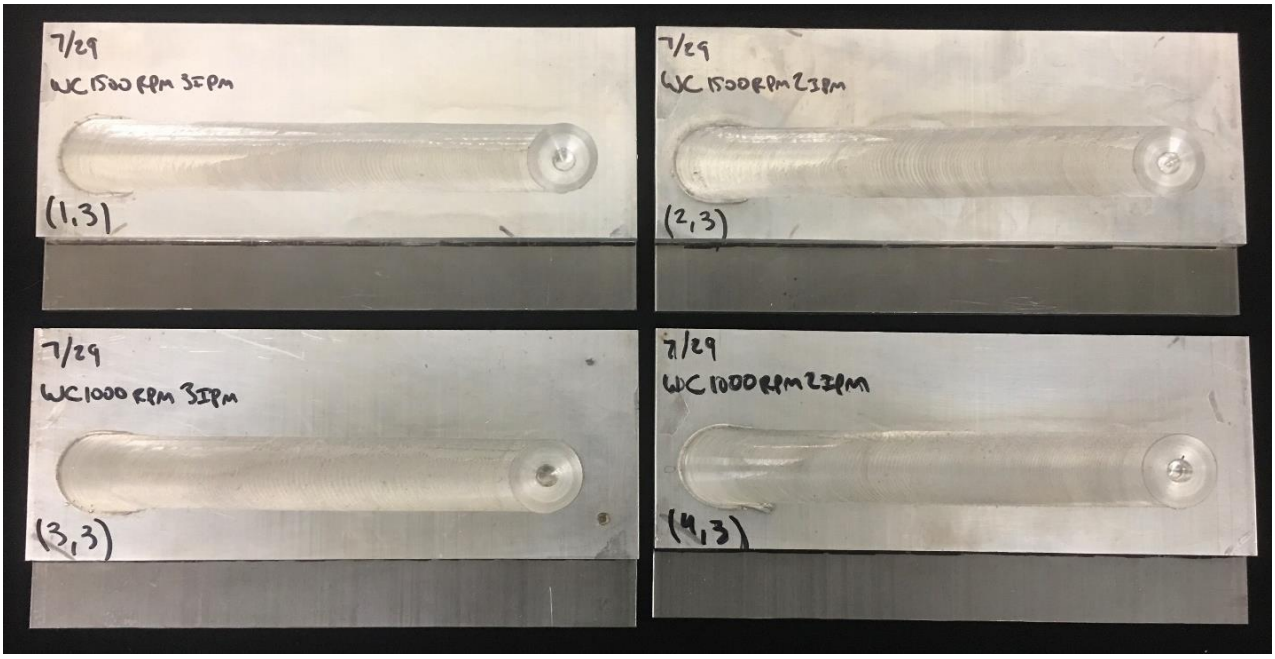

Figure A3 – WC welds with variable WP

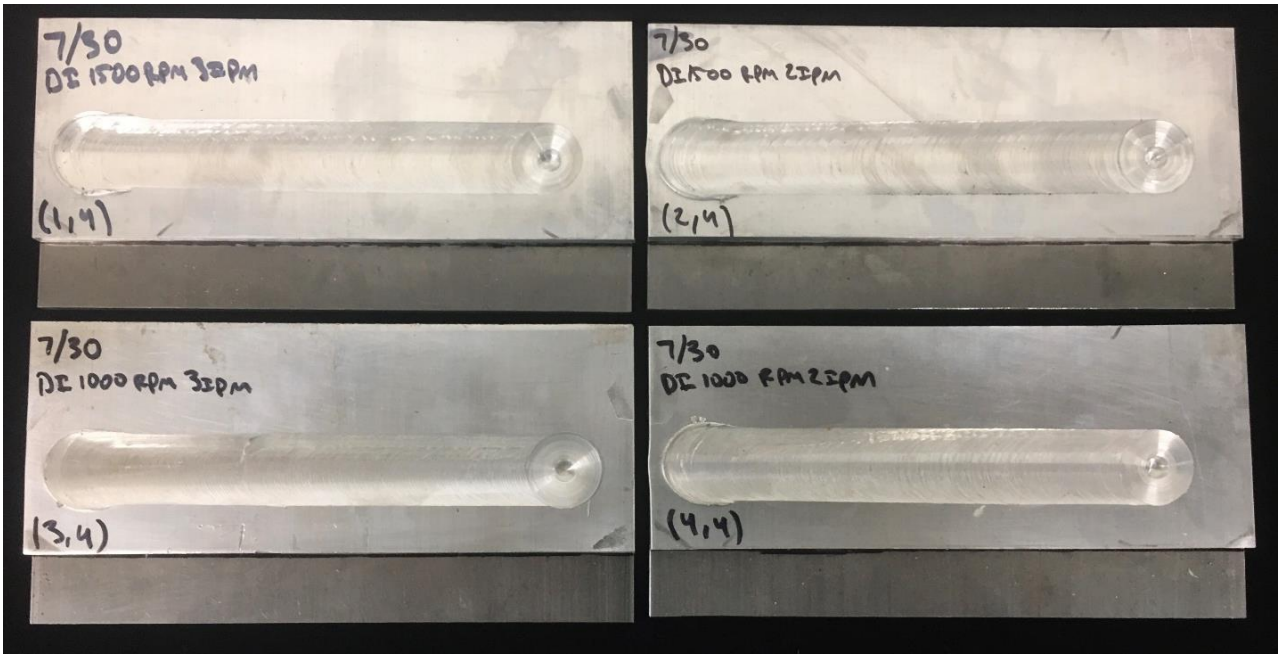

Figure A4 – DI welds with variable WP

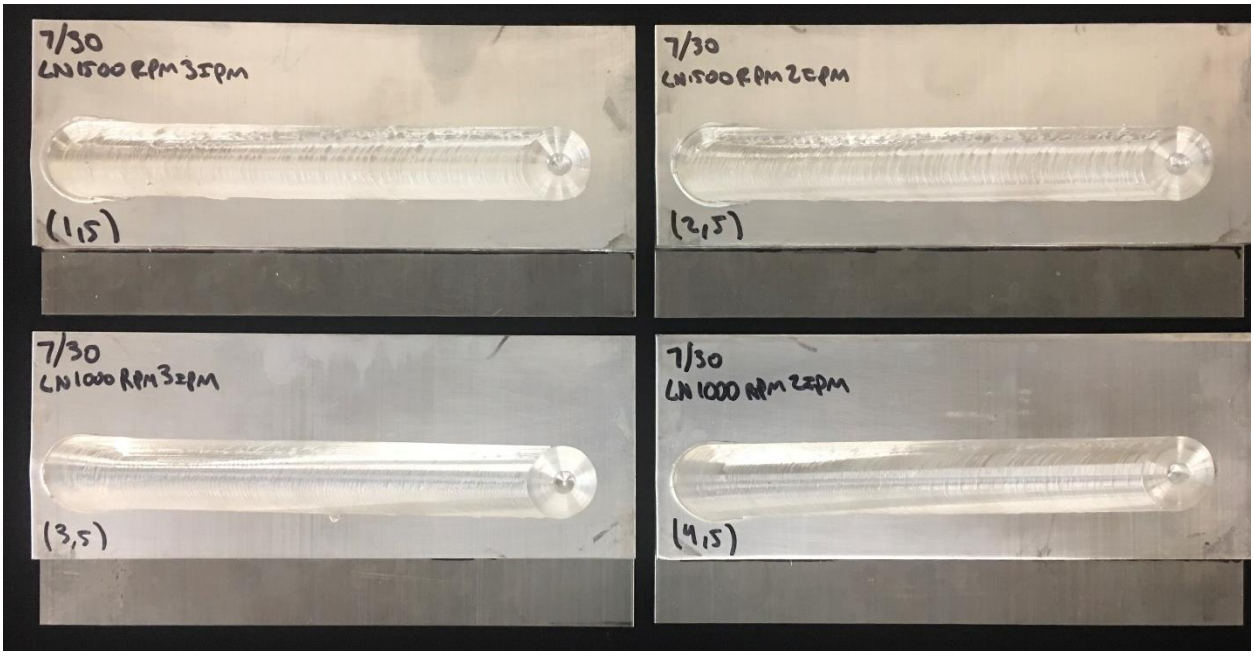

Figure A5 – LN welds with variable WP

Force Data

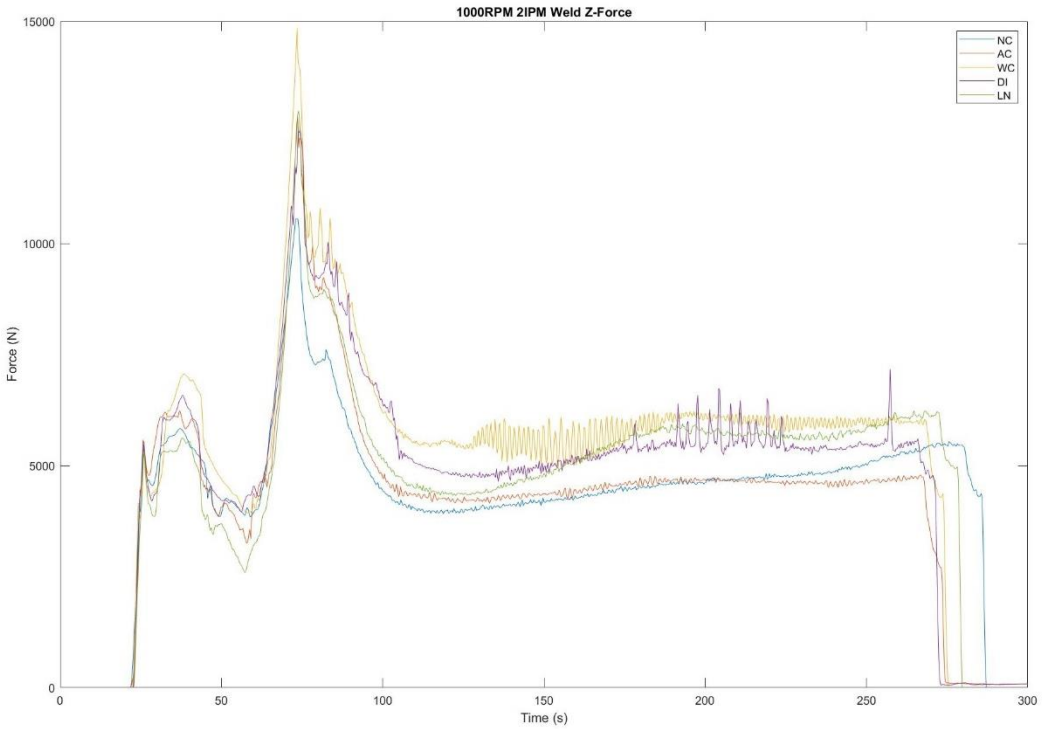

Figure A6 – Z-force plot of 1000RPM-2IPM weld with varying cooling sources

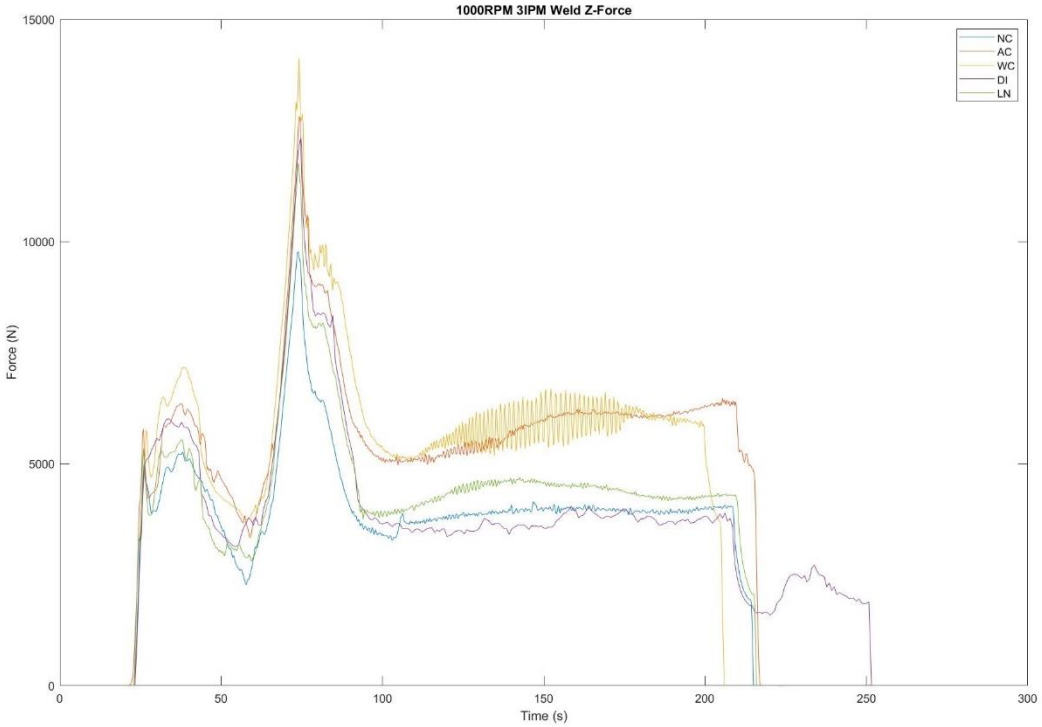

Figure A7 – Z-force plot of 1000RPM-3IPM weld with varying cooling sources

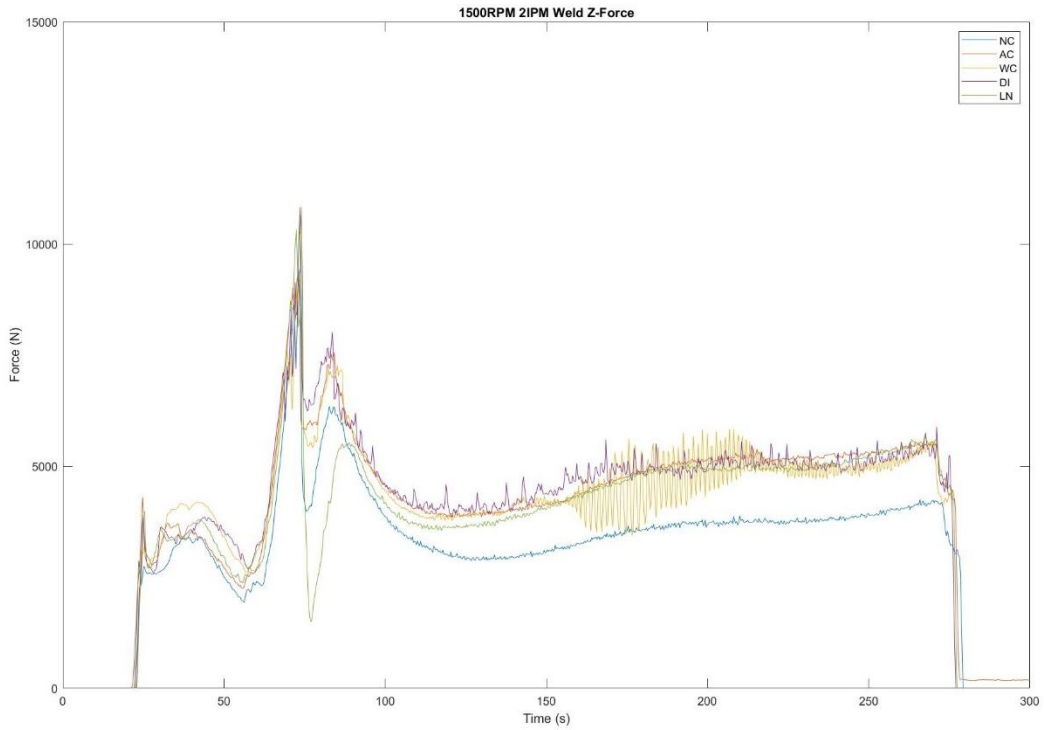

Figure A8 – Z-force plot of 1500RPM-2IPM weld with varying cooling sources

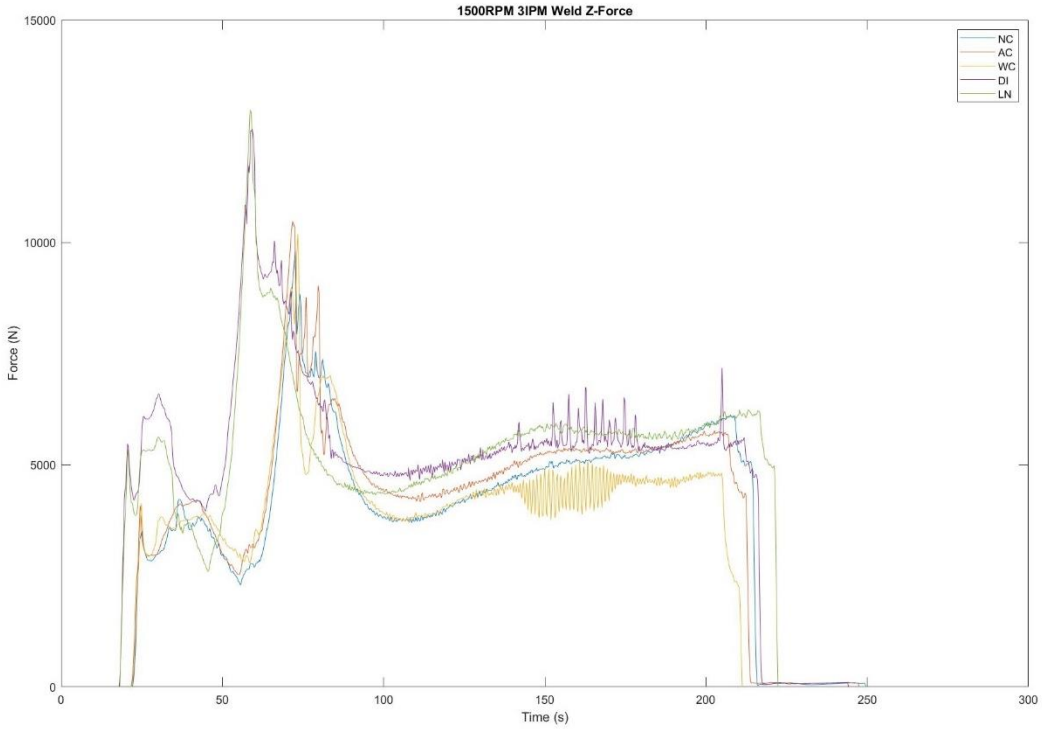

Figure A9 – Z-force plot of 1500RPM-3IPM weld with varying cooling sources

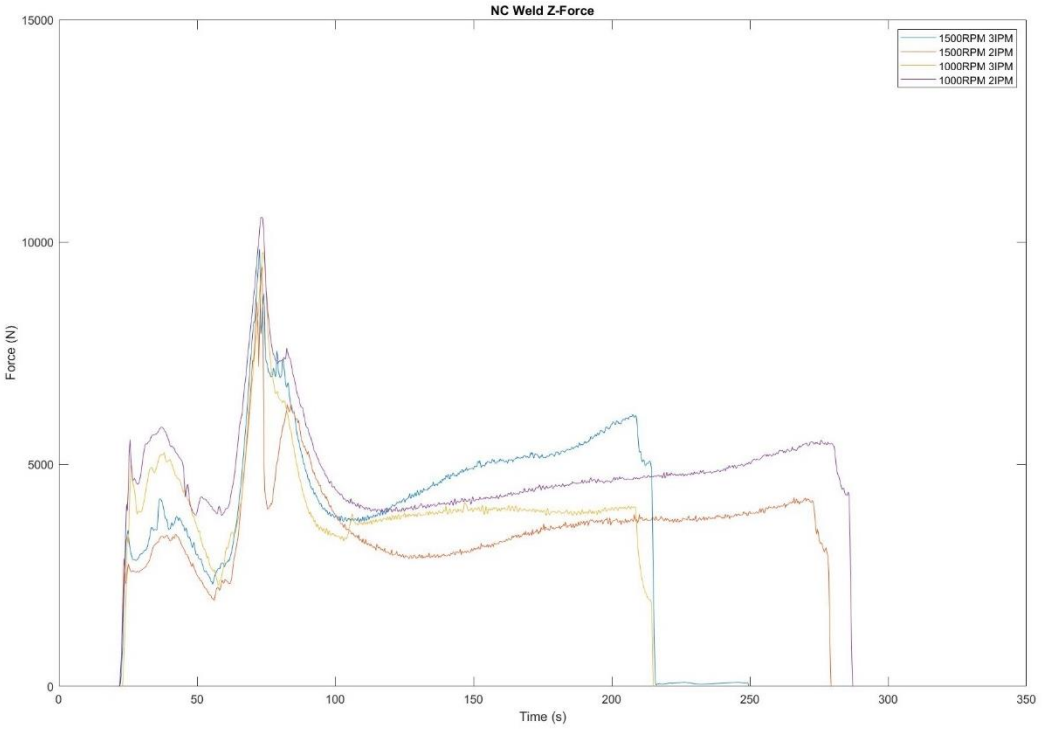

Figure A10 – Z-force plot of NC weld with varying weld parameters

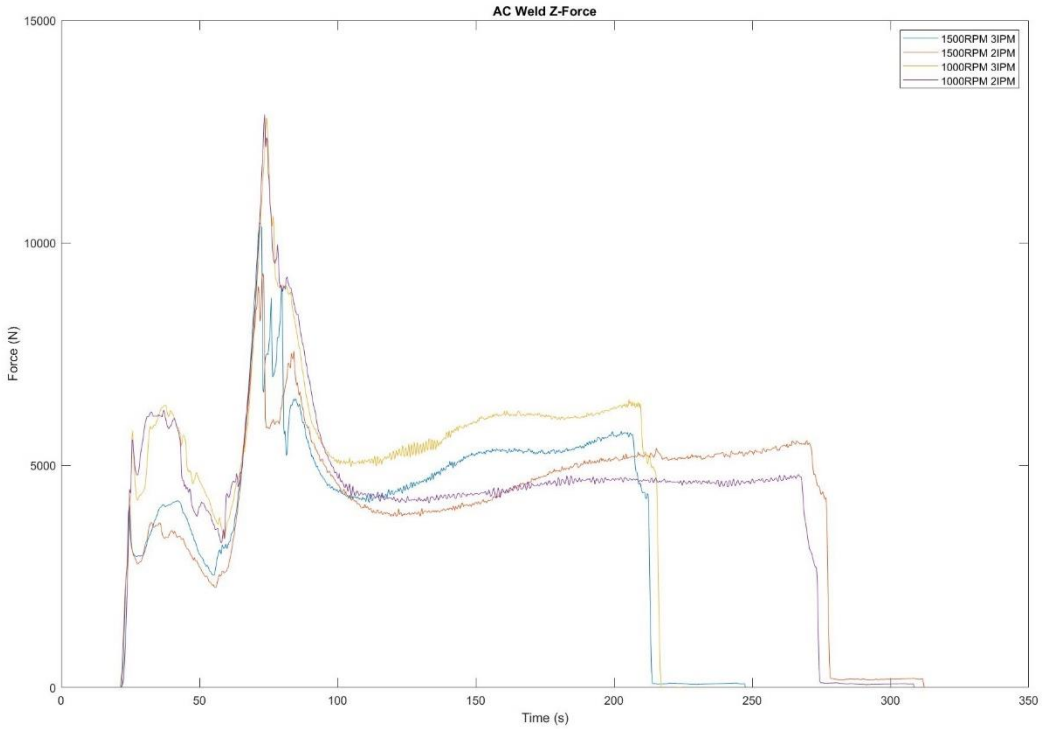

Figure A11 – Z-force plot of AC weld with varying weld parameters

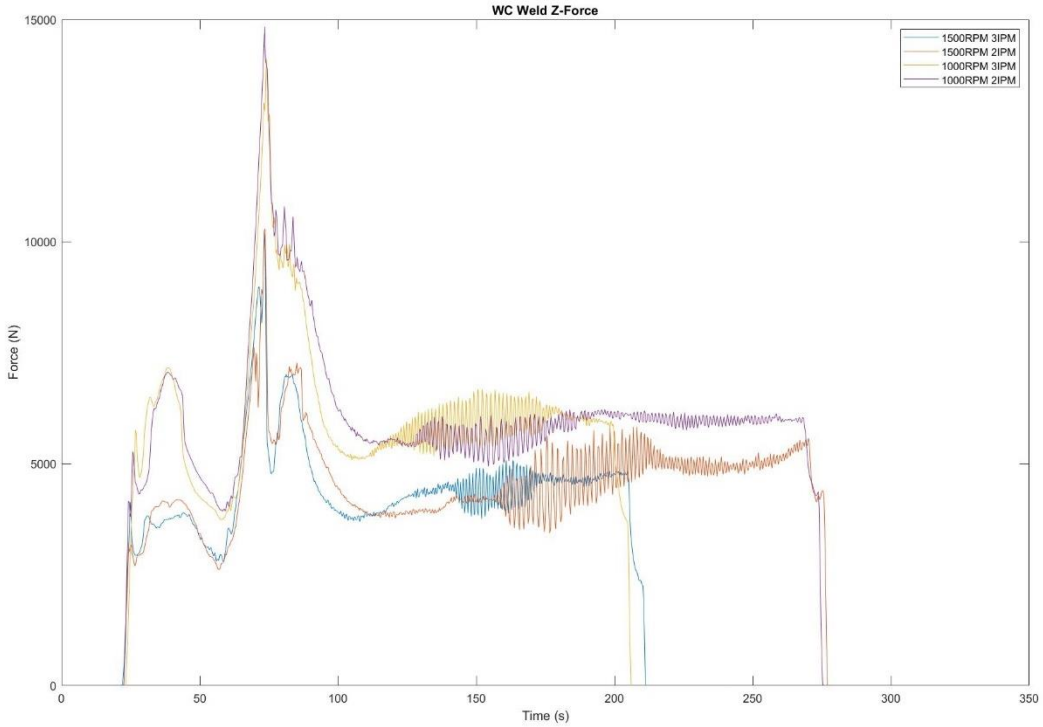

Figure A12 – Z-force plot of WC weld with varying weld parameters

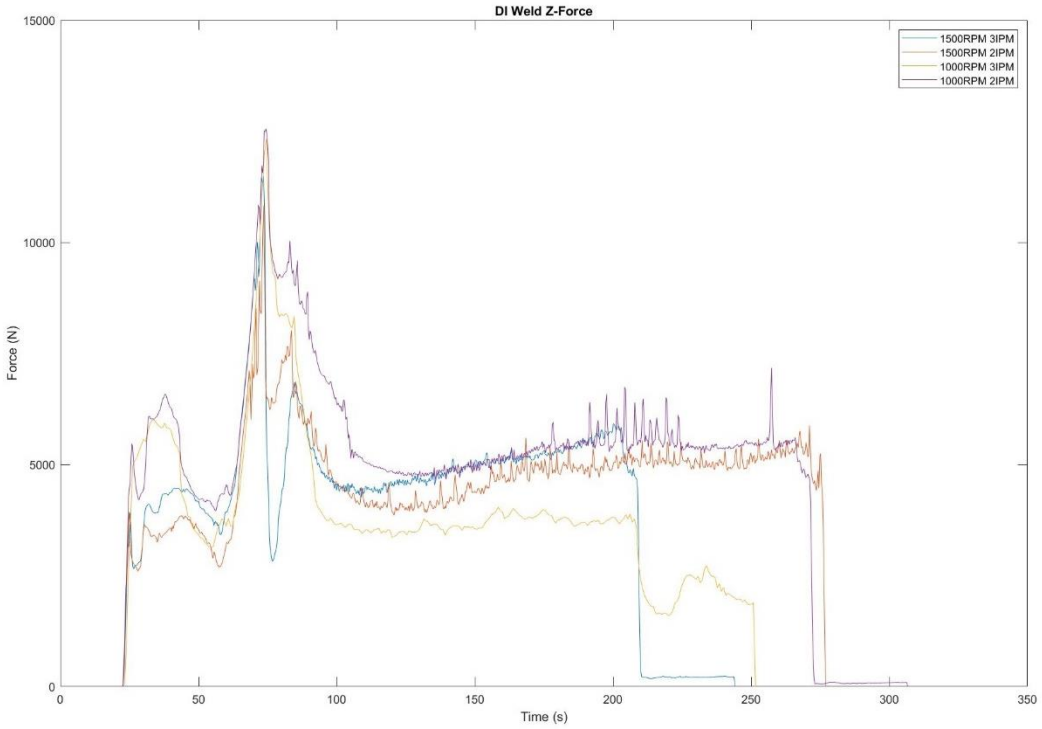

Figure A13 – Z-force plot of DI weld with varying weld parameters

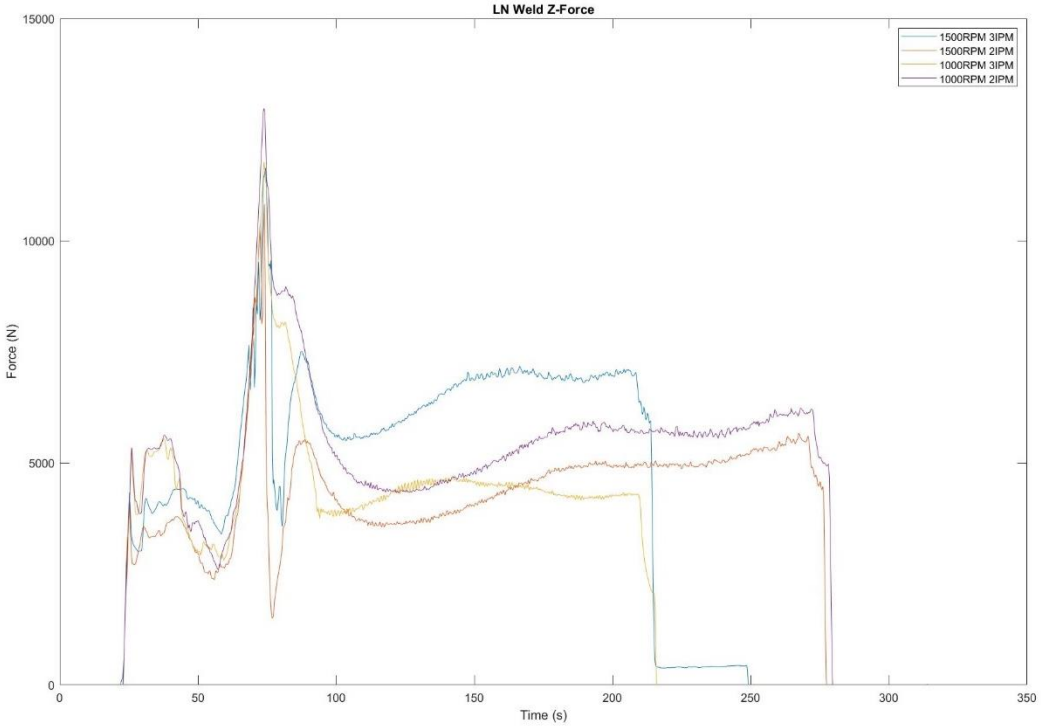

Figure A14 – Z-force plot of LN weld with varying weld parameters

Temperature Data

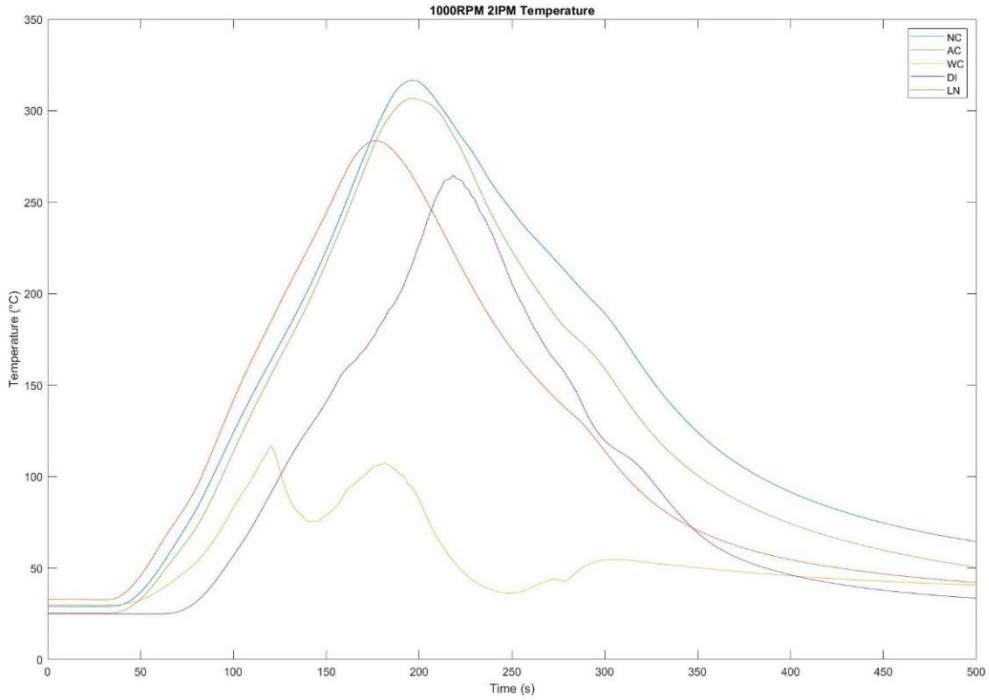

Figure A15 – Temperature plot of 1000RPM-2IPM weld with varying cooling sources

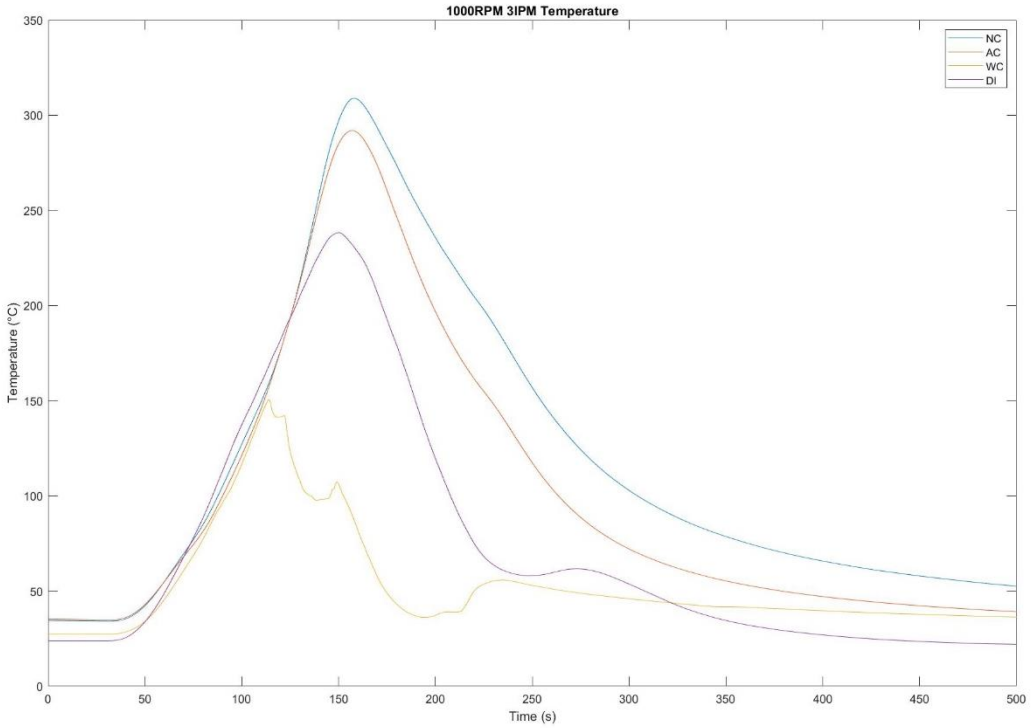

Figure A16 – Temperature plot of 1000RPM-3IPM weld with varying cooling sources

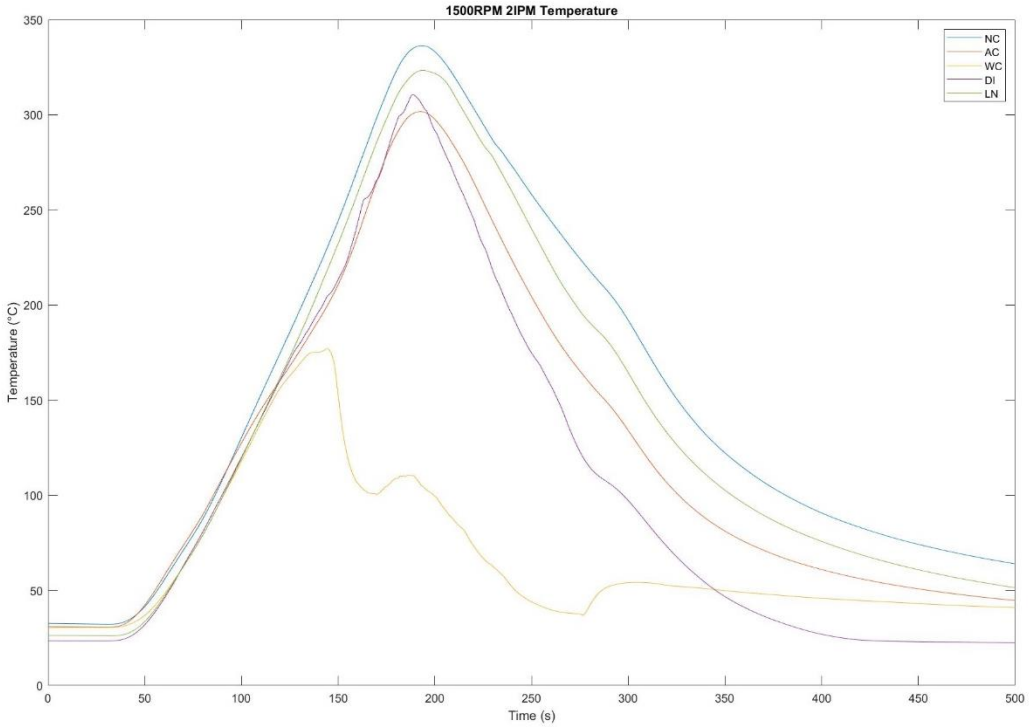

Figure A17 – Temperature plot of 1500RPM-2IPM weld with varying cooling sources

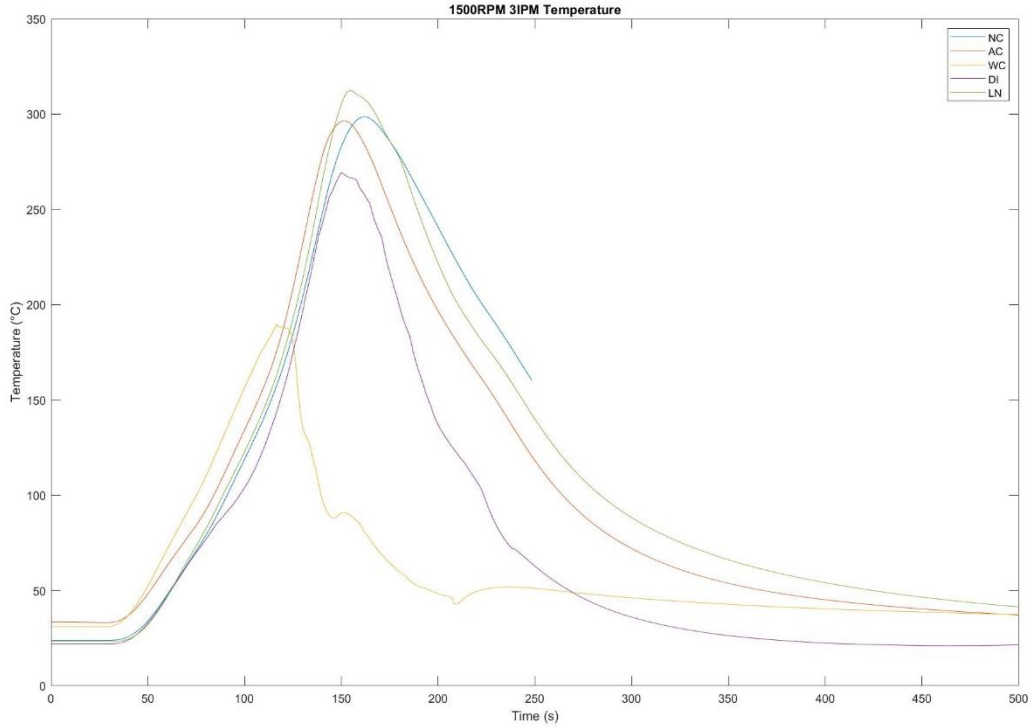

Figure A18 – Temperature plot of 1500RPM-3IPM weld with varying cooling sources

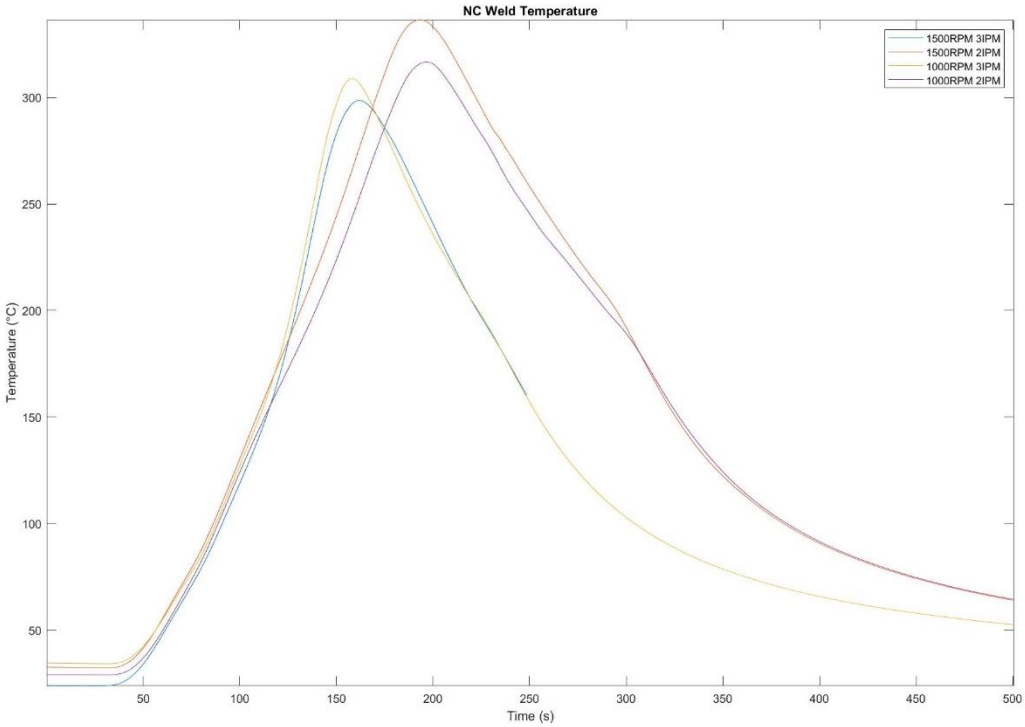

Figure A19 – Temperature plot of NC weld with varying weld parameters

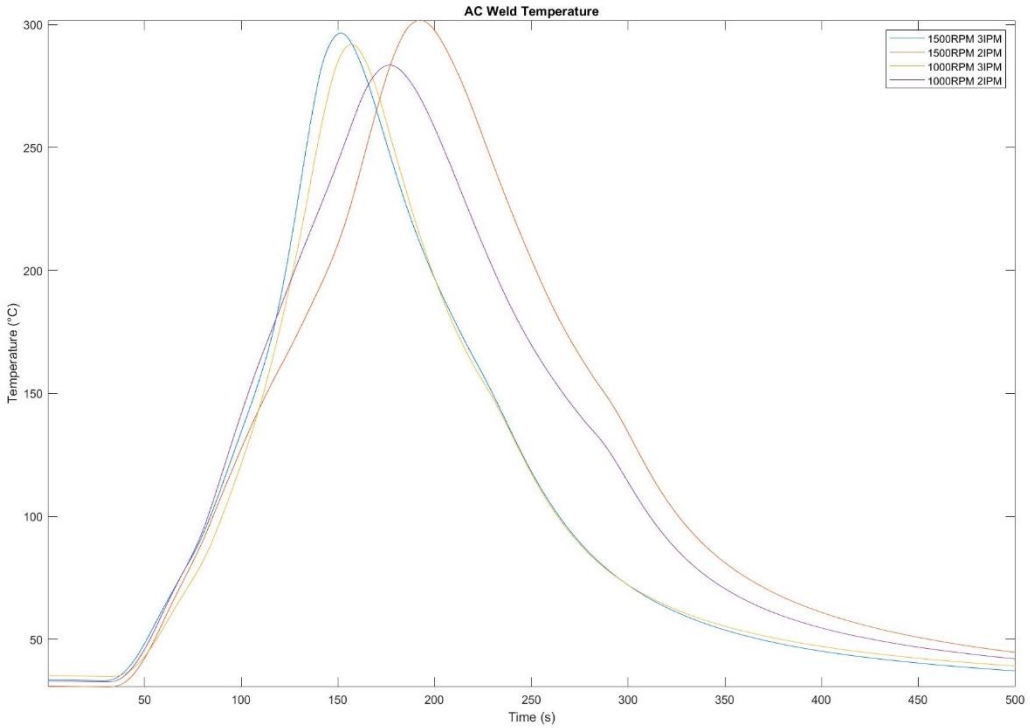

Figure A20 – Temperature plot of AC weld with varying weld parameters

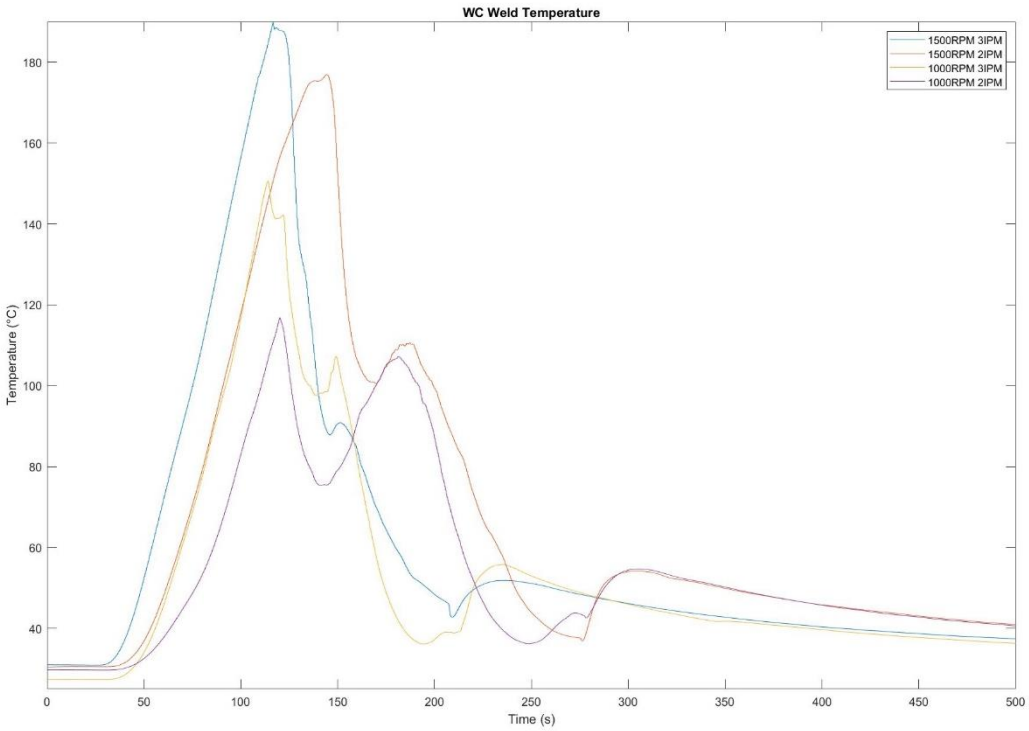

Figure A21 – Temperature plot of WC weld with varying weld parameters

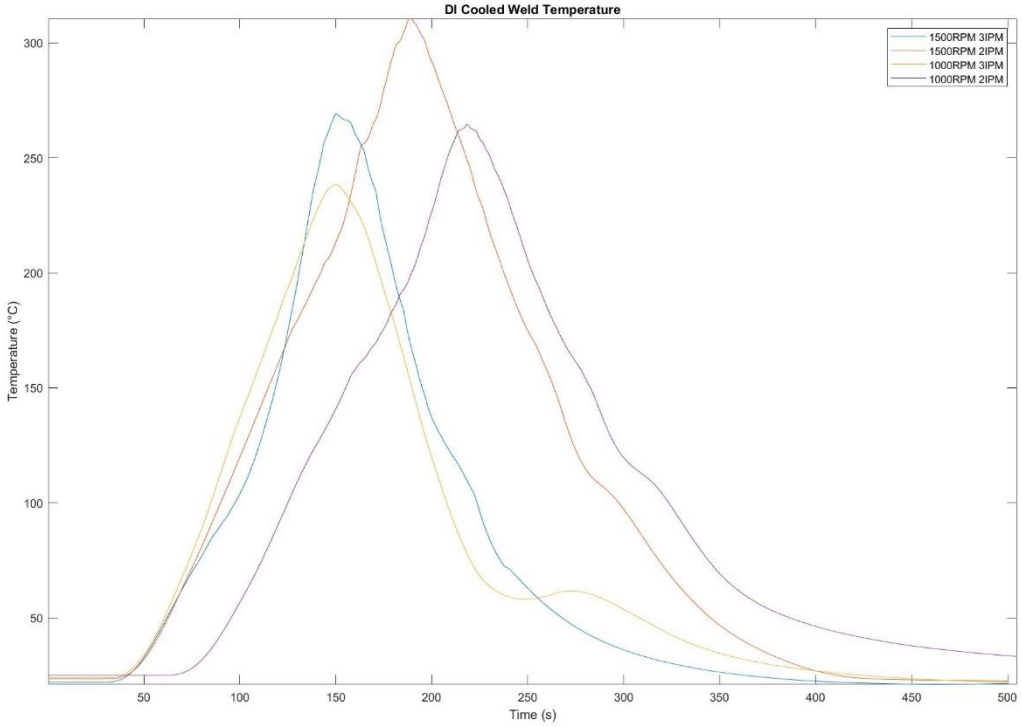

Figure A22 – Temperature plot of DI weld with varying weld parameters

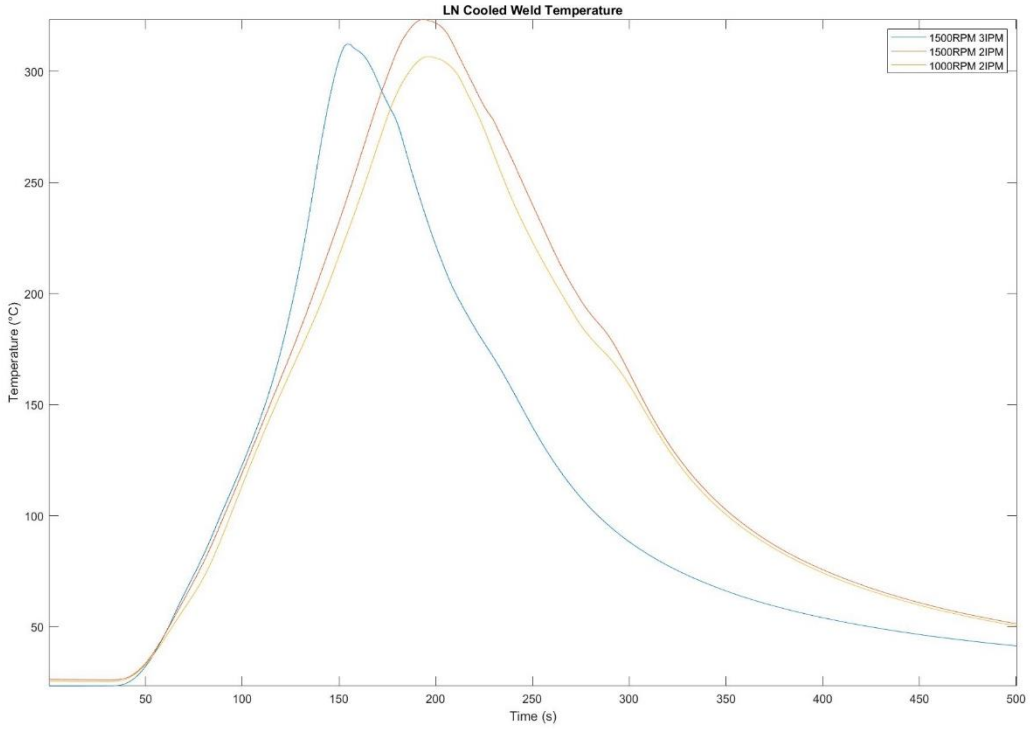

Figure A23 – Temperature plot of LN weld with varying weld parameters

Hardness Data

Table A1 – NC weld hardness data

				Hardness Values (HRF)																
Weld Name	**Matrix Number**	**Sample Number**	**Location of X-Sect**	**Loc 1**	**Loc 2**	**Loc 3**	**Loc 4**	**Loc 5**	**Loc 6**	**Loc 7**	**Loc 8**	**Loc 9**	**Loc 10**	**Loc 11**	**Loc 12**	**Loc 13**	**Loc 14**	**Loc 15**	**Loc 16**	**Extrusion**
NC1500RPM3IPM	(1,1)	1	M	82.6	84.5	85.2	83.7	82.0	78.5	75.1	62.9	42.5	45.0	66.7	65.7	43.9	49.8	57.3	55.9	52.0
		2	M	84.9	83.5	81.9	83.7	82.5	80.2	76.0	62.2	42.3	44.6	66.1	66.1	40.4	51.5	58.1	57.0	36.9
		3	M	80.7	76.9	80.5	79.3	77.5	74.9	68.6	55.9	37.0	42.6	63.5	62.4	35.6	45.8	54.8	51.3	47.5
		4	M	85.7	85.5	85.1	84.6	83.3	80.7	73.5	59.1	41.3	51.5	66.9	64.5	41.3	52.7	60.2	55.9	54.1
		5	M	86.1	85.3	84.7	84.6	83.4	78.3	73.1	56.8	42.9	58.7	64.9	64.0	43.0	51.8	60.0	57.9	43.1
		AVG	**M**	**84.0**	**83.1**	**83.5**	**83.2**	**81.7**	**78.5**	**73.3**	**59.4**	**41.2**	**48.5**	**65.6**	**64.5**	**40.8**	**50.3**	**58.1**	**55.6**	**46.7**
		STDEV	**M**	**2.0**	**3.2**	**1.9**	**2.0**	**2.2**	**2.0**	**2.6**	**2.8**	**2.2**	**5.9**	**1.3**	**1.3**	**2.9**	**2.4**	**2.0**	**2.3**	**6.2**
NC1500RPM2IPM	(2,1)	1	M	63.3	78.6	67.5	65.8	74.1	64.3	52.7	39.6	57.2	54.5	65.1	60.4	39.2	36.1	39.8		47.7
		2	M	80.6	78.4	79.6	77.3	73.7	65.7	58.4	39.2	60.7	58.3	65.9	64.0	29.9	42.0	42.8		42.9
		3	M	74.1	75.7	73.7	72.0	70.9	65.0	53.7	36.5	57.0	56.8	61.6	60.0	35.1	40.5	42.5		47.6
		4	M	64.7	75.7	78.0	77.9	75.6	68.5	55.8	42.7	61.6	57.8	64.8	61.9	36.0	41.7	42.9		31.5
		5	M	74.5	73.2	75.1	73.1	71.1	65.5	52.5	38.5	60.9	53.7	62.2	58.8	34.4	43.4	47.9		25.3
		AVG	**M**	**71.4**	**76.3**	**74.8**	**73.2**	**73.1**	**65.8**	**54.6**	**39.3**	**59.5**	**56.2**	**63.9**	**61.0**	**34.9**	**40.7**	**43.2**		**39.0**
		STDEV	**M**	**6.5**	**2.0**	**4.2**	**4.4**	**1.8**	**1.4**	**2.2**	**2.0**	**2.0**	**1.8**	**1.7**	**1.8**	**3.0**	**2.5**	**2.6**		**9.0**
NC1000RPM3IPM	(3,1)	1	M	79.8	84.5	84.5	82.2	79.1	75.7	66.7	46.6	36.2	58.3	63.3	40.1	51.8	62.8	61.1		21.5
		2	M	84.4	85.0	84.8	84.0	83.2	80.1	70.9	52.9	-16.0	63.8	64.7	44.3	61.8	69.5	69.8		21.4
		3	M	80.9	79.0	76.1	77.7	77.4	74.2	69.0	51.7	-18.5	61.9	59.5	37.1	56.3	67.6	70.6		41.5
		4	M	81.3	84.5	83.3	80.0	78.4	75.2	65.8	51.6	20.8	64.7	62.9	41.0	60.6	69.9	71.8		46.1
		5	M	83.3	85.2	83.1	82.4	79.8	75.9	65.9	47.5	-27.1	60.1	49.5	47.0	60.1	68.8	71.0		15.2
		AVG	**M**	**81.9**	**83.6**	**82.4**	**81.3**	**79.6**	**76.2**	**67.7**	**50.1**	**28.5**	**61.8**	**60.0**	**41.9**	**58.1**	**67.7**	**68.9**		**29.1**
		STDEV	**M**	**1.7**	**2.3**	**3.2**	**2.2**	**2.0**	**2.0**	**2.0**	**2.5**	**7.7**	**2.3**	**5.5**	**3.4**	**3.7**	**2.6**	**3.9**		**12.3**
NC1000RPM2IPM	(4,1)	1	M	80.6	80.8	81.0	79.7	76.9	71.6	62.0	47.7	40.1	55.7	61.6	58.9	39.0	47.5	52.5		53.0
		2	M	80.8	81.8	80.8	80.3	79.0	71.9	67.4	50.1	39.5	42.2	62.8	57.7	40.6	51.6	53.5		10.0
		3	M	76.5	77.2	76.8	76.5	73.5	69.0	58.4	44.2	30.1	54.0	57.8	49.7	38.4	47.6	53.4		46.4
		4	M	79.5	80.3	80.8	80.3	77.6	73.5	67.5	50.0	37.6	54.6	61.1	52.0	30.2	50.0	50.8		42.0
		5	M	72.0	79.0	79.0	75.3	74.1	71.4	63.8	46.8	33.8	55.5	59.9	53.1	37.0	48.9	56.1		5.8
		AVG	**M**	**77.9**	**79.8**	**79.7**	**78.4**	**76.2**	**71.5**	**63.8**	**47.8**	**36.2**	**52.4**	**60.6**	**54.3**	**37.0**	**49.1**	**53.3**		**31.4**
		STDEV	**M**	**3.3**	**1.6**	**1.6**	**2.1**	**2.1**	**1.4**	**3.4**	**2.2**	**3.8**	**5.1**	**1.7**	**3.5**	**3.6**	**1.5**	**1.7**		**19.6**

Table A2 – AC weld hardness data

				Hardness Values (HRF)																
Weld Name	**Matrix Number**	**Sample Number**	**Location of X-Sect**	**Loc 1**	**Loc 2**	**Loc 3**	**Loc 4**	**Loc 5**	**Loc 6**	**Loc 7**	**Loc 8**	**Loc 9**	**Loc 10**	**Loc 11**	**Loc 12**	**Loc 13**	**Loc 14**	**Loc 15**	**Loc 16**	**Extrusion**
AC1500RPM3IPM	(1,2)	1	M	72.2	84.2	84.1	82.9	80.0	75.6	63.9	43.9	64.7	69.2	68.7	59.2	47.6	60.1	65.5		60.6
		2	M	84.2	87.1	86.8	85.2	82.6	75.8	67.3	45.8	64.8	70.1	69.6	54.2	47.3	61.6	66.8		45.0
		3	M	84.0	82.7	85.4	84.2	80.2	73.6	67.4	45.5	59.8	65.5	64.9	45.5	35.7	60.7	65.6		62.2
		4	M	84.1	85.5	84.6	82.1	80.2	76.3	65.3	45.1	63.6	67.4	66.0	48.9	49.5	63.5	66.6		59.1
		5	M	86.3	86.0	85.6	84.0	81.1	75.1	65.0	41.5	65.5	65.3	64.5	52.7	43.8	56.3	64.9		59.4
		AVG	**M**	**82.2**	**85.1**	**85.3**	**83.7**	**80.8**	**75.3**	**65.8**	**44.4**	**63.7**	**67.5**	**66.7**	**52.1**	**44.8**	**60.4**	**65.9**		**57.3**
		STDEV	**M**	**5.1**	**1.5**	**0.9**	**1.1**	**1.0**	**0.9**	**1.4**	**1.6**	**2.0**	**1.9**	**2.0**	**4.7**	**4.9**	**2.4**	**0.7**		**6.2**
AC1500RPM2IPM	(2,2)	1	M	79.7	80.5	79.1	77.3	72.9	65.5	52.0	41.1	64.6	64.0	65.9	55.6	38.7	48.1	51.4		51.1
		2	M	82.4	82.0	80.4	78.0	76.8	69.1	51.7	40.7	62.7	66.6	66.9	50.6	45.2	55.1	57.5		51.6
		3	M	61.9	76.0	74.6	72.6	68.9	61.8	45.6	29.8	56.1	58.7	56.0	33.9	37.1	51.8	56.2		33.2
		4	M	78.0	83.4	80.7	78.9	76.0	69.6	53.7	34.3	61.2	63.0	62.3	40.4	40.9	56.6	59.9		46.5
		5	M	80.6	85.6	86.1	84.1	81.4	76.0	62.5	41.7	63.9	63.2	66.2	48.7	46.9	56.7	64.6		50.8
		AVG	**M**	**76.5**	**81.5**	**80.2**	**78.2**	**75.2**	**68.4**	**53.1**	**37.5**	**61.7**	**63.1**	**63.5**	**45.8**	**41.8**	**53.7**	**57.9**		**46.6**
		STDEV	**M**	**7.4**	**3.2**	**3.7**	**3.7**	**4.2**	**4.7**	**5.4**	**4.7**	**3.0**	**2.5**	**4.1**	**7.7**	**3.7**	**3.3**	**4.3**		**7.0**
AC1000RPM3IPM	(3,2)	1	M	83.2	85.3	81.6	82.3	80.1	73.8	62.1	43.2	13.3	67.1	62.2	43.1	62.4	67.6	66.4		30.1
		2	M	59.3	72.0	83.4	83.0	79.0	73.8	64.0	44.1	52.0	64.4	67.6	40.0	60.9	67.4	70.4		22.5
		3	M	77.7	78.1	75.6	74.5	71.9	67.6	53.7	34.3	50.2	60.8	59.7	35.2	53.5	65.3	66.1		51.8
		4	M	80.7	86.0	84.9	84.2	82.4	77.3	60.2	43.5	61.5	59.3	58.1	44.1	61.6	72.5	72.4		42.7
		5	M	86.4	87.1	86.2	83.3	80.8	71.0	62.1	41.0	58.2	52.4	68.0	44.8	61.9	71.8	74.6		15.4
		AVG	**M**	**77.5**	**81.7**	**82.3**	**81.5**	**78.8**	**72.7**	**60.4**	**41.2**	**55.5**	**60.8**	**63.1**	**41.4**	**60.1**	**68.9**	**70.0**		**32.5**
		STDEV	**M**	**9.5**	**5.8**	**3.7**	**3.5**	**3.6**	**3.2**	**3.6**	**3.6**	**4.6**	**5.0**	**4.0**	**3.5**	**3.3**	**2.8**	**3.3**		**13.2**
AC1000RPM2IPM	(4,2)	1	M	74.6	82.2	79.2	67.6	68.5	65.1	52.2	36.3	61.0	62.2	63.6	38.7	49.6	60.2	62.8		51.4
		2	M	81.1	82.8	77.5	82.3	79.8	71.0	67.7	49.2	31.8	65.4	67.5	41.3	54.0	67.0	71.9		40.6
		3	M	66.3	82.0	85.0	81.8	77.1	78.8	72.7	55.1	34.4	64.4	65.6	40.6	54.8	69.9	72.7		5.0
		4	M	77.8	83.6	82.6	80.7	75.2	75.5	69.9	51.0	22.7	59.8	60.6	31.6	51.1	63.1	61.7		24.8
		5	M	86.1	85.4	87.8	83.5	79.4	78.2	70.2	57.4	37.1	63.1	63.7	45.1	60.2	72.2	75.3		33.3
		AVG	**M**	**77.2**	**83.2**	**82.4**	**79.2**	**76.0**	**73.7**	**66.5**	**49.8**	**37.4**	**63.0**	**64.2**	**39.5**	**53.9**	**66.5**	**68.9**		**31.0**
		STDEV	**M**	**6.6**	**1.2**	**3.7**	**5.9**	**4.1**	**5.1**	**7.3**	**7.3**	**12.8**	**1.9**	**2.3**	**4.4**	**3.7**	**4.4**	**5.5**		**15.7**

Table A3 – WC weld hardness data

				Hardness Values (HRF)																
Weld Name	**Matrix Number**	**Sample Number**	**Location of X-Sect**	**Loc 1**	**Loc 2**	**Loc 3**	**Loc 4**	**Loc 5**	**Loc 6**	**Loc 7**	**Loc 8**	**Loc 9**	**Loc 10**	**Loc 11**	**Loc 12**	**Loc 13**	**Loc 14**	**Loc 15**	**Loc 16**	**Extrusion**
WC1500RPM3IPM	(1,3)	1	M	72.4	78.0	81.6	81.2	77.4	73.0	62.4	41.2	-4.8	71.9	69.7	44.4	51.2	63.9	66.7		61.1
		2	M	68.3	73.5	74.3	75.0	71.9	64.4	57.7	39.9	44.3	61.2	64.6	38.8	43.0	62.7	57.3		-5.4
		3	M	88.9	90.3	87.3	86.2	83.7	80.1	72.2	48.3	41.3	67.3	69.4	47.3	64.5	72.3	75.9		-62.7
		4	M	89.3	90.6	87.7	86.6	89.6	86.6	77.5	63.3	59.2	69.3	68.9	63.0	79.4	81.2	82.4		43.7
		5	M	89.6	94.1	93.6	93.3	93.0	92.5	87.6	70.5	40.2	69.2	67.2	67.7	84.0	89.2	88.4		4.6
		AVG	**M**	**81.7**	**85.3**	**84.9**	**84.5**	**83.1**	**79.3**	**71.5**	**52.6**	**46.3**	**67.8**	**68.0**	**52.2**	**64.4**	**73.9**	**74.1**		**36.5**
		STDEV	**M**	**9.4**	**8.0**	**6.5**	**6.1**	**7.7**	**9.9**	**10.7**	**12.2**	**7.6**	**3.6**	**1.9**	**11.1**	**15.8**	**10.2**	**11.1**		**23.6**
WC1500RPM2IPM	(2,3)	1	M	84.2	83.5	81.9	80.4	77.5	70.9	58.3	45.0	67.0	69.8	66.8	55.3	37.2	48.6	56.5		61.8
		2	M	82.3	82.2	82.1	80.5	79.0	70.8	62.2	41.8	65.0	59.6	68.5	51.7	39.5	53.6	57.8		52.2
		3	M	87.4	90.2	89.2	87.5	87.2	79.3	66.9	35.7	61.7	63.0	70.5	55.0	45.6	60.6	70.6		39.9
		4	M	88.9	91.5	89.9	90.1	87.5	85.2	75.5	62.7	42.4	62.9	68.3	36.9	65.3	75.7	78.3		61.2
		5	M	88.3	91.7	91.4	91.4	90.2	90.1	87.9	72.5	44.4	62.3	65.3	47.5	83.7	85.9	87.0		58.7
		AVG	**M**	**86.2**	**87.8**	**86.9**	**86.0**	**84.3**	**79.3**	**70.2**	**51.5**	**56.1**	**63.5**	**67.9**	**49.3**	**54.3**	**64.9**	**70.0**		**54.8**
		STDEV	**M**	**2.5**	**4.1**	**4.1**	**4.7**	**5.1**	**7.7**	**10.6**	**13.8**	**10.5**	**3.4**	**1.7**	**6.8**	**17.7**	**13.9**	**11.7**		**8.2**
WC1000RPM3IPM	(3,3)	1	M	80.1	85.6	80.3	84.6	83.0	78.9	73.3	59.2	57.0	69.5	70.7	53.1	51.6	65.3	72.7		59.1
		2	M	83.0	83.4	82.9	80.6	77.1	74.7	68.4	53.3	48.2	56.0	64.8	46.2	39.8	57.8	62.8		50.4
		3	M	88.9	90.9	92.2	90.5	89.7	90.2	84.0	71.7	46.7	60.2	70.4	54.6	59.3	75.2	76.0		59.7
		4	M	89.9	91.2	90.9	90.9	91.0	89.4	85.5	76.2	49.8	60.1	68.6	46.1	69.5	80.3	83.2		29.8
		5	M	91.0	89.0	92.1	90.9	91.0	89.6	82.6	85.0	53.7	62.9	69.1	48.0	71.9	84.6	87.2		-34.3
		AVG	**M**	**86.6**	**88.0**	**87.7**	**87.5**	**86.4**	**84.6**	**78.8**	**69.1**	**51.1**	**61.7**	**68.7**	**49.6**	**58.4**	**72.6**	**76.4**		**49.8**
		STDEV	**M**	**4.3**	**3.1**	**5.1**	**4.2**	**5.5**	**6.5**	**6.7**	**11.5**	**3.8**	**4.5**	**2.1**	**3.6**	**11.8**	**9.8**	**8.5**		**12.1**
WC1000RPM2IPM	(4,3)	1	M	87.8	87.9	87.5	85.0	81.7	78.2	68.1	45.9	67.3	66.3	68.2	43.9	53.4	67.3	70.2		57.0
		2	M	72.8	78.8	87.3	87.4	85.6	79.5	76.2	46.4	32.9	59.4	63.2	33.8	58.7	52.2	59.8		-81.2
		3	M	90.2	92.8	92.9	90.7	78.2	90.3	87.6	75.8	-1.5	65.7	55.4	57.2	80.5	84.8	64.4		-27.8
		4	M	90.4	91.7	90.4	91.8	86.2	88.3	86.6	72.8	-2.9	59.9	47.3	57.2	77.9	85.2	85.9		-59.1
		5	M	89.8	91.4	91.9	92.6	91.4	78.7	91.3	71.0	35.7	57.8	48.2	57.9	82.4	89.6	86.4		-50.6
		AVG	**M**	**86.2**	**88.5**	**90.0**	**89.5**	**84.6**	**83.0**	**82.0**	**62.4**	**45.3**	**61.8**	**56.5**	**50.0**	**70.6**	**75.8**	**73.3**		**57.0**
		STDEV	**M**	**6.8**	**5.1**	**2.3**	**2.9**	**4.5**	**5.2**	**8.6**	**13.3**	**15.6**	**3.5**	**8.2**	**9.7**	**12.1**	**14.1**	**11.0**		**0.0**

Table A4 – DI weld hardness data

				Hardness Values (HRF)																
Weld Name	**Matrix Number**	**Sample Number**	**Location of X-Sect**	**Loc 1**	**Loc 2**	**Loc 3**	**Loc 4**	**Loc 5**	**Loc 6**	**Loc 7**	**Loc 8**	**Loc 9**	**Loc 10**	**Loc 11**	**Loc 12**	**Loc 13**	**Loc 14**	**Loc 15**	**Loc 16**	**Extrusion**
DI1500RPM3IPM	(1,4)	1	M	87.1	88.0	86.7	85.3	82.6	79.0	70.1	49.9	65.1	69.7	69.0	46.1	54.9	70.9	75.1		44.7
		2	M	83.2	82.7	84.4	81.0	76.7	73.3	68.8	37.9	55.7	69.3	64.8	43.2	54.0	66.3	66.7		18.0
		3	M	88.5	90.9	90.1	87.0	83.2	78.4	71.1	44.8	61.3	70.5	68.4	53.0	54.3	69.1	73.9		15.4
		4	M	87.6	89.9	89.5	85.6	85.5	73.8	70.8	33.0	65.3	67.6	68.7	61.0	54.4	70.1	73.8		-49.1
		5	M	88.4	89.9	90.3	87.6	84.4	77.1	67.8	45.1	66.0	66.2	69.2	50.6	52.1	70.4	74.1		-24.6
		AVG	**M**	**87.0**	**88.3**	**88.2**	**85.3**	**82.5**	**76.3**	**69.7**	**42.1**	**62.7**	**68.7**	**68.0**	**50.8**	**53.9**	**69.4**	**72.7**		**26.0**
		STDEV	**M**	**1.9**	**2.9**	**2.3**	**2.3**	**3.1**	**2.3**	**1.2**	**6.0**	**3.9**	**1.6**	**1.6**	**6.1**	**1.0**	**1.6**	**3.0**		**13.2**
DI1500RPM2IPM	(2,4)	1	M	71.5	78.7	79.0	77.3	73.8	63.6	48.2	50.2	64.5	59.0	67.1	45.3	41.3	48.8	51.8		62.6
		2	M	66.2	75.9	75.2	70.9	66.5	57.1	36.8	44.9	61.3	57.6	62.4	33.3	37.7	47.4	51.1		38.1
		3	M	85.6	86.5	84.9	81.9	79.3	69.7	50.3	49.4	61.4	67.5	68.5	44.8	47.5	57.4	61.6		53.2
		4	M	84.7	86.8	78.4	83.7	76.2	69.4	48.8	57.2	61.3	66.6	68.6	48.7	50.9	62.7	65.4		49.8
		5	M	87.1	88.6	83.7	82.4	78.3	71.5	46.9	64.1	58.0	72.3	68.7	46.2	49.6	58.8	62.2		50.8
		AVG	**M**	**79.0**	**83.3**	**80.2**	**79.2**	**74.8**	**66.3**	**46.2**	**53.2**	**61.3**	**64.6**	**67.1**	**43.7**	**45.4**	**55.0**	**58.4**		**50.9**
		STDEV	**M**	**8.5**	**5.0**	**3.6**	**4.7**	**4.6**	**5.3**	**4.8**	**6.7**	**2.1**	**5.5**	**2.4**	**5.4**	**5.1**	**5.9**	**5.8**		**7.8**
DI1000RPM3IPM	(3,4)	1	M	82.9	83.8	83.3	82.3	80.5	77.6	70.1	54.3	46.3	-50.1	65.4	64.8	42.2	55.4	65.6	64.4	42.7
		2	M	73.1	88.6	86.2	87.1	84.4	81.0	75.8	62.5	46.3	-58.3	66.2	61.6	47.7	62.9	72.8	72.7	50.8
		3	M	88.5	88.1	86.4	82.3	80.7	74.2	68.8	56.7	37.4	49.6	62.6	51.1	29.8	54.1	63.0	67.5	-3.3
		4	M	88.6	92.4	92.1	91.1	90.2	83.9	69.2	61.9	45.3	55.2	68.6	67.3	45.1	64.0	73.3	74.0	-55.7
		5	M	90.7	93.2	94.7	90.3	85.2	82.9	78.6	62.0	44.9	63.1	64.8	67.6	46.8	66.0	74.7	71.6	-22.9
		AVG	**M**	**84.8**	**89.2**	**88.5**	**86.6**	**84.2**	**79.9**	**72.5**	**59.5**	**44.0**	**56.0**	**65.5**	**62.5**	**42.3**	**60.5**	**69.9**	**70.0**	**46.8**
		STDEV	**M**	**6.4**	**3.4**	**4.2**	**3.8**	**3.5**	**3.6**	**4.0**	**3.3**	**3.4**	**5.5**	**1.9**	**6.1**	**6.5**	**4.8**	**4.7**	**3.6**	**4.1**
DI1000RPM2IPM	(4,4)	1	M	81.2	83.2	82.3	76.9	72.7	73.7	59.8	42.6	64.5	65.6	66.8	46.5	47.5	62.2	69.7		48.7
		2	M	90.0	77.8	76.7	75.3	73.5	66.9	48.1	25.7	47.7	37.0	54.5	27.8	30.4	46.5	54.9		11.9
		3	M	89.6	90.5	89.5	83.8	82.7	80.8	66.0	40.2	60.6	65.5	67.6	56.2	46.1	62.4	66.8		-50.2
		4	M	86.5	89.2	87.3	87.4	81.8	79.4	69.5	42.6	55.3	62.3	67.3	58.0	44.7	56.6	64.9		12.8
		5	M	87.9	90.0	89.6	89.0	87.6	78.6	68.9	38.1	62.0	47.5	66.5	58.0	38.0	57.7	65.7		-18.1
		AVG	**M**	**87.0**	**86.1**	**85.1**	**82.5**	**79.7**	**75.9**	**62.5**	**37.8**	**58.0**	**55.6**	**64.5**	**49.3**	**41.3**	**57.1**	**64.4**		**24.5**
		STDEV	**M**	**3.2**	**4.9**	**5.0**	**5.5**	**5.7**	**5.1**	**8.0**	**6.3**	**6.0**	**11.4**	**5.0**	**11.6**	**6.4**	**5.8**	**5.0**		**17.1**

Table A5 – LN weld hardness data

				Hardness Values (HRF)																
Weld Name	**Matrix Number**	**Sample Number**	**Location of X-Sect**	**Loc 1**	**Loc 2**	**Loc 3**	**Loc 4**	**Loc 5**	**Loc 6**	**Loc 7**	**Loc 8**	**Loc 9**	**Loc 10**	**Loc 11**	**Loc 12**	**Loc 13**	**Loc 14**	**Loc 15**	**Loc 16**	**Extrusion**
LN1500RPM3IPM	(1,5)	1	M	77.7	81.8	78.2	80.5	77.6	71.2	59.5	41.4	66.4	69.5	66.9	51.3	44.7	62.1	68.4		56.1
		2	M	61.9	78.9	81.5	79.6	76.9	72.1	58.3	42.2	66.5	64.1	66.1	42.7	43.9	61.2	67.5		44.4
		3	M	76.2	82.9	83.2	82.9	79.2	74.3	61.1	41.0	66.3	69.5	68.5	52.0	52.5	65.6	71.5		58.3
		4	M	79.4	77.7	79.3	80.3	79.2	72.5	59.8	42.1	67.4	61.7	67.4	50.1	48.8	63.8	67.5		-17.6
		5	M	85.6	85.2	84.0	78.6	78.3	66.7	59.9	30.9	65.4	66.8	68.6	57.8	49.9	61.9	68.7		60.4
		AVG	**M**	**76.2**	**81.3**	**81.2**	**80.4**	**78.2**	**71.4**	**59.7**	**39.5**	**66.4**	**66.3**	**67.5**	**50.8**	**48.0**	**62.9**	**68.7**		**54.8**
		STDEV	**M**	**7.8**	**2.7**	**2.2**	**1.4**	**0.9**	**2.5**	**0.9**	**4.3**	**0.6**	**3.1**	**1.0**	**4.8**	**3.2**	**1.6**	**1.5**		**6.2**
LN1500RPM2IPM	(2,5)	1	M	80.0	72.0	78.3	74.6	74.6	67.5	54.2	39.6	63.9	64.0	65.2	45.4	41.3	48.6	53.1		46.9
		2	M	70.7	73.6	72.9	69.6	63.1	55.1	47.5	31.6	60.1	57.7	60.8	46.4	34.5	40.1	36.5		25.7
		3	M	79.3	80.8	79.7	78.3	74.3	66.0	52.0	36.9	62.7	63.2	65.8	55.4	42.0	50.1	53.8		35.0
		4	M	78.5	81.5	81.0	79.3	75.5	66.7	51.5	39.6	57.5	62.2	65.3	58.0	42.4	49.6	53.9		16.6
		5	M	80.4	78.2	79.4	77.2	73.4	63.3	50.3	39.0	62.1	60.8	64.8	52.4	41.9	48.3	53.5		30.2
		AVG	**M**	**77.8**	**77.2**	**78.3**	**75.8**	**72.2**	**63.7**	**51.1**	**37.3**	**61.3**	**61.6**	**64.4**	**51.5**	**40.4**	**47.3**	**50.2**		**30.9**
		STDEV	**M**	**3.6**	**3.8**	**2.8**	**3.5**	**4.6**	**4.5**	**2.2**	**3.0**	**2.2**	**2.2**	**1.8**	**4.9**	**3.0**	**3.7**	**6.8**		**10.0**
LN1000RPM3IPM	(3,5)	1	M	76.7	85.3	86.3	84.3	84.0	80.6	73.3	58.6	43.4	27.5	65.7	40.0	55.5	70.3	73.7		39.2
		2	M	85.0	76.4	73.7	74.4	73.9	69.0	64.1	44.9	29.5	56.2	58.8	30.2	42.1	56.6	57.2		3.1
		3	M	80.9	81.0	81.3	77.7	76.4	68.0	65.0	46.8	28.5	54.6	63.6	48.6	43.7	59.2	69.3		23.1
		4	M	77.4	89.5	76.9	80.8	73.6	84.7	78.9	60.8	43.8	65.7	67.1	50.4	54.2	69.5	72.1		11.9
		5	M	68.4	87.5	84.9	88.7	86.1	83.6	76.7	59.7	43.9	63.3	63.6	54.0	55.7	66.4	71.6		-0.5
		AVG	**M**	**77.7**	**83.9**	**80.6**	**81.2**	**78.8**	**77.2**	**71.6**	**54.2**	**37.8**	**53.5**	**63.8**	**44.6**	**50.2**	**64.4**	**68.8**		**19.3**
		STDEV	**M**	**5.5**	**4.7**	**4.7**	**5.0**	**5.2**	**7.2**	**6.0**	**6.8**	**7.2**	**13.6**	**2.8**	**8.6**	**6.0**	**5.5**	**6.0**		**13.5**
LN1000RPM2IPM	(4,5)	1	M	82.2	79.4	73.7	75.8	76.7	72.2	62.7	44.0	40.7	56.9	64.8	60.0	39.7	50.4	55.8		37.9
		2	M	76.7	79.6	78.4	76.6	74.3	68.8	56.5	37.1	44.3	50.2	62.2	51.0	28.8	40.1	41.0		17.9
		3	M	76.2	84.6	83.7	82.6	81.1	77.1	63.8	45.3	60.3	59.4	66.0	64.5	39.6	51.2	58.8		41.2
		4	M	80.3	69.6	80.4	80.4	79.0	75.2	62.9	46.4	54.7	59.3	64.9	62.1	35.0	49.4	53.6		33.4
		5	M	81.2	82.8	82.7	77.2	78.9	74.5	63.8	42.9	60.2	61.4	64.9	60.5	40.8	51.8	57.7		37.9
		AVG	**M**	**79.3**	**79.2**	**79.8**	**78.5**	**78.0**	**73.6**	**61.9**	**43.1**	**52.0**	**57.4**	**64.6**	**59.6**	**36.8**	**48.6**	**53.4**		**33.7**
		STDEV	**M**	**2.4**	**5.2**	**3.6**	**2.6**	**2.3**	**2.8**	**2.8**	**3.2**	**8.1**	**3.9**	**1.3**	**4.6**	**4.5**	**4.3**	**6.4**		**8.3**

Table A6 – AA6061-T6 unwelded base metal hardness data

Aluminum 6061 T-6 Unwelded Hardness Values (HRF)																
Loc 1	**Loc 2**	**Loc 3**	**Loc 4**	**Loc 5**	**Loc 6**	**Loc 7**	**Loc 8**	**Loc 9**	**Loc 10**	**Loc 11**	**Loc 12**	**Loc 13**	**Loc 14**	**Loc 15**	**Loc 16**	
78.2	86.2	86.8	86.4	86.5	87.3	86.1	87.7	87.2	87.3	87.8	88.0	89.4	87.3	85.5	87.0	

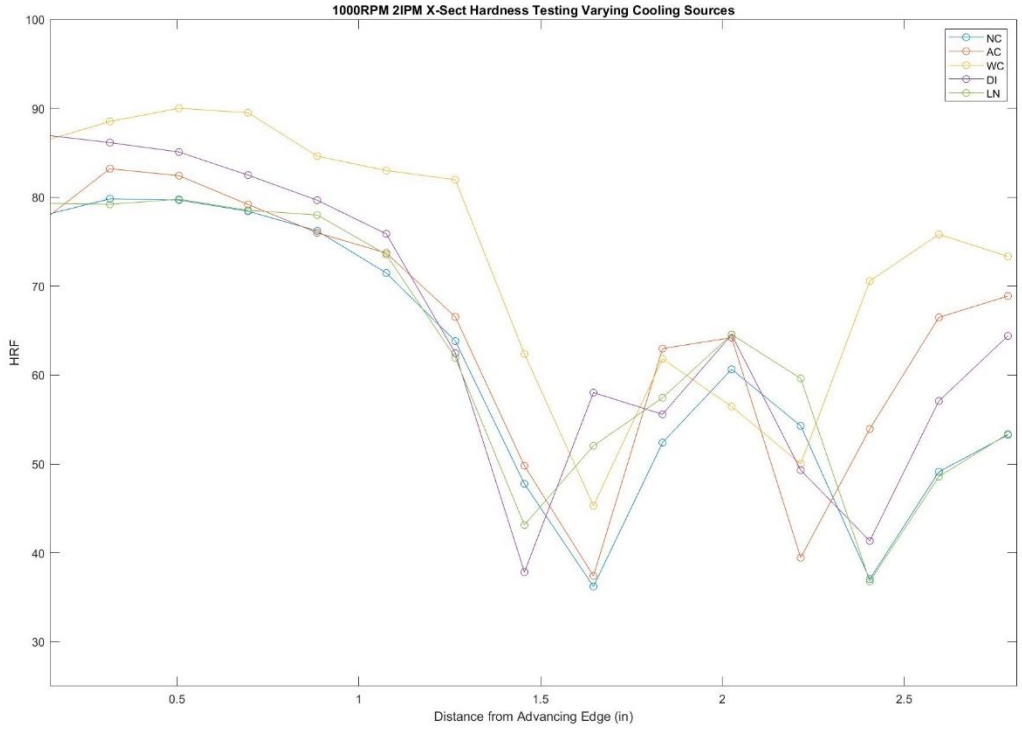

Figure A24 – X-Sect hardness plot of 1000RPM-2IPM weld with varying cooling sources

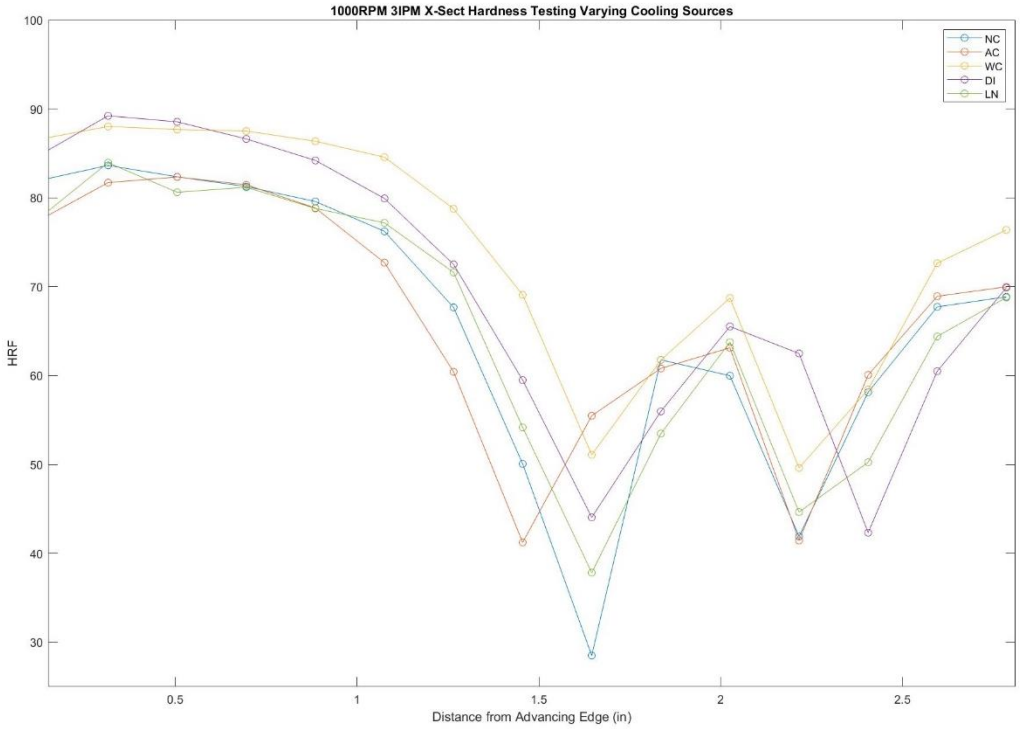

Figure A25 – X-Sect hardness plot of 1000RPM-3IPM weld with varying cooling sources

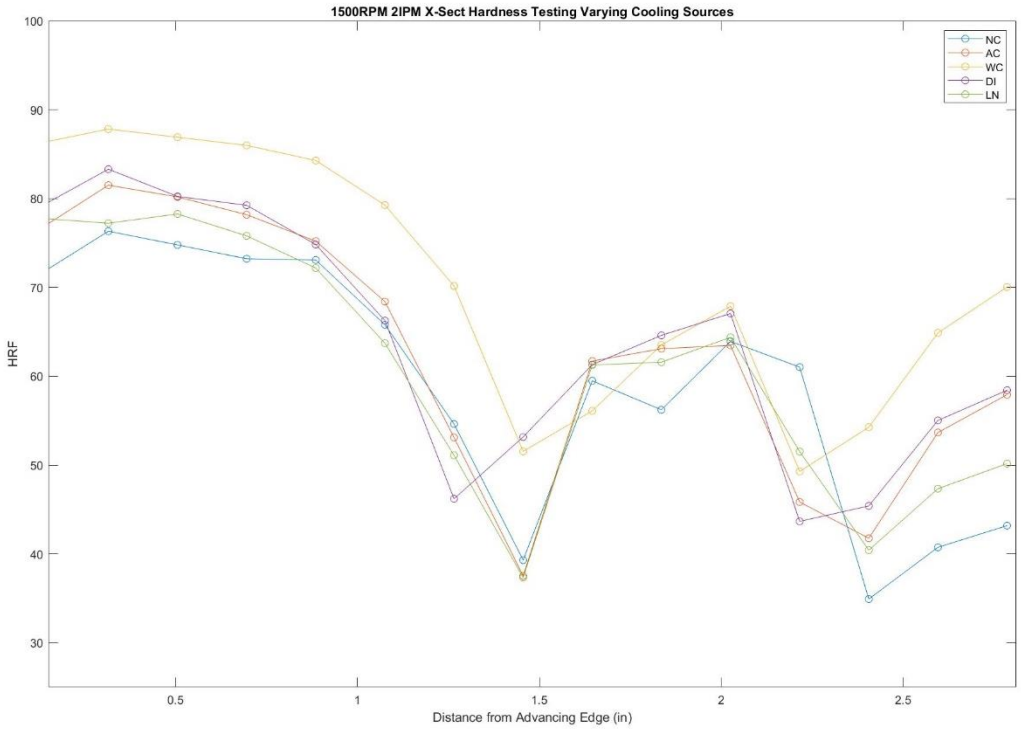

Figure A26 – X-Sect hardness plot of 1500RPM-2IPM weld with varying cooling sources

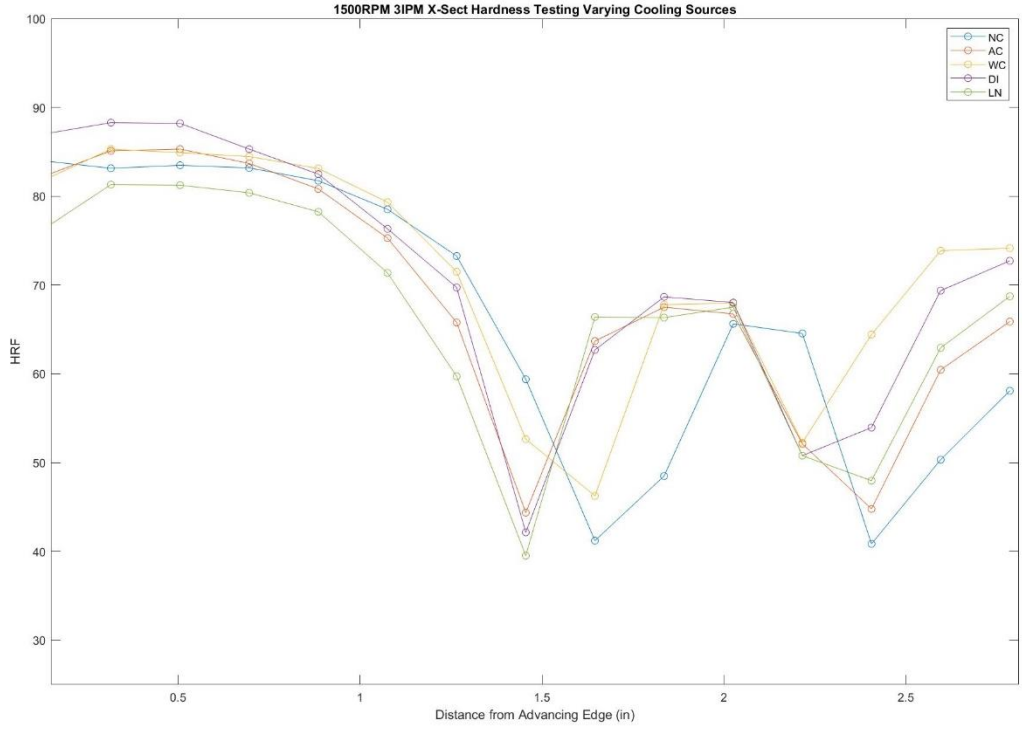

Figure A27 – X-Sect hardness plot of 1500RPM-3IPM weld with varying cooling sources

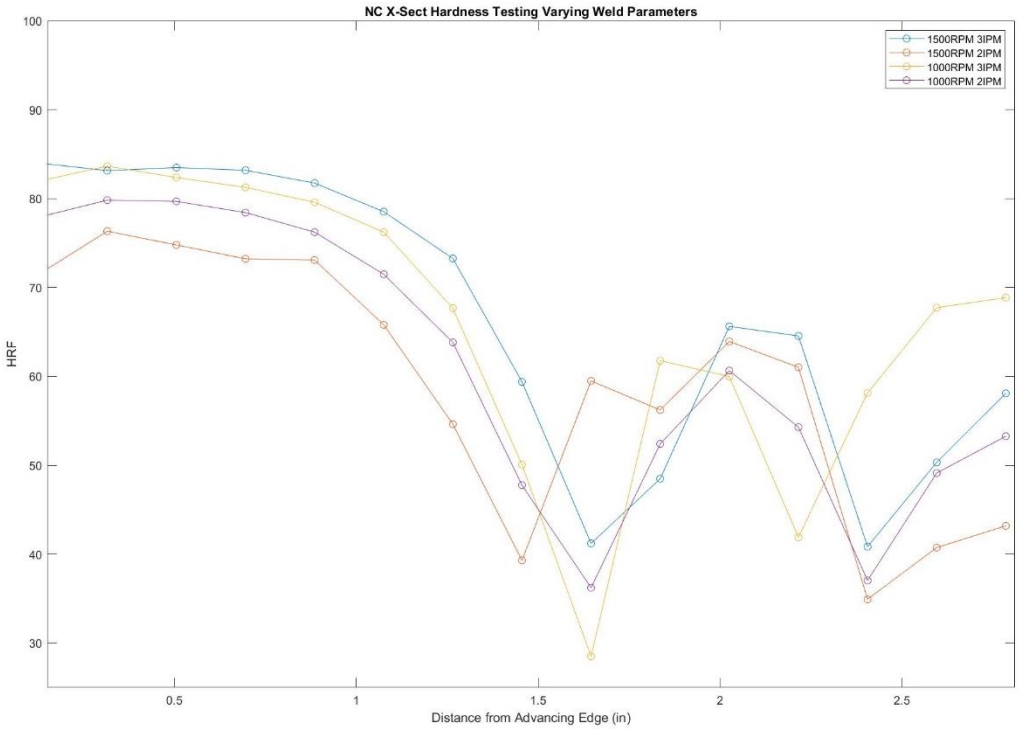

Figure A28 – X-Sect hardness plot of NC weld with varying weld parameters

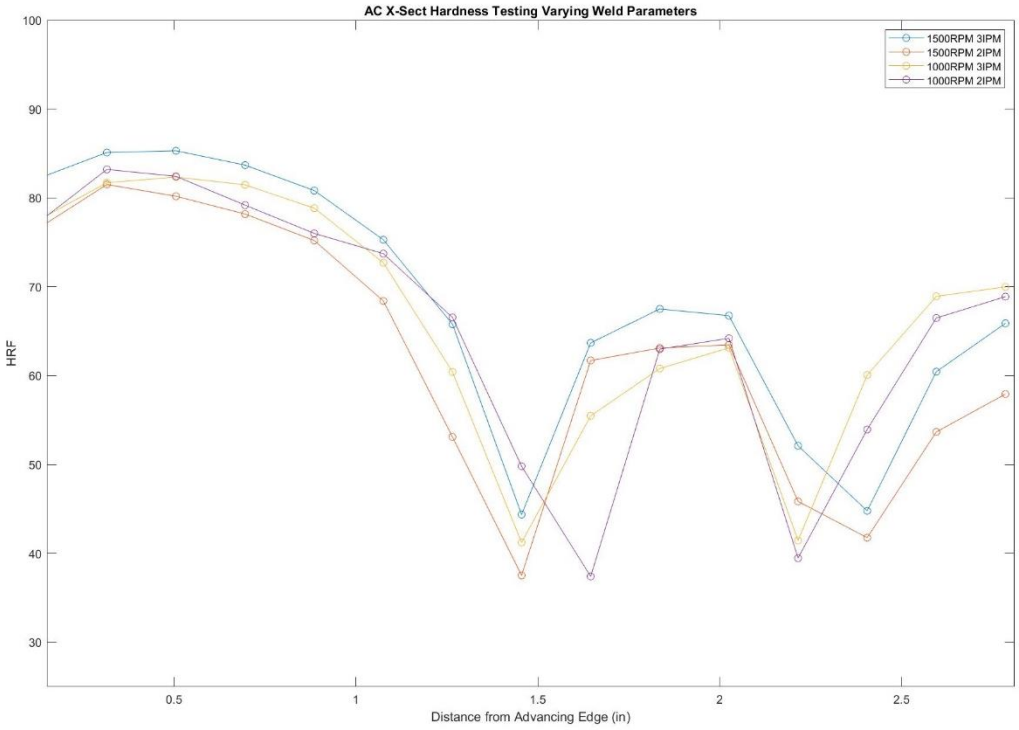

Figure A29 – X-Sect hardness plot of AC weld with varying weld parameters

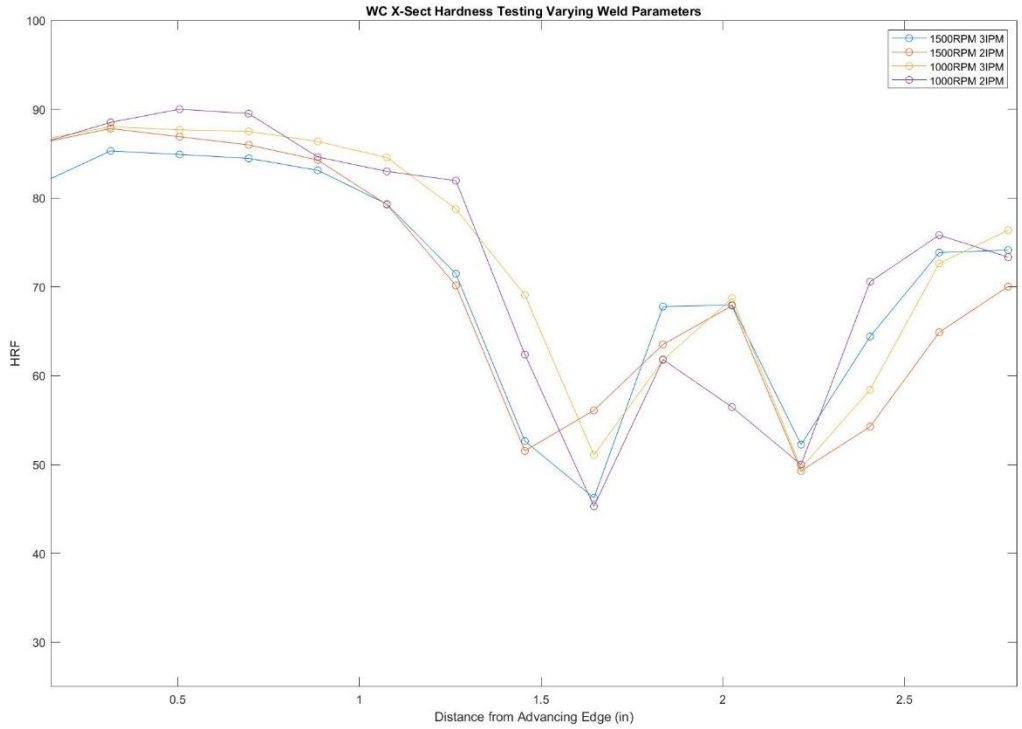

Figure A30 – X-Sect hardness plot of WC weld with varying weld parameters

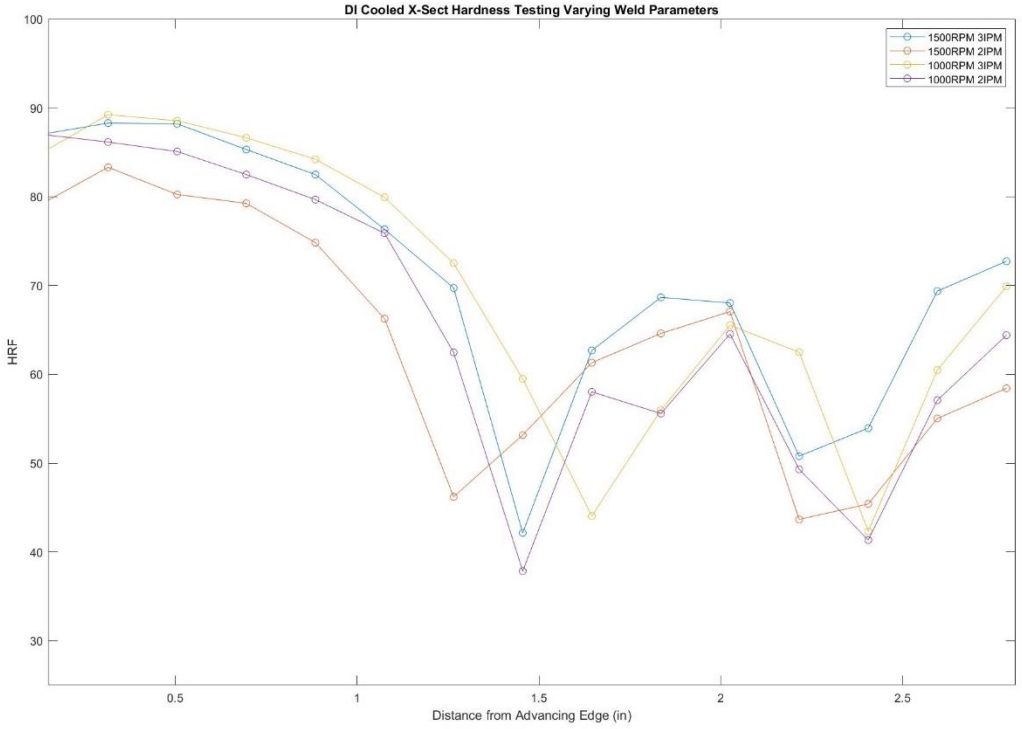

Figure A31 – X-Sect hardness plot of DI weld with varying weld parameters

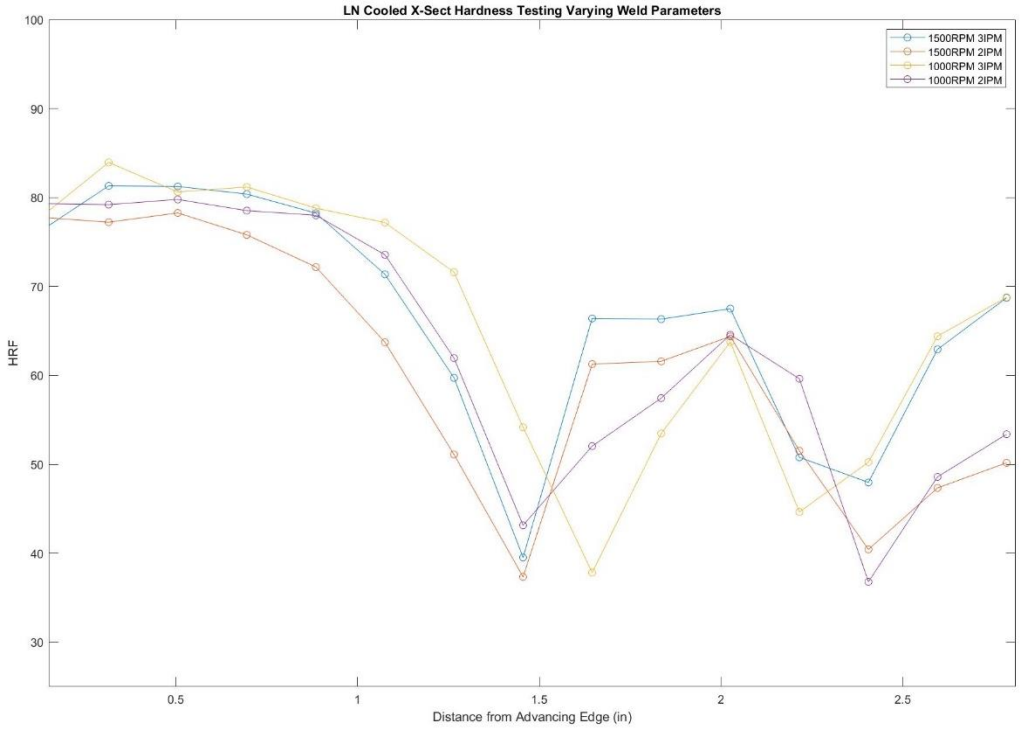

Figure A32 – X-Sect hardness plot of LN weld with varying weld parameters

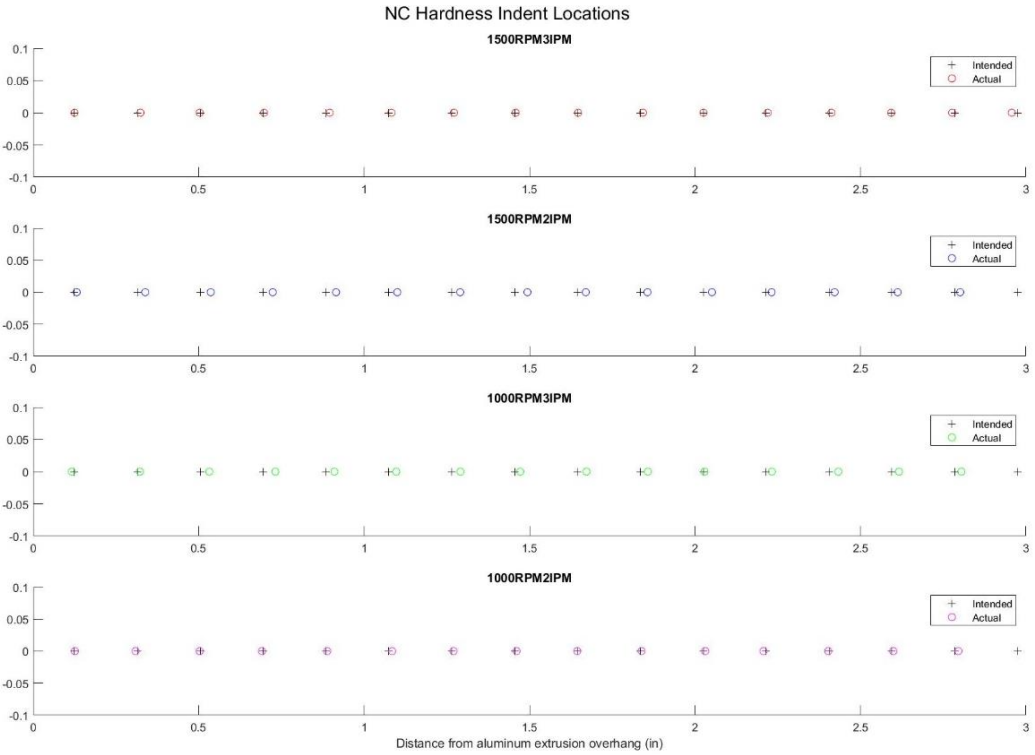

Figure A33 – X-Sect hardness indent location of NC weld with varying weld parameters

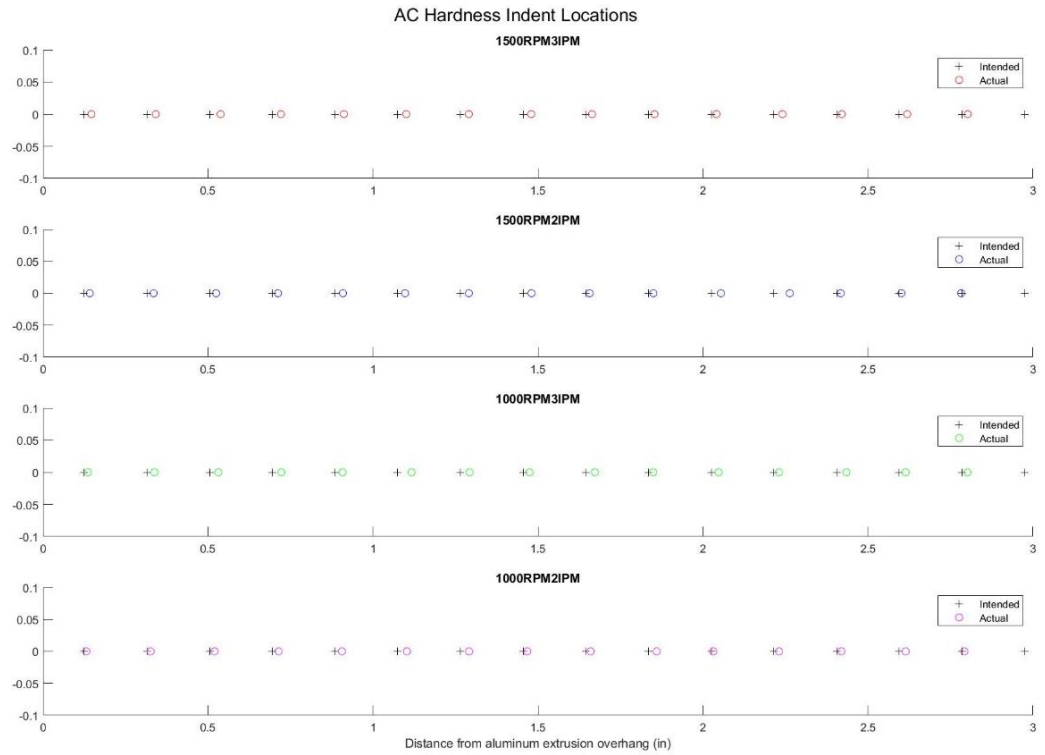

Figure A34 – X-Sect hardness indent location of AC weld with varying weld parameters

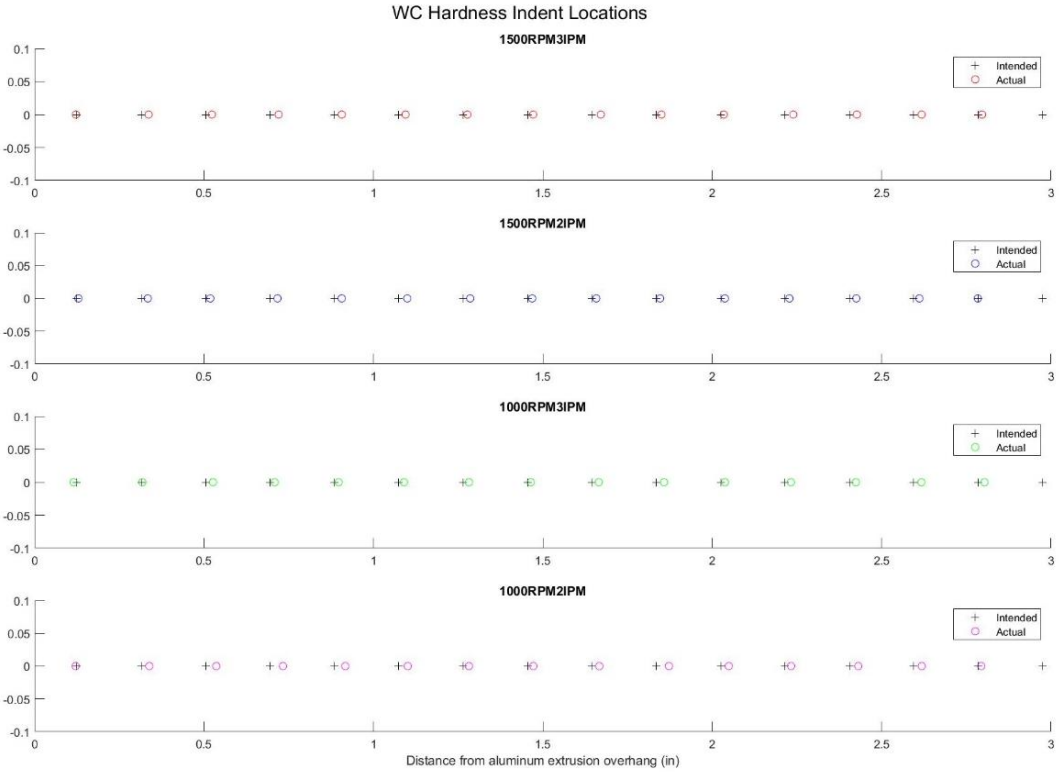

Figure A35 – X-Sect hardness indent location of WC weld with varying weld parameters

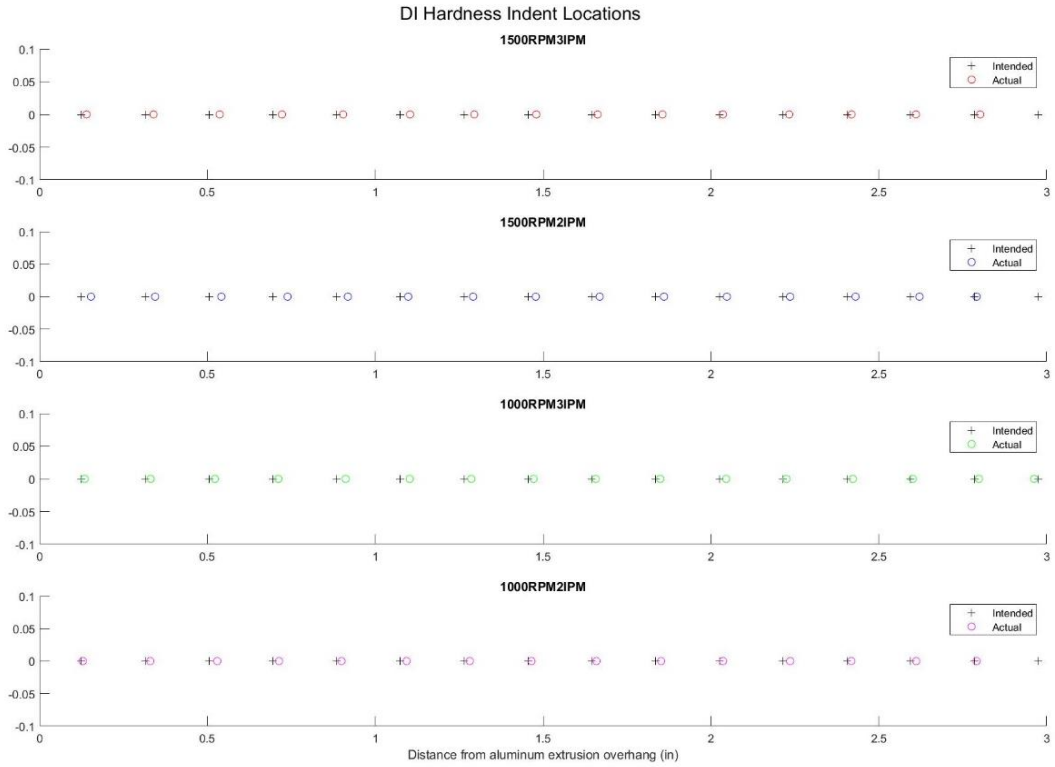

Figure A36 – X-Sect hardness indent location of DI weld with varying weld parameters

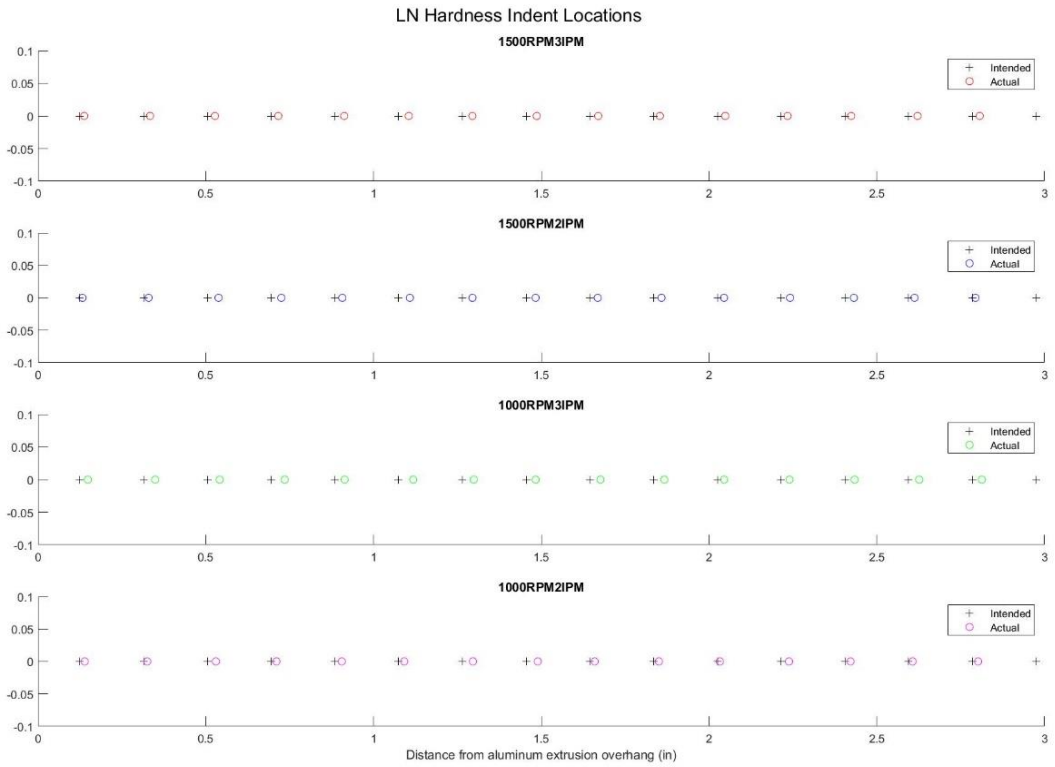

Figure A37 – X-Sect hardness indent location of LN weld with varying weld parameters

Shear Testing Data

Table A7 – NC weld shear stress data

Non Cooled Welds							
Weld Name	**Matrix Number**	**Sample Number**	**Sample Thickness (in)**	**Peak Load (N)**	**Peak Shear Stress (MPa)**	**Averaged Shear Stress (MPa)**	**Standard Deviation**
NC1500RPM3IPM	(1,1)	1	0.248	2577.83	128.89	126.87	3.62
		2	0.252	2461.44	121.12		
		3	0.24	2530.91	130.76		
		4	0.235	2401.39	126.71		
NC1500RPM2IPM	(2,1)	1	0.247	2481.11	124.56	122.08	1.43
		2	0.242	2365.63	121.21		
		3	0.23	2252.07	121.42		
		4	0.245	2393.58	121.14		
NC1000RPM3IPM	(3,1)	1	0.255	2205.28	107.24	114.75	4.52
		2	0.236	2193.17	115.23		
		3	0.248	2355.55	117.78		
		4	0.25	2393.97	118.74		
NC1000RPM2IPM	(4,1)	1	0.25	2311.72	114.66	115.07	0.84
		2	0.227	2096.82	114.54		
		3	0.233	2189.55	116.53		
		4	0.247	2282.16	114.57		

Table A8 – AC weld shear stress data

Air Cooled Welds							
Weld Name	**Matrix Number**	**Sample Number**	**Sample Thickness (in)**	**Peak Load (N)**	**Peak Shear Stress (MPa)**	**Averaged Shear Stress (MPa)**	**Standard Deviation**
AC1500RPM3IPM	(1,2)	1	0.239	2429.37	126.04	127.98	1.39
		2	0.235	2415.89	127.48		
		3	0.252	2613.25	128.59		
		4	0.248	2595.96	129.80		
AC1500RPM2IPM	(2,2)	1	0.256	2584.37	125.18	127.35	1.79
		2	0.234	2383.65	126.31		
		3	0.249	2570.10	127.99		
		4	0.251	2629.90	129.92		
AC1000RPM3IPM	(3,2)	1	0.247	2490.48	125.03	126.99	1.86
		2	0.235	2378.12	125.48		
		3	0.253	2607.83	127.81		
		4	0.249	2603.23	129.64		
AC1000RPM2IPM	(4,2)	1	0.252	2392.78	117.74	114.24	2.05
		2	0.24	2197.78	113.55		
		3	0.221	2008.42	112.69		
		4	0.24	2186.35	112.96		

Table A9 – WC weld shear stress data

Water Cooled Welds							
Weld Name	**Matrix Number**	**Sample Number**	**Sample Thickness (in)**	**Peak Load (N)**	**Peak Shear Stress (MPa)**	**Averaged Shear Stress (MPa)**	**Standard Deviation**
WC1500RPM3IPM	(1,3)	1	0.25	2600.15	128.97	129.51	0.63
		2	0.24	2521.34	130.27		
		3	0.217	2274.89	129.99		
		4	0.21	2181.60	128.82		
WC1500RPM2IPM	(2,3)	1	0.251	2718.56	134.30	131.56	2.16
		2	0.254	2704.62	132.04		
		3	0.227	2410.20	131.66		
		4	0.223	2306.55	128.26		
WC1000RPM3IPM	(3,3)	1	0.25	2566.26	127.29	123.79	3.29
		2	0.252	2500.33	123.03		
		3	0.241	2450.26	126.07		
		4	0.233	2231.58	118.76		
WC1000RPM2IPM	(4,3)	1	0.249	2610.40	130.00	115.42	10.21
		2	0.254	2443.67	119.30		
		3	0.244	2149.64	109.24		
		4	0.234	1946.19	103.13		

Table A10 – DI weld shear stress data

Dry Ice Cooled Welds							
Weld Name	**Matrix Number**	**Sample Number**	**Sample Thickness (in)**	**Peak Load (N)**	**Peak Shear Stress (MPa)**	**Averaged Shear Stress (MPa)**	**Standard Deviation**
DI1500RPM3IPM	(1,4)	1	0.231	2464.01	132.27	131.92	0.75
		2	0.242	2553.96	130.86		
		3	0.244	2591.00	131.67		
		4	0.247	2647.01	132.89		
DI1500RPM2IPM	(2,4)	1	0.25	2512.52	124.62	123.74	2.53
		2	0.248	2549.84	127.49		
		3	0.243	2383.31	121.62		
		4	0.225	2200.05	121.25		
DI1000RPM3IPM	(3,4)	1	0.221	2188.53	122.79	115.44	4.34
		2	0.22	2030.57	114.45		
		3	0.246	2227.27	112.27		
		4	0.251	2272.17	112.25		
DI1000RPM2IPM	(4,4)	1	0.238	2487.65	129.61	124.56	3.08
		2	0.249	2480.60	123.53		
		3	0.248	2425.57	121.28		
		4	0.253	2526.50	123.83		

Table A11 – LN weld shear stress data

Liquid Nitrogen Cooled Welds							
Weld Name	**Matrix Number**	**Sample Number**	**Sample Thickness (in)**	**Peak Load (N)**	**Peak Shear Stress (MPa)**	**Averaged Shear Stress (MPa)**	**Standard Deviation**
LN1500RPM3IPM	(1,5)	1	0.24	2549.30	131.71	130.13	1.20
		2	0.25	2636.95	130.79		
		3	0.251	2604.37	128.66		
		4	0.26	2712.05	129.34		
LN1500RPM2IPM	(2,5)	1	0.253	2489.09	121.99	121.24	1.92
		2	0.243	2423.46	123.67		
		3	0.227	2167.12	118.38		
		4	0.236	2301.52	120.93		
LN1000RPM3IPM	(3,5)	1	0.25	2279.13	113.04	114.64	2.39
		2	0.25	2269.16	112.55		
		3	0.23	2120.59	114.33		
		4	0.248	2372.58	118.63		
LN1000RPM2IPM	(4,5)	1	0.253	2439.60	119.57	121.37	1.04
		2	0.236	2320.68	121.93		
		3	0.241	2369.35	121.91		
		4	0.238	2343.18	122.08		